CHARACTERIZATION OF ANTIMICROBIAL COMPOUNDS SECRETED BY *BURKHOLDERIA THAILANDENSIS* OUTER MEMBRANE VESICLES

AN ABSTRACT SUBMITTED ON THE TWELFTH DAY OF NOVEMBER 2019

TO THE GRADUATE PROGRAM IN BIOMEDICAL SCIENCES

IN PARTIAL FULFILLMENT OF THE REQUIREMENTS

OF THE SCHOOL OF MEDICINE OF TULANE UNIVERSITY

FOR THE DEGREE OF

DOCTOR OF PHILOSOPHY

BY

Yihui Wang

APPROVED:

Lisa A. Morici, Ph.D. Chair

William C. Wimley, Ph.D.

Jacob P. Bitoun, Ph.D.

Kerstin Höner zu Bentrup, Ph.D.

Joseph A. Fuselier, MBA

ABSTRACT

Gram-negative bacteria secrete outer membrane vesicles (OMVs) that play critical roles in intraspecies, interspecies, and bacteria-environment interactions. Some OMVs, such as those produced by *Pseudomonas aeruginosa,* have previously been shown to possess antimicrobial activity against competitor species. In the current work, we demonstrate that OMVs from *Burkholderia thailandensis* inhibit the growth of drug-sensitive and drug-resistant bacteria and fungi and exhibit antibiofilm activity against methicillin-resistant *S. aureus* (MRSA) and *Streptococcus mutans*. We show that a number of compounds, including peptidoglycan hydrolases, 4-hydroxy-3-methyl-2-(2-non-enyl)-quinoline (HMNQ) and long-chain rhamnolipid present in *B. thailandensis* OMVs exert antimicrobial activity. Furthermore, we demonstrate that HMNQ and rhamnolipid possess antimicrobial and antibiofilm properties against various microbes. Rhamnolipid is superior at reducing the integrity of biofilms while HMNQ displays greater bactericidal activity. We attempted to use HMNQ and rhamnolipid to combat MRSA and promote wound healing in a murine full-thickness wound model. However, further optimization of the model and characterization of the molecules in antimicrobial efficacy, wound healing, and host immune responses are required. Overall, this work indicates that *B. thailandensis* secretes antimicrobial OMVs that may impart a survival advantage by eliminating competition. In addition, bacterial OMVs may represent an untapped resource of novel therapeutics effective against biofilm-forming and multidrug-resistant organisms.

CHARACTERIZATION OF ANTIMICROBIAL COMPOUNDS SECRETED BY *BURKHOLDERIA THAILANDENSIS* OUTER MEMBRANE VESICLES

A DISSERTATION SUBMITTED ON THE TWELFTH DAY OF NOVEMBER 2019

TO THE GRADUATE PROGRAM IN BIOMEDICAL SCIENCES

IN PARTIAL FULFILLMENT OF THE REQUIREMENTS

OF THE SCHOOL OF MEDICINE OF TULANE UNIVERSITY

FOR THE DEGREE OF

DOCTOR OF PHILOSOPHY

BY

Yihui Wang

APPROVED:

Lisa A. Morici, Ph.D. Chair

William C. Wimley, Ph.D.

Jacob P. Bitoun, Ph.D.

Kerstin Höner zu Bentrup, Ph.D.

Joseph A. Fuselier, MBA

ACKNOWLEDGEMENTS

I first would like to thank my advisor, Dr. Lisa Morici. Thank you for all your support and guidance on my research, personal improvement, as well as career development. Thank you for providing funding and giving me freedom to explore in science here. I always feel very lucky to join your lab where I get trained to be a scientist in so many ways and met other talented lab members. Thank you for establishing this enjoyable, supportive, and collaborative family, which I am proud and grateful to be part of. You always seem to have simple solutions every time I came to you with complex problems. Thank you for showing me how to think as a scientist. I appreciate and enjoyed every opportunity to have your guidance on how to present and write in science, which will benefit me for life. Thank you for everything you did that makes me enjoy my life as a graduate student here.

I also would like to thank all my committee members: Drs. William Wimley, Jacob Bitoun, Kerstin Höner zu Bentrup, and Joseph Fuselier. Thank you for your advice and expertise, and for providing this collaborative research environments. I appreciate the opportunities to work with you in many of your labs and your guidance on the exploration of my research project. I also thank Drs. James McLachlan, Lucia Freytag, and Derek Pociask for your life and career advice and guidance for my study and research.

I thank all my fellow lab members. Thank you, Joe Hoffmann and Sally Baker, for all the experiments we did together, for helping me with my presentations and writings, and for the fun we had moving lab. Thank you, Chris Davitt, Josh Hart, Rani Brooks, and

Patrick Gellings, for your help and support along the way. I also would like to thank the members of the Wimley Lab and McLachlan Lab for your help and insights.

I want to thank other faculty members, staff, and students in the Department of Microbiology and Immunology and the Biomedical Sciences Graduate Program. Thank you for contributing to this supportive and collaborative environment that I always enjoy. I also thank all my friends, old and new, for spending good times together and helping me go through my journey here.

Lastly, I would like to thank my family back in China. Thank you to my parents who always respect and support my passions and decisions. Thank you for all the video calls, listening me out and providing advice. Thank you for letting me travel this far and become who I am. You probably will never read this, but I hope you already know.

TABLE OF CONTENTS

LIST OF FIGURES

LIST OF TABLES

CHAPTER 1: Introduction

1.1 Antimicrobial resistance

Antimicrobial resistant (AMR) infections caused by multidrug-resistant microorganisms have increasingly become a problem crisis in recent years, not only due to the misuse of antimicrobials but also due to the lack of novel antimicrobial development. Mathematical models predict that by 2050, approximately ten million people will die annually with a cost up to 100 trillion USD if the current trend is not altered[1].

Most of the antibiotics against bacterial infections in use today were discovered between 1940s to 1980s including the β-lactam antibiotics (penicillin, methicillin), polymyxins (colistin), glycopeptides (vancomycin), aminoglycosides (gentamicin), tetracyclines, macrolides (erythromycin), fluoroquinolones (ciprofloxacin), and lipopeptides (daptomycin). Their natural scaffolds were mostly identified from the metabolites of bacteria and fungi. Further chemical modifications were applied to improve potency and reduce toxicity. However, with the misuse and overuse of antibiotics, bacteria evolved with more resistance mechanisms including enzymatic degradation or modification of antibiotics, alteration of antibiotic targets, active efflux of antibiotics, and reduced permeability of their cell membrane under the antibiotic selection pressure[2,3]. Furthermore, many of these resistance mechanisms are mediated through bacterial plasmids, can undergo horizontal gene transfer and spread worldwide[4]. Although many derivatives of old class antibiotics were launched later, the resistance developed even sooner as documented in a 2013 report from CDC (**Figure 1-1**)[5]. In addition, after 2000, few novel-classes of antibiotics was discovered exacerbating this crisis.

Antifungal resistance is another alarming problem in recently years facilitated by the limited classes of antifungal drugs that are available clinically (polyenes, triazoles, and echinocandins)[6]. Additionally, the occurrence and severity of fungal infections have significantly increased since the late 1960s with the development of antibacterial therapies[7]. Mechanisms of antifungal resistance are similar to those of antibacterial resistance including increase of drug efflux, target alteration, and metabolism modification[8]. *Candida* as one of the most common cause of bloodstream infections in the US has been shown to become increasingly resistant to first-line (fluconazole) and second-line (echinocandins) antifungal medications[9,10]. Notably, fluconazole-resistant *Candida* is categorized as a serious threats to the United States by CDC[5]. Another frequent pathogen involved in systemic fungal infections is *Cryptococcus*. As an encapsulated opportunistic pathogen, they are ubiquitous in the environment and easily inhaled into the lungs. Failure of the clearance usually results in pulmonary infection and subsequent dissemination to the central nervous system[11]. Although antifungal resistant *Cryptococcus* has not yet become a clinically significant problem, isolates are recommended to be tested for antifungal susceptibility in persistent or relapsed cases due to the widespread use of fluconazole[12].

1.2 Multidrug-resistant organisms

The first well known threat of AMR was the rise of drug-resistant *Staphylococcus aureus*. The initial resistance of *S. aureus* happened only a few years after the introduction of penicillin into clinical practice in the 1940s, which quickly spread from hospitals to communities[13]. In 1960s, the widespread use of methicillin led to the almost immediate emergence of methicillin-resistant *S. aureus* (MRSA) resistant to a wide range of β-lactam

antibiotics[14]. The resistance is predominantly spread through the horizontal transfer of genes[13]. Beginning in 1980s it has been reported that MRSA accounts for over 50% bacterial isolates in hospitals[15,16]. Later, vancomycin-intermediate and vancomycin-resistant *S. aureus* were isolated following the general use of the antibiotic[17,18]. Nevertheless, *S. aureus* is part of the normal bacterial flora colonizing the nasopharynx and skin[19]. Thus, MRSA carriers are at higher risk of infection and transmission[20]. In recent years, MRSA has been categorized as a serious threat by CDC, which is responsible for the more than 80,000 severe infections and 11,000 deaths in the US each year[5].

Because of the significance of MRSA, the development of antibiotics was mainly focused on targeting Gram-positive bacteria before 2000. With the neglect of Gram-negative bacteria, the number of clinical isolates with resistance to seven out of ten antibiotics increased from 5% to between 6% and 18% from 1999 to 2008[21]. The now leading species of AMR, *Acinetobacter baumannii*, is an opportunistic pathogen and commonly involved in nosocomial infections causing a wide range of infections. Ventilator-associated pneumonia and bloodstream infections caused by *A. baumannii* have been shown to lead to 52% morbidity and mortality[22,23]. In addition, *A. baumannii* is associated with skin and soft-tissue infections[24], wound infections[25], urinary-tract infections[26], and secondary meningitis[27] within hospital settings. Although it can be spread through the air in water droplets, its most common mode of transmission is from the skin contacts with hospital staff[28,29]. More importantly, multidrug-resistant (MDR) *A. baumannii* has become more and more prevalent with some strains resistant to nearly all antibiotics including carbapenems which are considered antibiotics of last resort[5]. The resistance of these MDR strains was shown to be mediated by all the resistance

mechanisms that are known including producing β-lactamases and other enzymes against β-lactams and aminoglycosides[30,31], altering the targets of fluoroquinolones through point mutations[32], and expressing genes that encode tetracycline-specific efflux pumps[33]. Further evidence suggests that these resistance genes are transmitted by horizontal transfer[34].

Due to the severity of AMR and the critical need for new antimicrobials, in 2017 the World Health Organization published a global priority list of antibiotic-resistant species to guide urgent research, discovery, and development of new antibiotics (**Figure 1-2**). Among this list, the bacterial species *A. baumannii, Pseudomonas aeruginosa,* and *Enterobacteriaceae* are of critical priority, followed by *Enterococcus faecium, S. aureus* and others[35]. Importantly, many of these organisms are well known for their propensity to form biofilms which are 10- to 1000-fold more resistant to antimicrobials than planktonic organisms[36].

1.3 Biofilms

Despite the fact that the majority of antimicrobial development focuses on free-living planktonic bacteria and fungi, microorganisms predominantly exist within biofilms in both natural environment[37] and infections[38]. Biofilms are bacterial communities surrounded by extracellular polymeric substances (EPS) and are one of the most diverse and complex systems[39,40]. The development of a biofilm is a dynamic and well-regulated process that includes stage-specific expression of genes and proteins and involves the early attachment to the surface, microcolony formation, subpopulation interactions during structure development, maturation, and even the reactivation and dispersion in some bacterial species (**Figure 1-3**)[41]. It has become apparent that biofilms are secreted by many

pathogenic microorganisms as a principle virulence mechanism and are involved in over 80% of microbial infections[42]. Biofilm-related infections often result from microbial colonization of soft tissues or medical implants and can manifest as persistent or chronic disease[43]. The sticky and hydrated gel-like biofilm extracellular matrix composed primarily of polysaccharides, proteins, and lipids, leads to remarkable complexity of the biofilms[44] with steep nutrient and oxygen gradients[45], high biodiversity[46], and complex social interactions[39] that can result a wide variety of phenotypic states in a given species[47]. These highly heterogeneous matrices encase and protect microbes from antimicrobials, obstructing the eradication of infections caused by biofilm-forming pathogens and contributing to antimicrobial resistance[48]. Several mechanisms of biofilm tolerance have been proposed (**Figure 1-4**) including poor penetration of antimicrobial agents[39,49], metabolic inactive and persister cells with reduced susceptibility[50,51], and varieties of adaptive responses[36,38,52].

1.4 Efforts and challenges in the development of novel antimicrobials

Many past efforts were directed at the development of novel antimicrobials to combat AMR and biofilm-related infections. In 1995, the sequencing of the first complete bacterial genome provided new tools for identifying new antibacterial targets, which led to the massive efforts in developing high-throughput screens (HTS) for novel antibiotics[53]. Unfortunately, none of these efforts resulted in any promising drug candidates[54]. In the example of GlaxoSmithKline, despite more than 350 candidate target genes from a broad variety of pathways and processes identified from *Streptococcus pneumoniae, S. aureus*, and *Heamophilus influenzae*, only 5 leads were identified when screened with the

compound collection which consisted of 260,000-530,000 compounds and none of them advanced into development candidates[53]. The main reason for the failure is the fundamental difference between the development of antimicrobials and other medicines in that the antimicrobial agents require much higher exposures and doses. This makes it critical and challenging to balance their antimicrobial activity, drug metabolism, pharmacokinetic properties and safety[55]. Moreover, it is likely that the target genes identified are only essential for the growth of bacteria in nutrient-rich media. On the contrary, essential genes for bacteria *in vivo* or during infections may be cryptic and encode proteins with unknown functions, which makes it difficult to build chemical screening assays[56]. To tackle this problem, recent studies screened chemical libraries on target bacteria in non-conventional growth media and host models of disease and yielded promising drug candidates against *P. aeruginosa* and *Mycobacterium tuberculosis*[57,58]. In another study, researchers identified compounds targeting quorum-sensing virulence pathway in mouse models of *P. aeruginosa* infection without perturbing bacterial growth *in vitro*[59]. These findings suggest that *in vivo* essential genes represent a set of emerging targets that remain untested in modern antibacterial drug discovery[56]. Besides developing novel classes of antimicrobials, more approaches were proposed to combat AMR. Among them, antibiotic adjuvants, hybrids and prodrugs were designed to potentiate the antimicrobial activity or promote the uptake of the current antibiotics[60,61]. Other approaches such as vaccines, phage therapy, monoclonal antibodies, modulation of host microbiome and immunity opens more avenues for solving this crisis[55,62].

Furthermore, the highly drug-resistant biofilm-related infections highlight the importance of not only the development of new antimicrobials but also novel therapeutic

strategies that target multiple pathways with the ability to diffuse into or disrupt biofilms, and kill persister cells (**Figure 1-5**)[63-65]. Not surprisingly, current therapies targeting individual cells with antibiotics are restrained by the poor penetration of the biofilms or adaptive responses [66]. EPS targeting strategies with inhibitors[67,68], degrading enzymes[69], quorum sensing regulators[70-72] and vaccination[73,74] are promising adjunctive approaches for combination therapies with other antimicrobials. Unfortunately, few of them were successful or clinically viable thus far[75]. To overcome these obstructions caused by biofilms, researchers have proposed to exploit nanoparticles, which can be designed to enhance drug delivery with increased penetration, selective targeting and local drug release in existing biofilms[75-79].

1.5 Bacteria as sources of antimicrobial products

Although the first antibiotic, sulfonamides, were discovered by screening libraries of synthetic chemicals, starting from the discovery of streptomycin in 1943, the main antibiotics scaffolds we are using today were mined from bacteria and fungi. Microbes in the environment especially soil bacteria produce metabolites with remarkable efficacy and minimal toxic side effects[56]. The mining platform of streptomycin developed by Selman Waksman was then widely adopted and yielded many classed of antibiotics in the following 20 years known as the golden era of antibiotics[80]. Actinomycetes are the source of about 75% of known antibiotics with 75% of them produced by a single genus, *Streptomyces*. Another major source of antimicrobials are derived from non-filamentous bacteria including *Bacillus*, which produce over 60 antibiotics[62]. Unfortunately, the overmining quickly resulted a depleted pool of natural antimicrobials from the available soil bacteria

(less than 1% of all soil bacteria were culturable) with the same compounds repeatedly identified. Thus, in the following years, synthetic modifications were mostly made to improve the efficacy of known antibiotics.

In recent years, newer tools and technologies were applied to advance this field. Novel methods were developed for growing "nonculturable" microorganisms, which can now be a source for more antimicrobials. An antibiotic resistance platform was developed to identify new antibiotics and adjuvants and to dereplicate known naturally occurring antibiotic scaffolds[81]. Genome-guided approaches were used for the discovery of natural products[82]. Notably, bacterial genome sequences shed lights on cryptic biosynthetic genes which encode products that were unrecognizable before. To activate silent gene clusters, libraries of small molecules were tested as elicitors which awakened the production of different profiles of secondary metabolites[83]. Furthermore, many silent genes are regulated by growth conditions, signals and stressors from the environment, which can be manipulated for extended profiles of natural products[84].

1.6 *Burkholderia* species

In recent years, due to the development of novel tools and technologies, *Burkholderia* species have emerged as a new source of diverse natural products especially novel antibiotics and bioactive secondary metabolites[82,85,86]. The genus *Burkholderia* represents an expanding group of diverse and versatile Gram-negative, obligately aerobic, rod-shaped bacteria with over 80 species. They inhabit ecological niches such as water, soil, plant surfaces and rhizosphere, and even occur in association with animal hosts including humans[87,88]. The *Burkholderia* was previously part of the *Pseudomonas* genus

and first described in 1992[89]. The versatility of *Burkholderia* is likely due to their large genomes. The median genome size of *Burkholderia* species is 7.27 Mb revealed by the complete genome sequencing of 36 *Burkholderia* strains, ranking in the top 5% of all bacteria[82]. The genome indicates a large number of putative natural product biosynthetic gene clusters, ranging from 7 to 27 in different strains as predicted by the antiSMASH (antibiotic & Secondary Metabolite Analysis Shell) program, which identifies biosynthetic loci covering the whole range of known secondary metabolite compound classes[90,91]. Some of the best known *Burkholderia* species are the *B. cepacia* complex which are opportunistic pathogens primarily causing diseases in immunocompromised individuals such as cystic fibrosis patients[92]. Other pathogenic members are *B. pseudomallei* as the etiological agent of melioidosis in both animals and humans[93], and *B. mallei* which causes glanders in horses and is also highly virulent in humans[94].

B. thailandensis is closely related and coexists with *B. pseudomallei* in the soil but rarely causes disease and is approximately 10^5-fold less virulent than *B. pseudomallei* in Syrian hamsters or mice[95]. Previous studies suggests that *B. thailandensis* E264 is unequivocally the most promising source of bioactive natural products among the *Burkholderia* strains explored, harboring 21 biosynthetic gene clusters which include predicted polyketide synthase (PKS) or nonribosomal peptide synthase (NRPS) that are associated with synthesis of putative natural products (**Table 1-1**)[82,90,91]. Studies have shown that *B. thailandensis* produces capistruin[96], malleilactone[97], thailandamide[98], burkholdacs[99], thailanstatins[100], bactobolin[101], rhamnolipid[102], and hydroxyalkylquinoline[103] in the culture supernatant. Many of them were identified through a genome-guided approach[82], while others were discovered with a conventional natural

product approach[101,104]. Notably, capistruin, malleilactone, bactobolin, rhamnolipid, and 4-hydroxy-2-alkylquinoline (HAQ), have been previously shown to express weak to moderate antimicrobial activity[96,97,105-107].

The production of multiple products in *B. thailandensis* is tightly regulated under the quorum sensing (QS) system[86,101,108]. *B. thailandensis* is also well known for producing QS signals with antimicrobial functions[103,107]. HAQs were originally characterized in *P. aeruginosa* and recognized as a class of quorum sensing molecules that exhibit numerous functions, including iron chelation, immune modulation, and intercellular communication[109]. Recently, HAQ derivatives were reported in *B. thailandensis* as quorum sensing signals with synergistic effects that could inhibit *E. coli* growth in planktonic cultures[103,107]. Specifically, 4-hydroxy-3-methyl-2-(2-non-enyl)-quinoline (HMNQ) is the dominant form of HAQs produced by *B. thailandensis*. HMNQ was shown to function as an ionophore, to disrupt proton motive force, and to inhibit pyrimidine biosynthesis in *E. coli*[103].

Another example of natural products produced by *B.* thailandensis is rhamnolipid. Rhamnolipids are glycolipidic surfactant with up to two rhamnoses (mono or di-rhamnolipids) linked through a β-glycosidic bond to up to two 3-hydroxyfatty acids with various chain lengths[110]. Rhamnolipids are well studied in *P. aeruginosa*, which predominantly produces short chain rhamnolipids (Rha-Rha-C_{10}-C_{10}), for their applications in pharmaceutical, chemical, cosmetic and food industries, replacing surfactants of petrochemical origins[111]. Recent studies have shown that rhamnolipids are also produced by the non-pathogenic *B. thailandensis,* predominantly in a form with longer fatty acid chains (Rha-Rha-C_{14}-C_{14}), which may provide additional industrial

applications[102,112]. The antimicrobial and antibiofilm activities of rhamnolipids have also been previously characterized[102,113-115]. A recent study showed that the production of rhamnolipids in *B. thailandensis* is regulated by QS[116]. Although HMNQ has been shown to play a key role in the QS of *B. thailandensis*, the correlation between the two molecules remains unknown. Besides these well characterized small molecules, more metabolites likely remain cryptic with unknown regulatory factors.

1.7 Bacterial outer membrane vesicles

Most if not all living cells from prokaryotes to more complex eukaryotic cells naturally secrete membrane vesicles that serve numerous and versatile roles in intra- and interspecies interactions[117,118]. Gram-negative bacteria constitutively shed outer membrane vesicles (OMVs) from their surface that contain numerous components including proteins[119], lipids[120], polysaccharides[121], RNA/DNA[122,123], and small molecules[124]. These components either associate with the bi-layered membrane or are located within the vesicle's lumen (**Figure 1-6A**). The production and cargo selection of OMVs is in response to stressors and environmental signals[125]. Thus, OMVs serve various offensive and defensive roles contributing to bacterial survival (**Figure 1-6B**). OMVs also interact with other microorganisms in nature[126] or host cells in the context of colonization and infection[127], protecting cargo molecules from degradation and delivering them at high concentrations over long distances[128,129]. Because of their ability to stimulate host innate and adaptive immunity, OMVs have been used as a vaccine platform. In particular, an OMV-containing meningococcal vaccine (Bexsero®, 4CMenB; GSK) is now used in the routine immunization schedules for infants in the United Kingdom and Ireland[130]. In

addition, the roles of OMVs in various biological process such as nutrient acquisition, defense, and intercellular communication lend them to other diverse biotechnological applications.

OMVs are also a ubiquitous and important constituent of Gram-negative and mixed bacterial biofilms. It has been documented that OMVs from planktonic and biofilm cultures were significantly different, suggesting diverse functional roles in different environments[131]. As one of their functions contributing to bacterial survival and competition, OMVs have been shown to possess antimicrobial activity against other microorganisms. *P. aeruginosa* OMVs was first reported to possess antimicrobial activity against competitor Gram-negative and Gram-positive planktonic bacteria twenty years ago[129]. The activity was attributed to the presence of hydrolytic enzymes, in particular a 26-kDa peptidoglycan hydrolase that degraded the cell well of competitor bacterial species[129,132]. OMVs from more than fifteen strains of Gram-negative species were tested for their bactericidal activity. *P. aeruginosa* OMVs possessed the most potent killing capacity against other species[133,134]. More recently, *Lysobacteri* sp. XL1 has been shown to secret bacteriolytic endopeptidases within OMVs against *S. aureus* and *Erwinia marcescens*[135]. Similarly, *Myxococcus xanthus* predate upon various bacteria and fungi with OMVs containing hydrolytic enzymes and secondary metabolites including myxochelines, myxalamids, myxovirescin A, and cittlin A, with antimicrobial activity[136,137]. Both *Lysobacter* and *Myxococcus* are social bacterial predators. Their predation can be accomplished remotely via OMVs that kill and decompose neighboring competitors[138,139].

The majority of the bacteriolytic enzymes found in OMVs are peptidoglycan hydrolases such as amidases, endopeptidases, transglycosylases, and glucosaminidases with different specificity on bacterial peptidoglycan[140]. Peptidoglycan as the major components of bacterial cell wall are made of glycan strands cross-linked by short peptides, which are highly diverse in their composition and sequence between bacterial species[141]. For instance, peptidoglycan structures are well studied in *S. aureus* with conserved disaccharide (*N*-acetylglucosamine and *N*-acetylmuramic acid), a pentapeptide stem (L-alanine-D-*iso*-glutamine-L-lysine-D-alanine-D-alanine), and a pentaglycyl bridge[142]. Their glycosidic bond between *N*-acetylglucosamine and *N*-acetylmuramic acid, peptide bonds, and amide groups linking L-alanine and *N*-acetylmuramic acid could potentially be cleaved by transglycosylases, peptidases, and amidases, respectively.

1.8 Significance and hypothesis

Although the bactericidal activity of OMVs was documented, their roles in targeting bacterial biofilms were not characterized. With the mounting crisis of antimicrobial resistance, new antimicrobial agents and therapeutic strategies with novel mechanisms of action against multidrug-resistant organisms and biofilms are urgently needed to prevent chronic and life-threatening infections. As a non-pathogenic soil saprophyte, *Burkholderia thailandensis* is closely related to *P. aeruginosa* and presumably evolved mechanisms to produce predatory OMVs to increase nutrient load in poor growth conditions at the expense of surrounding microbes. Thus, we hypothesized that *B. thailandensis* produces OMVs with antimicrobial activity that are naturally used as a

survival strategy to compete with surrounding microflora. We further hypothesized that the OMVs may penetrate biofilms.

In the current study, we initially evaluated the antimicrobial activity of OMVs against representative Gram-positive and -negative bacteria, multidrug-resistant bacteria and fungi. The reproducibility of purified OMV was evaluated by chemical composition and physical appearance using gel electrophoresis, liquid chromatography, and transmission electron microscopy. The antimicrobial activity was measured against planktonic and agar cultures of individual microorganisms.

We also investigated the antibiofilm activity of OMVs with various microorganisms. The ability of OMVs to disrupt pre-formed biofilms was first screened using representative biofilm-forming bacteria. We then characterized the ability of *B. thailandensis* OMVs to disrupt the model biofilm forming bacterium, MRSA and *Streptococcus mutans* in well-established biofilm assays using multiple imaging techniques. The synergistic effect of OMVs with an antibiotic was also evaluated against *S. mutans* biofilms.

To better understand the antimicrobial and antibiofilm properties of OMVs, we confirmed the existence of peptidoglycan hydrolases and successfully identified HMNQ and rhamnolipid within *B. thailandensis* OMVs with analytical chemistry methods. The quorum sensing antimicrobial molecule, HMNQ, and biosurfactant, rhamnolipid, were further evaluated for their ability to inhibit the growth of various bacteria and fungi.

Finally, we characterized the roles of HMNQ and rhamnolipid in killing and disrupting MRSA biofilms using confocal microscopy and COMSTAT analyses. The

efficacy and safety of HMNQ and rhamnolipid was eventually evaluated *in vivo* using a murine wound model infected with bioluminescent MRSA.

Figure 1-1

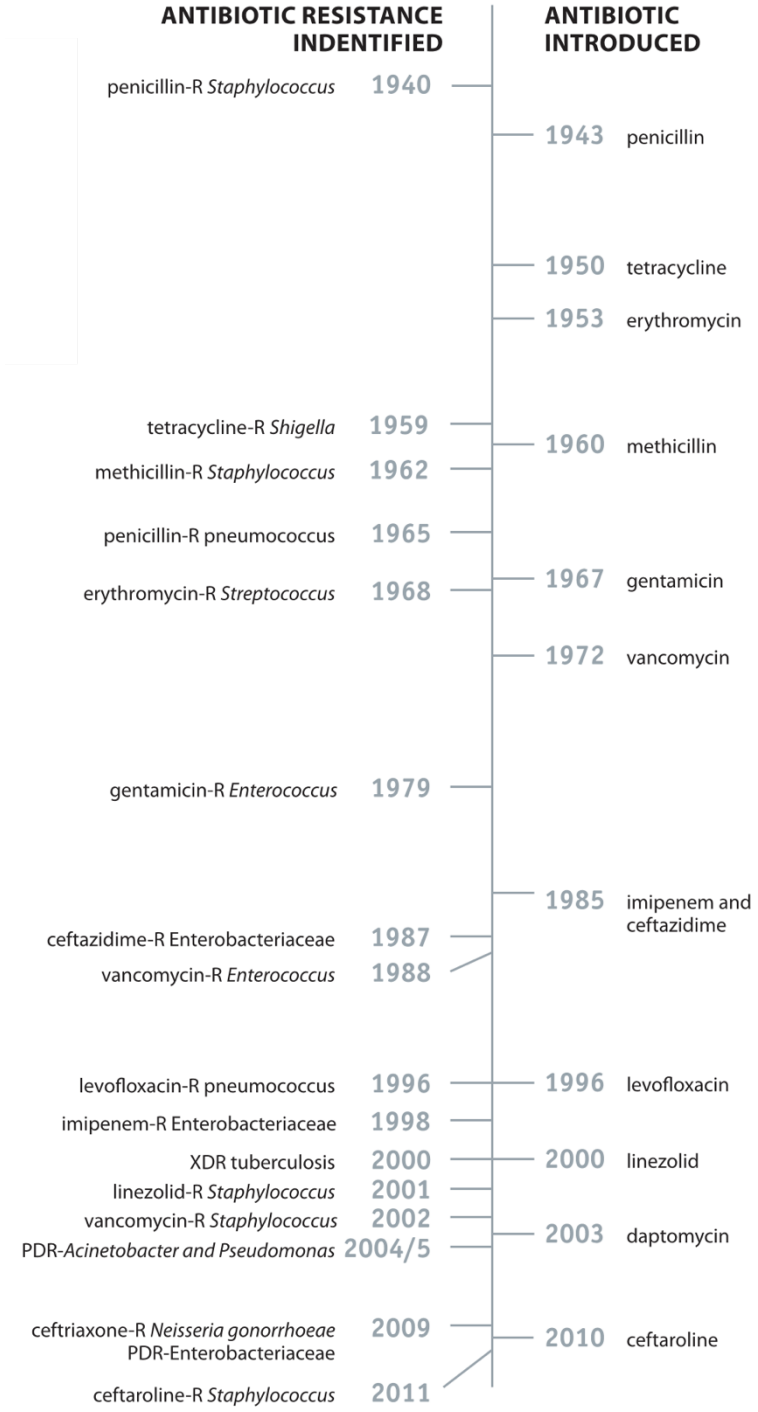
ANTIBIOTIC RESISTANCE INDENTIFIED
ANTIBIOTIC INTRODUCED
penicillin-R Staphylococcus 1940
1943 penicillin
1950 tetracycline
1953 erythromycin
tetracycline-R Shigella 1959
1960 methicillin
methicillin-R Staphylococcus 1962
penicillin-R pneumococcus 1965
erythromycin-R Streptococcus 1968
1967 gentamicin
1972 vancomycin
gentamicin-R Enterococcus 1979
1985 imipenem and ceftazidime
ceftazidime-R Enterobacteriaceae 1987
vancomycin-R Enterococcus 1988
levofloxacin-R pneumococcus 1996
1996 levofloxacin
imipenem-R Enterobacteriaceae 1998
XDR tuberculosis 2000
2000 linezolid
linezolid-R Staphylococcus 2001
vancomycin-R Staphylococcus 2002
2003 daptomycin
PDR-Acinetobacter and Pseudomonas 2004/5
ceftriaxone-R Neisseria gonorrhoeae 2009
PDR-Enterobacteriaceae
2010 ceftaroline
ceftaroline-R Staphylococcus 2011

Figure 1-1. Timeline of key antibiotic resistance events

Dates are based upon early reports of resistance in the literature. In the case of pan drug-resistant (PDR) – *Acinetobacter* and *Pseudomonas*, the date is based upon reports of healthcare transmission or outbreaks. Note: penicillin was in limited use prior to widespread population usage in 1943. This timeline was originally published by CDC[5].

Figure 1-2

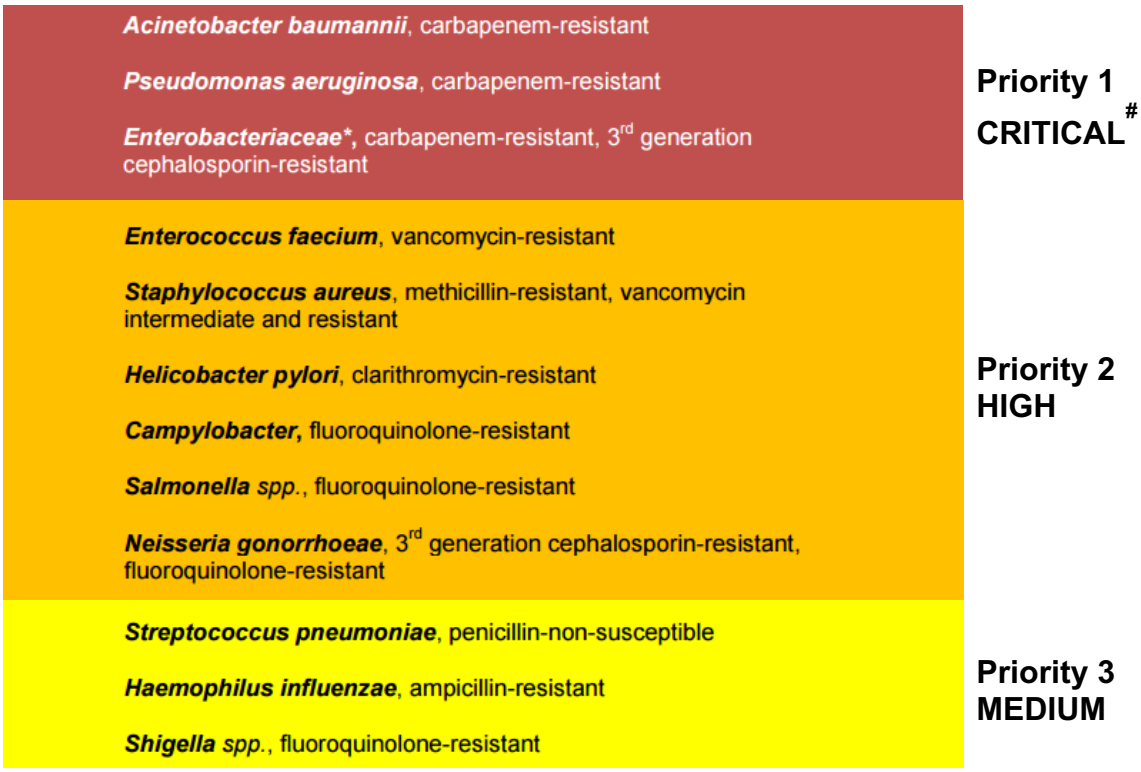
Acinetobacter baumannii, carbapenem-resistant
Pseudomonas aeruginosa, carbapenem-resistant
Enterobacteriaceae*, carbapenem-resistant, 3rd generation cephalosporin-resistant
Priority 1
CRITICAL #
Enterococcus faecium, vancomycin-resistant
Staphylococcus aureus, methicillin-resistant, vancomycin intermediate and resistant
Helicobacter pylori, clarithromycin-resistant
Campylobacter, fluoroquinolone-resistant
Salmonella *spp.*, fluoroquinolone-resistant
Neisseria gonorrhoeae, 3rd generation cephalosporin-resistant, fluoroquinolone-resistant
Priority 2
HIGH
Streptococcus pneumoniae, penicillin-non-susceptible
Haemophilus influenzae, ampicillin-resistant
Shigella *spp.*, fluoroquinolone-resistant
Priority 3
MEDIUM

Figure 1-2. WHO priority pathogens list for research and discovery of new antibiotics

[#] *Mycobacteria* (including *Mycobacterium tuberculosis*, the cause of human tuberculosis), was not subjected to review for inclusion in this prioritization exercise as it is already a globally established priority for which innovative new treatments are urgently needed.

[*] Enterobacteriaceae include: *Klebsiella pneumonia, Escherichia coli, Enterobacter* spp., *Serratia* spp., *Proteus* spp., and *Providencia* spp., *Morganella* spp. The list was originally published by the World Health Organization[35].

Figure 1-3

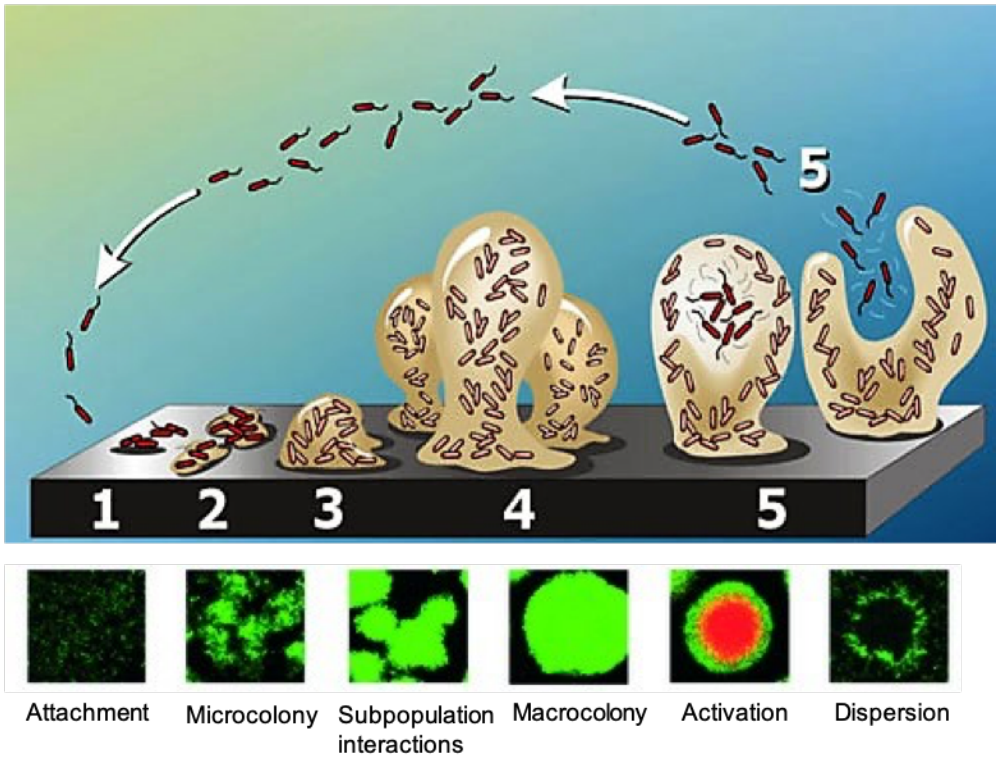
5
1
2
3
4
5
Attachment
Microcolony
Subpopulation interactions
Macrocolony
Activation
Dispersion

Figure 1-3. Biofilm development stages

The biofilm starts with individual planktonic cells attach to the surface following by extracellular polysaccharide production and microcolony formation. During biofilm structure development, subpopulations interact with each other through signaling molecules. In the following development, macrocolonies are formed in mature biofilms. Under stress conditions, dead cells are accumulated. In certain species like *Pseudomonas aeruginosa*, cells can be released from the biofilm macrocolonies to start this process again. In the bottom fluorescent images, biofilms formed by green fluorescent protein-tagged *P. aeruginosa* were stained with propidium iodine (red fluorescent, labeling extracellular DNA). The illustration was modified from the original image published by the Montana State University Center for Biofilm Engineering. The fluorescent images were originally published by Yang, L. *et al.*[41].

Figure 1-4

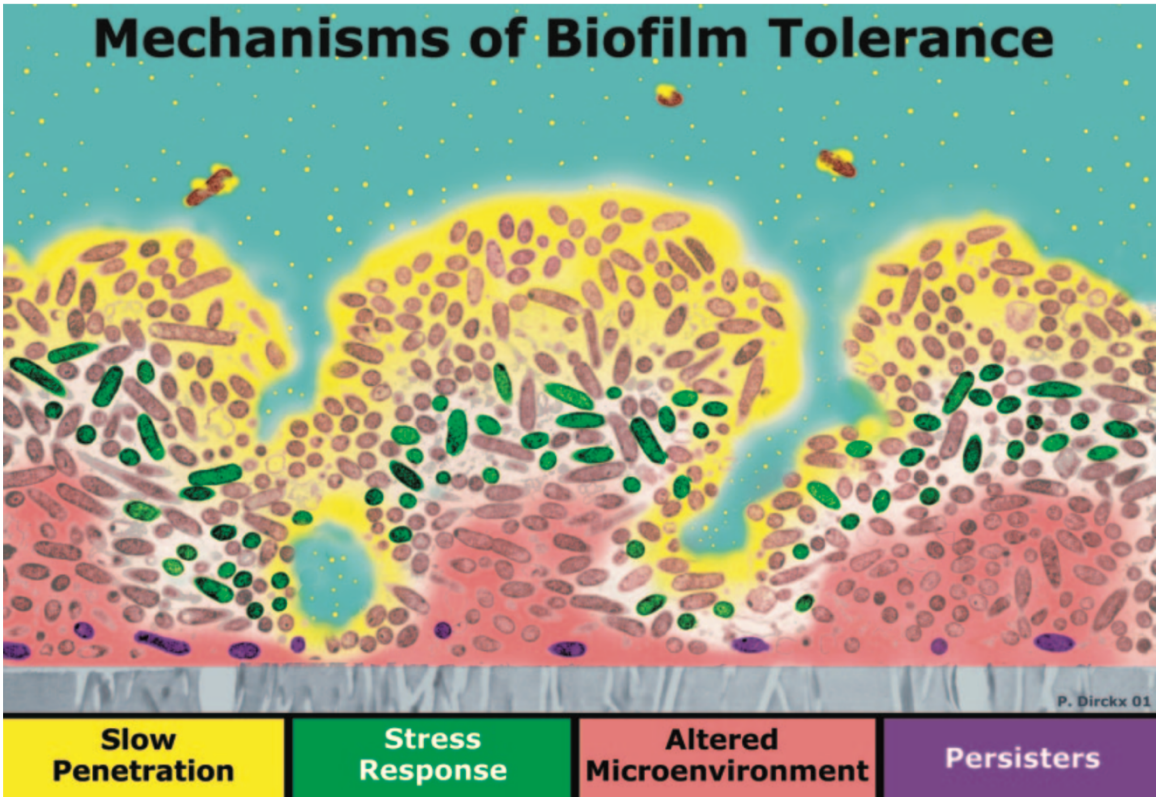
Mechanisms of Biofilm Tolerance
P. Dirckx 01
Slow Penetration
Stress Response
Altered Microenvironment
Persisters

Figure 1-4. Mechanisms for biofilm tolerance

Four possible mechanisms of biofilm antibiotic resistance. The image is a cross section of a biofilm with the attachment surface (gray) at the bottom and the aqueous containing the antibiotic (yellow) at the top. In zones where there is nutrient depletion (red), antibiotic action may be antagonized. Some bacteria may activate stress responses (green), with other may differentiate into a protected phenotype (purple). The illustration was previously published by Chambless, J. D. *et al*.[143].

Figure 1-5

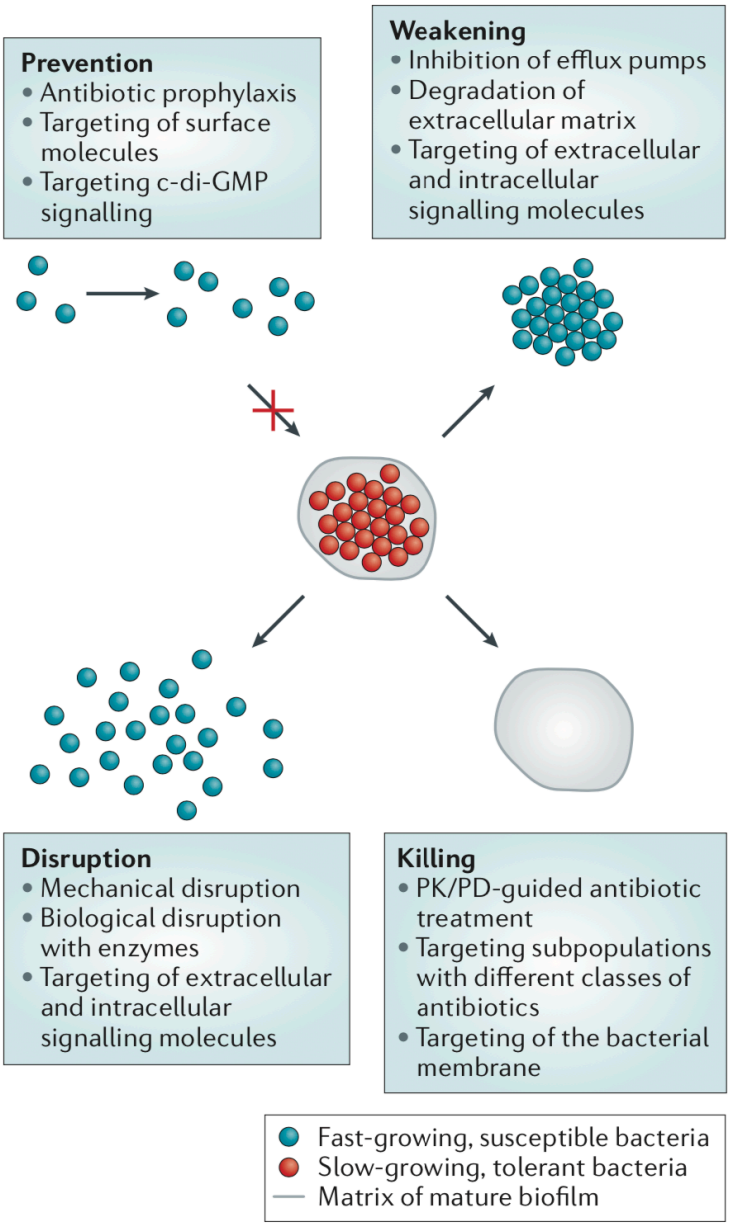
Prevention
• Antibiotic prophylaxis
• Targeting of surface molecules
• Targeting c-di-GMP signalling
Weakening
• Inhibition of efflux pumps
• Degradation of extracellular matrix
• Targeting of extracellular and intracellular signalling molecules
Disruption
• Mechanical disruption
• Biological disruption with enzymes
• Targeting of extracellular and intracellular signalling molecules
Killing
• PK/PD-guided antibiotic treatment
• Targeting subpopulations with different classes of antibiotics
• Targeting of the bacterial membrane
Fast-growing, susceptible bacteria
Slow-growing, tolerant bacteria
Matrix of mature biofilm

Figure 1-5. The four anti-biofilm strategies

The blue circles represent susceptible bacteria and the red circles represent tolerant bacteria. The large light blue circles represent susceptible bacteria and the red circles represent tolerant bacteria. The large light gray circle represents the matrix of mature biofilms. c-di-GMP, cyclic diguanosine-5'-monophosphate; PK/PD, pharmacokinetics/pharmacodynamics. The illustration was previously published by Bjarnsholt, T. *et al*.[144].

Figure 1-6

A

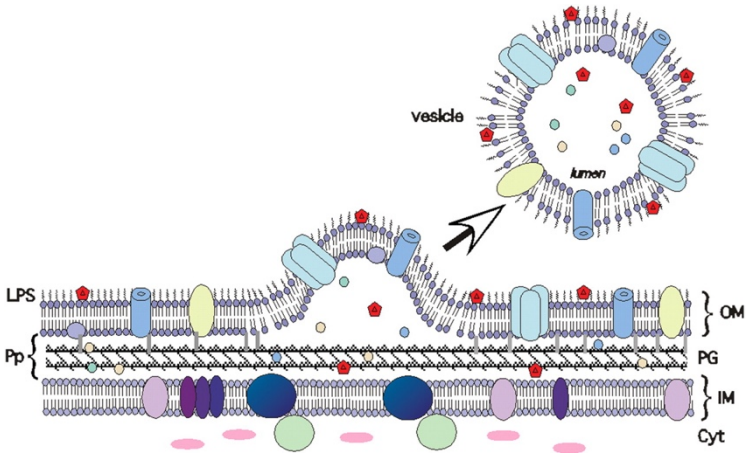
vesicle
lumen
LPS
Pp
OM
PG
IM
Cyt

B

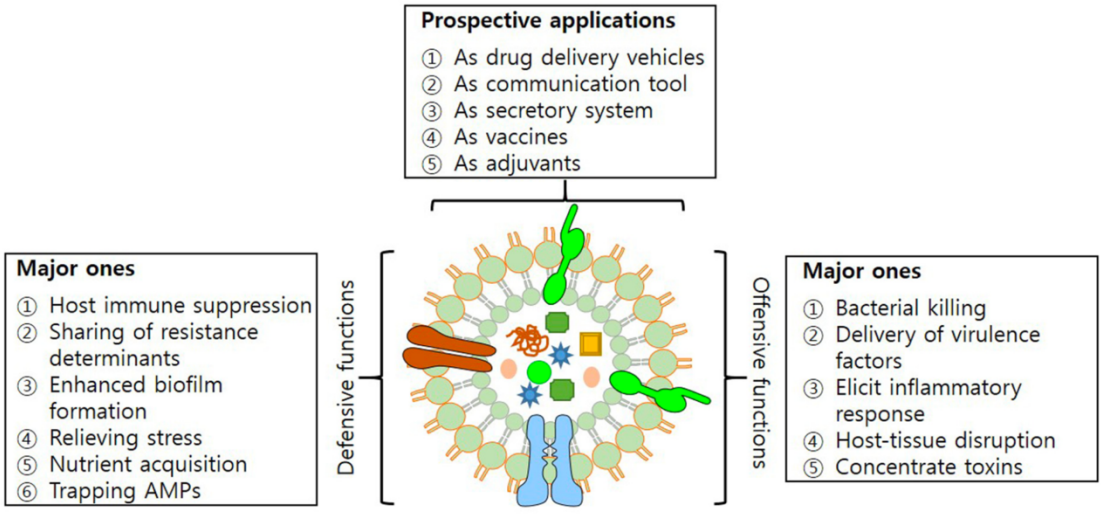
Prospective applications
① As drug delivery vehicles
② As communication tool
③ As secretory system
④ As vaccines
⑤ As adjuvants
Major ones
① Host immune suppression
② Sharing of resistance determinants
③ Enhanced biofilm formation
④ Relieving stress
⑤ Nutrient acquisition
⑥ Trapping AMPs
Defensive functions
Offensive functions
Major ones
① Bacterial killing
② Delivery of virulence factors
③ Elicit inflammatory response
④ Host-tissue disruption
⑤ Concentrate toxins

Figure 1-6. Bacterial outer membrane vesicles

(**A**) Model of OMV biogenesis. OMVs are proteoliposomes consisting of outer membrane phospholipids and LPS, a subset of outer membrane proteins, periplasmic proteins, DNA/RNA, and small molecules. Vesicles are likely to bud at sites where the links between the peptidoglycan and outer membrane are infrequent, absent, or broken. Other mechanisms were also proposed for OMV biogenesis. LPS, lipopolysaccharide; Pp, periplasm; OM, outer membrane; PG, peptidoglycan; IM, inner membrane; Cyt, cytosol. The illustration was previously published by Kuehn, M. J. *et al*.[145]. (**B**) Offensive and defensive roles of OMVs utilized in bacteria-bacteria and bacteria-host interactions; and their potential applications. The illustration was previously published by Jan, A. T. *et al*.[146].

Table 1-1

B. thailandensis E264 genome	Gene cluster #	Category of predicted gene cluster	Identified natural product
Chromosome I	1	Bacteriocin	
	2	Type I PKS	
	3	NRPS	
	4	Terpene	
	5	NRPS	Thailandepsins
	6	NRPS	
	7	Bacteriocin	Capistruin
Chromosome II	1	Bacteriocin	
	2	Other	Betulinan/terferol analogues
	3	Homoserine lactone	
	4	Other	
	5	NRPS-type I PKS-homoserine lactone	Bactobolins[a]
	6	Homoserine lactone	
	7	*Trans*-AT PKS-type II PKS-NRPS	Thailandamides
	8	Bacteriocin	
	9	NRPS	
	10	Phosphonate	
	11	Other	
	12	NRPS-type I PKS-*trans*-AT PKS	Burkholderic acid
	13	Terpene	
	14	PKS-terpene	

Table 1-1. Putative natural product biosynthetic gene clustered predicted in the genome of *B. thailandensis* E264 and compounds actually identified

The table was originally published by Lix, X. *et al*.[82].

CHAPTER 2: The antimicrobial activity of outer membrane vesicles derived from *Burkholderia thailandensis*

Introduction

Bacterial outer membrane vesicles have been documented to play numerous roles including, but not limited to, cargo delivery[126], cell-to-cell communication[127,147], genetic exchange[148], and predation[129,137]. Because of their versatility, the secretory contents of OMVs can respond to the bacterial growth environment such as nutrient availability, waste product concentration, population density and other related factors[149]. To enhances OMV production, stress-inducing conditions including iron depletion[150], oxidative stress[151], temperature stress[125], and chemical supplementation[125], are frequently used. However, the OMV contents under these conditions are difficult to control especially when they induce accumulation and aggregation of misfolded proteins in the bacterial periplasm. In the current study, OMVs were cultivated in nutrient-rich broth and harvested at late-log, early-stationary phase (**Figure 2-1**) when vesiculation more frequently occurs[152].

Precipitation and ultrafiltration are the most commonly used techniques for OMV isolation (**Figure 2-1**). Frequently employed in protein purification, addition of high concentration of a salt into a solution perturbs the hydrogen bonds and surface charges of proteins and OMVs, leads to their aggregation. This process is usually followed by centrifugation separating the precipitated proteins and OMVs from soluble contaminants. For this purpose, ammonium sulfate is commonly used for its high solubility, adequate ionic strength, and the ability to prevent microbial contamination during the incubation. Previous studies have shown that the concentration of ammonium sulfate must be

determined carefully in order to prevent the enrichment of non-OMV-associated proteins and the non-specific binding of free extracellular proteins to OMVs[153,154]. For instance, in *P. aeruginosa* the ammonium sulfate precipitation increases the amount of secreted protease which subsequently degrades OMV proteins[155]. Ultrafiltration is achieved by passing bacterial supernatant through a membrane with a given molecular cut-off. In the current study, a polyethersulfone (PES) membrane with a cut-off of 100 kDa was used with a tangential flow filtration (TFF) system to remove non-OMV-associated proteins. The TFF system allows the solution to flow through the device under gentle pressure in a parallel direction to the membrane, protecting it from clogging[149]. Moreover, it gives the option of buffer exchange separating the OMVs from the growth medium, which facilitates the following purification process.

Since neither precipitation nor ultrafiltration separates OMVs from other bacterial components like flagella, pili, and protein aggregates, further purification steps are necessary for pure OMV preparations (**Figure 2-1**). Density-gradient centrifugation is commonly used for small-scale OMV purifications[121,154]. Compared to bacterial flagella, pili, and protein aggregates, OMVs have a lower density due to their lipid content. In the current study, crude OMVs are suspended with high-density sucrose solution and overlaid with step gradients of low-density sucrose solutions. During centrifugation, OMVs migrate and equilibrate into sucrose layers with similar density. The final preparations of OMVs are further extracted from these sucrose fractions by ultracentrifugation. Although OMVs purified with density-gradient centrifugation usually show great purity, the yield is limited by the volume of centrifuge bottles. Additionally, OMVs are prone to aggregation under these purification conditions. Alternatively, gel filtration chromatography has been shown

to yield OMVs with high purity and size homogeneity[156]. Specifically, size exclusion chromatography (SEC) separate OMVs from other contaminants based on their size difference, which can be optimized with choice of resin and column sizes. In most cases, vesicles with larger sizes than the resin's pores travel quicker along the column and elute first, right after the column's void volume[157]. Although less commonly used in bacterial membrane vesicle purifications, ion exchange chromatography and other affinity chromatography are used for extracellular vesicle purification from mammalian cell cultures and biological samples[158]. Compared to the density-gradient centrifugation method, gel filtration chromatography can be more easily scaled up for mass production and manufacturing[157].

In the current study, the ultracentrifugation method with ammonium sulfate precipitation and density-gradient centrifugation was previously developed and optimized by our laboratory[159,160]. OMVs were predominantly purified by this method for their superior purity. To rule out the possibility that the antimicrobial properties of OMVs were purification method-dependent, OMVs were also concentrated with ultrafiltration and purified with SEC prior to testing.

Nearly two decades ago, OMVs from *P. aeruginosa* were shown to possess antimicrobial activity against *E. coli* and *S. arueus*[129]. Of fifteen bacterial strains examined, *P. aeruginosa* produced OMVs with the broadest antimicrobial activity[133]. Given its relatedness to *P. aeruginosa*, we hypothesized that *B. thailandensis* produces OMVs with antimicrobial activity. Due to the significant problem caused by antimicrobial resistance, *B. thailandensis* OMVs were screened for their antimicrobial activity against Gram-negative bacteria, *A. baumannii*, *P. aeruginosa*, *Enterobacteriaceae* including *E. coli*, and

Klebsiella pneumoniae, Gram-positive bacteria, *S. aureus*, *Enterococcus faecalis*, and *S. mutans*. They were further evaluated against drug-resistant bacterial strains including MDR *A. baumannii*, MRSA, carbapenem-resistant *K. pneumoniae*, and the fungal pathogens, *C. albicans* and *C. neoformans.*

Materials and Methods

Bacterial strains and growth conditions

Burkholderia thailandensis E264, *Burkholderia pseudomallei* Bp82, *Acinetobacter baumannii,* multidrug-resistant *Acinetobacter baumannii, Pseudomonas aeruginosa* PAO1, *Staphylococcus aureus* ATCC 6538*,* methicillin-resistant *Staphylococcus aureus* ATCC 43300, *Enterococcus faecalis* ATCC 29212*, Escherichia coli* ATCC 25922*, Klebsiella pneumoniae* ATCC 1706, carbapenem-resistant *Klebsiella pneumoniae* ATCC 1705, *Streptococcus mutans* UA159, *Cryptococcus neoformans* and *Candida albicans* ATCC 14053 were maintained in lysogeny broth (LB) or brain heart infusion broth (BHI), while solid medium was made by adding 1.5% (wt/vol) agar. All bacterial cultures were incubated at 37 ºC with 233 rpm oscillation. *S. mutans* cultures and plates were maintained at 37 °C in an aerobic chamber containing 5% CO_2 under static conditions. Drug-sensitive and multidrug-resistant (MDR) *A. baumannii* strains and *C. neoformans* we used for current study were isolated from Tulane hospital. The MDR strain was resistant to all the antibiotic tested (**Table 2-1**).

OMV purification with ultracentrifugation

OMVs were prepared as previously described[159,160]. Briefly, bacteria were grown in LB at 37 ºC until late-log phase (18 hours). The intact bacteria were pelleted by centrifugation (Thermo Scientific, Sorvall RC5C plus) at 6,000 x g for 60 minutes at 4 ºC, and the supernatant was removed and filtered through a 0.22 μm polyethersulfone (PES) filter (Millipore) in order to remove any remaining bacteria or large bacterial fragments. To ensure the supernatant was free of viable bacteria, one milliliter of filtered supernatant was streaked onto Pseudomonas isolation agar (BD) and incubated for 48 hours at 37 ºC. The OMVs were precipitated by slowly adding 1.5 M solid ammonium sulfate while stirring gently and incubated overnight at 4 ºC before harvested by centrifugation at 11,000 x g for 45 minutes at 4 ºC. The resulting pellet, consisting of crude vesicles, was resuspended with 60% sucrose in 30 mM Tris-HCl pH 8.0 (wt/vol), which was filter sterilized through a 0.22 μm PES filter and layered at the bottom of a centrifuge tube. A sucrose gradient was prepared by slowly layering 55%, 50%, 45%, 40%, and 35% sucrose in 30 mM Tris-HCl pH 8.0 over the crude OMV preparation. The sucrose gradient with crude OMVs was ultracentrifuged (Beckman Coulter, Optima XL-100K) at 200,000 x g for 3 hours at 4 ºC. Equal 3 mL fractions were removed sequentially from the top and stored at 4 ºC. To determine the purity of the fraction, 200 μL of each was precipitated with 20% Tri-chloroacetic acid (TCA). The resulting protein pellets were run on an SDS-PAGE gel (4-20%, Bio-Rad). The final OMV preparation was recovered by pooling the purest fractions in 30 mM Tris-HCl pH 8.0 followed by centrifugation at 200,000 x g for 19 hours at 4 ºC. The resulting pellet, containing OMVs, was resuspended in Hyclone™ sterile cell culture water (GE LifeSciences) and quantified using a Bradford Protein Assay (Bio-Rad).

Transmission electron microscopy

To visually confirm the presence and purity of purified OMVs, one microgram OMVs were loaded on copper grid (Electron Microscopy Sciences) and stained with 1% uranyl acetate (Electron Microscopy Sciences) before imaging with a FEI G^2 F30 Tecnai transmission electron microscope.

Gel electrophoresis

After OMV purification, five micrograms of OMVs were 1:1 mixed with 2x Laemmli loading buffer (Bio-Rad) containing 100 mM dithiothreitol (DTT), boiled for 10 min and loaded onto an SDS-PAGE polyacrylamide gel (4-20%, Bio-Rad) running at 200 V. The gel was further stained with Coomassie Blue (Sigma-Aldrich) or silver (GBiosciences) to visualize the protein patterns.

HPLC analysis

B. thailandensis OMVs (100 μg) purified with equilibrium density-gradient ultracentrifugation were first extracted with MeOH/$CHCl_3$ mix (1:2, v/v) at 45 ºC until complete separation for three times. The extracts from organic phase was then resuspended with MeOH and separated with HPLC. The HPLC (Shimadzu) was carried out on with a UV-Fluorescence detector and an automated fraction collector. A C2 column (250/4.6 Nucleosil 100-7, Macherey-Nagel) was used with a flow of 0.5 mL/min and a gradient of 5% MeOH in H_2O to 100% MeOH (with 50 mM NH_4OAc, pH 5.6) over 80 mins. The injection volume was 70 μL. The elution started with 5% MeOH isocratic for 5 min, from 5 to 10 min a linear increase from 5 to 45% MeOH was applied, followed by a second

linear increase from 45% to 100% MeOH (10 to 55 min). An isocratic step (100% MeOH) was then maintained for 10 min and ended with a return to 5% MeOH in 2 min. The re-equilibration was done with 5% MeOH isocratic for 13 min. The spectra were detected at UV 214 nm.

Liposome preparation

To make liposomes with a diameter of 100 nm containing small molecule dye, four milliliter phosphatidylcholine (POPC) at a concentration of 50 mM in chloroform was added into a 20 ml glass vial and dried in a vacuum overnight. The lipids were then resuspended with a solution of ANTS/DPX dye (5 mM HEPES, 20 mM NaCl, 12.5 mM ANTS, 45 mM DPX, in 5 mL MilliQ H_2O). To hydrate and incorporate them into vesicles, the lipids solution was frozen with liquid nitrogen and warmed with tap water for 10 cycles. To make uniform liposomes, the ANTS/DPX vesicles were extruded 10 times in an extruder with one 100 nm nitrocellulose polycarbonate filter (Whatman).

OMV purification with size exclusion chromatography

Bacteria were grown in LB at 37 ºC until late-log-phase (18 hours). The intact bacteria were pelleted by centrifugation (Thermo Scientific, Sorvall RC5C plus) at 6,000 x g for 60 minutes at 4 ºC, and the supernatant was removed and filtered through a 0.22 μm PES filter (Millipore) in order to remove any remaining bacteria or large bacterial fragments. Two liters of the sterile supernatant was concentrated with a Pellicon XL Cassette filter (PES, 100 kDa cutoff, Millipore) in a tangential flow filtration system (TFF) to about 15 mL. The concentrated supernatant was then centrifuged at 10,000 x g for 15

min with a SA-600 rotor to remove clustered materials and prevent potential clotting in the chromatography.

To prepare the column, five grams of Sephadex G-200 resin was hydrated with 200 mL 10 mM Tris-HCl (pH 7.5) for three days and filled in the column with 2.5 cm diameter and 30 cm length. After the column was packed, Tris-HCl buffer (10 mM) was run overnight through the column with a flow rate of 0.4 mL/min to further pack the resin. Five-milliliter sample was injected onto the column for each run and eluted with 10 mM Tris-HCl at a flow rate of 0.4 mL/min. The spectra were detected at UV 280 nm for the presence of proteins. Five-milliliter fractions were collected for further characterization.

Bacterial susceptibility assays

The antimicrobial activity of OMVs was evaluated with a Kirby Bauer-like method. For ultracentrifugation-purified OMVs, a fresh culture of microorganism was streaked heavily onto an agar plate, and 10 μg OMVs (adjusted in 10 μL with PBS) from each preparation were applied compared with 10 μL PBS as negative control. The plate was incubated at room temperature for up to 48 hours at which time the plates were examined for antimicrobial activity.

For OMVs and other fractions eluted from SEC, materials from representative fractions (400 μL) were extracted with MeOH/$CHCl_3$ mix (1:2, v/v). Both aqueous (left) and organic (right) phases were desiccated under vacuum before resuspended with 20% MeOH and spotted on plates spread with MRSA.

Microorganism growth inhibitions assay

The ability of OMVs to inhibit the growth of representative microorganism was examined by this assay. Microorganism was cultured overnight in 5 mL LB or BHI broth at 37 ºC. The suspension was further 1:1000 diluted in nutrient broth and added into a 96-well plate (Costar) at 80 μL/well followed by treatments with 20 μL of PBS or OMVs. Optical density at 600 nm was monitored until the culture reached plateau.

Statistics

The Chi squared test was applied to compare two curves, which measures the deviations between a measured and an expected value, divided by the uncertainty.

Results

Production and characterization of B. thailandensis OMVs isolated with ammonium sulfate precipitation and purified with equilibrium density-gradient ultracentrifugation

B. thailandensis OMVs used in the current study were predominantly isolated with ammonium sulfate precipitation and purified using equilibrium density-gradient ultracentrifugation. Experiments and statistics are based on four independent preparations. Purified OMVs ranged in size from 20 to 50 nm and were free of contaminants (**Figure 2-2**). As demonstrated by SDS-PAGE and HPLC, independent batches of OMVs isolated under identical growth conditions demonstrate consistent and reproducible compositions (**Figure 2-3)**. To determine if purified OMVs possessed antimicrobial activity, 10 μL of OMVs were spot-plated onto MRSA-streaked agar plates. Inhibition of MRSA growth was observed at the site of OMV delivery for all preparations (**Figure 2-4**).

Method development and characterization of OMVs isolated with ultrafiltration and purified with size exclusion chromatography

To exclude the possibility that the antimicrobial activity of *B. thailandensis* OMVs were method-dependent, OMVs were further isolated with ultrafiltration and purified with SEC (**Figure 2-5**). We first validated this method by separating liposomes (100 nm) from small molecule dye that were mixed with them. Large-sized liposomes were eluted within the void volume before the elution of other small molecule contaminants (**Figure 2-5A**). For OMV purification with SEC, bacterial supernatant was first concentrated with TFF system and centrifuged to remove the clustered materials before separated on the column. OMVs from *B. thailandensis* and *B. pseudomallei* with sizes range from 20 to 200 nm were eluted within the void volume at similar elution time of the liposomes (**Figure 2-5A**). In additions, the chromatography successfully separated the OMVs from the proteins and small molecules secreted in the supernatant (**Figure 2-5A**). Five-milliliter fractions were collected from the *B. thailandensis* OMV purification, and representative fractions as shown in **Figure 2-5B** were further characterized for their physical appearance, protein composition, and antimicrobial activity.

Electron microscopy revealed the sizes of SEC-purified OMVs ranging from 20 to 100 nm. The purified OMVs were relative pure with some pili contamination (**Figure 2-6**). Proteins from fraction 13, 15, 20, 29, 39 (20 μL each) were separated with SDS-PAGE and visualized with silver staining. Protein patterns of F13 and F15 showed a wide range of molecular weights suggesting these fractions contain materials in forms of complexes, such as OMVs. From F20 to F29, the molecular weights of proteins went down, whereas F39 showed no protein on the gel, which suggests the successful separation with SEC

(**Figure 2-7A**). In addition, crude OMVs concentrated with TFF (TFF) and ammonium sulfate precipitation (AS) showed similar protein compositions with more proteins less than 37 kDa compared to ultracentrifugation-purified OMVs (UO) and SEC-purified OMVs (F13, F15) (**Figure 2-7A**). The antimicrobial activity of OMVs (F13,16) and representative fractions (F20, 29, 39, 43) from SEC was examined against MRSA. To further characterize their chemical properties, materials in these fractions were extracted with organic solvent. Both aqueous and organic phases were concentrated and tested for their antimicrobial activity. For OMV fractions (F13,16), the majority of the antimicrobial activity was retained in the organic phase, whereas the antimicrobial molecules in F39 were more likely to partition in aqueous phase suggesting their relative hydrophilic propensity (**Figure 2-7B**). Thus, we showed here *B. thailandensis* OMVs purified with both ultracentrifugation method and chromatography method exhibited antimicrobial activity against MRSA.

Evaluation of the antimicrobial activity of B. thailandensis OMVs against representative Gram-negative and -positive bacteria, multidrug-resistant bacteria, and fungi

Next, we examined the spectrum of OMV antimicrobial activity by screening for growth inhibition of additional bacterial and fungal species of clinical importance. Among Gram-negative bacteria, OMVs inhibited the growth of *A. baumannii*, but not *P. aeruginosa*, *E. coli*, or *K. pneumoniae* (**Figure 2-8A-D**). Notably, *Burkholderia spp*. are closely related to *Pseudomonas spp.* which potentially explains why *B. thailandensis* OMVs did not inhibit the growth of *P. aeruginosa*. OMVs also inhibited the growth of Gram-positive bacteria, *S. aureus*, *S. mutans*, but not *E. faecalis* (**Figure 2-8E-G**). Further

screening indicated the antimicrobial activity of OMVs against a MDR clinical isolate of *A. baumannii*, MRSA, and the fungal pathogens *C. albicans* and *C. neoformans*, but not carbapenem-resistant *K. pneumoniae* (**Figure 2-9**).

To confirm our observations, OMV inhibitory activity was also evaluated using planktonic cultures of each organism. Again, OMVs inhibited the growth of *A. baumannii*, MDR *A. baumannii*, *S. aureus*, MRSA, *S. mutans*, *C. albicans*, and *C. neoformans* (**Figure 2-10, 2-11**). Furthermore, the inhibitory activity of OMVs against each organism was shown to be dose-dependent (**Figure 2-10, 2-11**). The MDR *A. baumannii* strain we used in the current study was isolated from Tulane hospital and was resistant to all the antibiotics tested (**Table 2-1**). Taken together, these results indicate that *B. thailandensis* OMVs inhibits both drug-sensitive and MDR microbial species.

Discussion

We have demonstrated here that OMVs purified with ultracentrifugation display great consistency in their physical appearance and chemical composition with no visible flagella or pili contamination revealed by electron microscopy. Size exclusion chromatography successfully separated OMVs from other soluble contaminants. However, further optimization is necessary to separate OMVs from bacterial pili when using SEC. Gel electrophoresis demonstrated considerable similarity of protein composition between ultracentrifugation-purified and chromatography-purified OMVs. Importantly, both methods isolated OMVs with antimicrobial activity against MRSA.

When screened against representative Gram-negative and Gram-positive bacteria, drug-resistant bacteria, and fungi, OMVs inhibit their growth implying specific

mechanisms of action against some but not all microbes. On agar plates and in planktonic cultures, OMVs significantly inhibited the growth of *A. baumannii*, *S. aureus*, and *S. mutans*, but had no effect on the growth of *K. pneumoniae* and *E. faecalis*. Seemingly, OMVs promoted the growth of *P. aeruginosa* and *E. coli*. However, the increased optical density was potentially caused by materials secreted in the cultures by the bacteria when treated with OMVs, especially in the case of *E. coli* when the growth was initially inhibited. Additionally, OMVs exhibited antimicrobial activity against a clinical isolate of *A. baumannii* that was resistant to multiple classes of antibiotics. According to the Centers for Disease Control, MDR *A. baumannii* strains have the potential to resist all clinically approved antibiotics including colistin[5]. OMVs derived from *B. thailandensis* could represent a source of new antibacterial agents that are effective against MDR species. Lastly, OMVs showed potent antifungal activity against *C. neoformans*, but slightly inhibited the growth of *C. albicans*. Different from other microbes inhibited by the OMVs, *C. neoformans* is well characterized for its thick polysaccharide capsule surrounding the cell body[161]. How the OMVs interact with Cryptococcal cells and penetrate the polysaccharide capsule remain unknown.

It has been shown that to initiate the killing OMVs first associate with the targeted bacteria through salt-bridge and deliver the killing materials directly onto Gram-positive bacteria or intermingle and fuse with the outer membrane of Gram-negative bacteria (**Figure 2-12**)[129]. This enables the delivery of concentrated cargos into the periplasm of the targeted cells where they can better access the cell wall or further diffuse into the cytoplasm. In this way, OMVs can be seen as something of a “Trojan Horse” where they

deliver soldiers past the bacterial outer membrane barrier and directly into the part of the bacteria where they can do the most damage.

Compared to biological nanoparticles like liposomes, OMVs have many advantages in terms of lipid composition and cargo packaging. Studies characterizing phospholipids in *P.* aeruginosa OMVs showed a higher membrane rigidity of the vesicles compared to their outer membrane, which makes them more resistant to environmental pertubation[120]. It has been demonstrated that bacteria protects secretory cargos from degradation through directed packaging into OMVs[128]. Protein cargos within OMVs are relatively stable at room temperature and resistant to freeze-thaw cycles, which makes them ideal for lyophilization and storage[128].

In future studies, it will be interesting to test *B. thailandensis* OMVs against agricultural pathogens since *B. thailandensis* inhabits ecological niches primarily composed of soil, plant surfaces, and rhizospheres. The antibiofilm activity of OMVs against representative bacteria will be characterized in the next chapter.

Figure 2-1

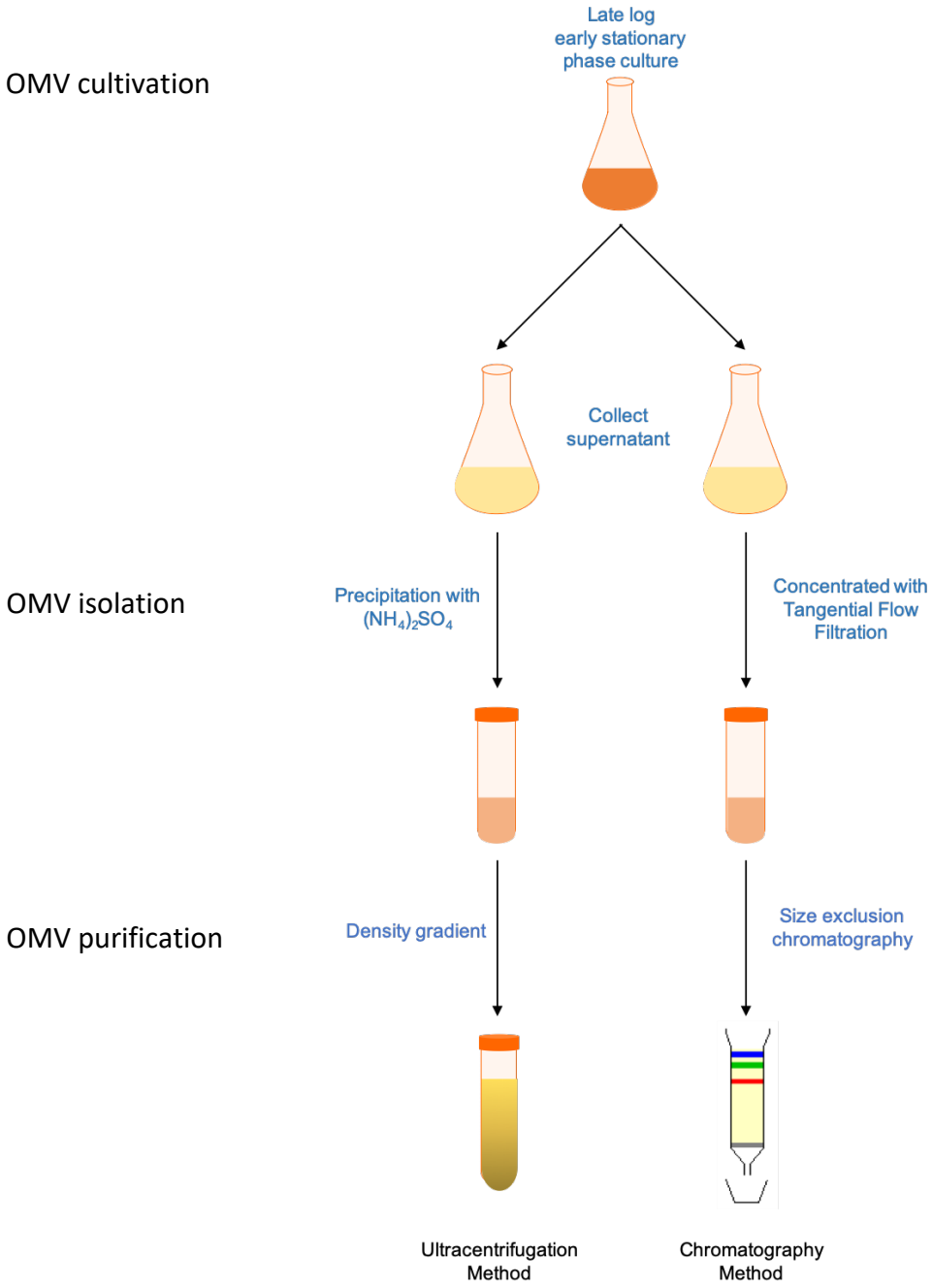
OMV cultivation
OMV isolation
OMV purification
Late log
early stationary
phase culture
Collect
supernatant
Precipitation with
$(NH_4)_2SO_4$
Concentrated with
Tangential Flow
Filtration
Density gradient
Size exclusion
chromatography
Ultracentrifugation
Method
Chromatography
Method

Figure 2-1. Illustration of outer membrane vesicle purification methods

Ultracentrifugation method (left): OMVs isolated with ammonium sulfate precipitation and purified with density-gradient ultracentrifugation. The crude vesicles were first harvested by precipitating the supernatant of bacteria culture with a high concentration of ammonium sulfate. To separate the OMVs from bacterial cell debris and other secretory proteins, the precipitated crude vesicles were subjected for sucrose density-gradient purification based on vesicle density. The final OMV preparation was recovered by pooling the purest fractions by ultracentrifugation. Chromatography method (right): OMVs was isolated by ultrafiltration and purified with size exclusion chromatography. The crude vesicles were first concentrated from the supernatant of bacteria culture by tangential flow filtration with a cut off of 100 kDa. The cell debris and clustered secretory proteins were pelleted at 10,000 x g for 15 minutes. OMVs within the supernatant were separated from the unpelleted components with size exclusion chromatography.

Figure 2-2

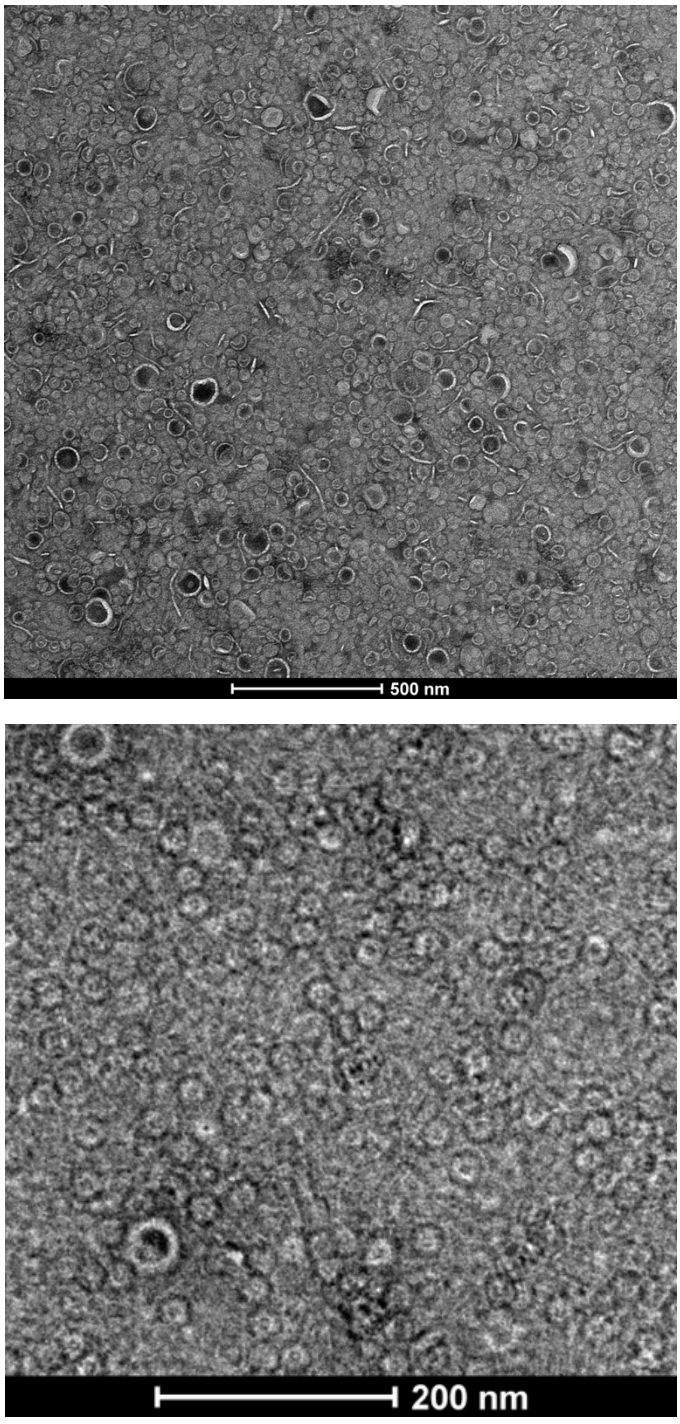

Figure 2-2. TEM image of ultracentrifugation-purified *B. thailandensis* OMVs

Purified OMVs were negatively stained with 1% uranyl acetate and visualized by transmission electron microscopy. Size of OMVs purified with ultracentrifugation ranges from 20 to 100 nm.

Figure 2-3

A

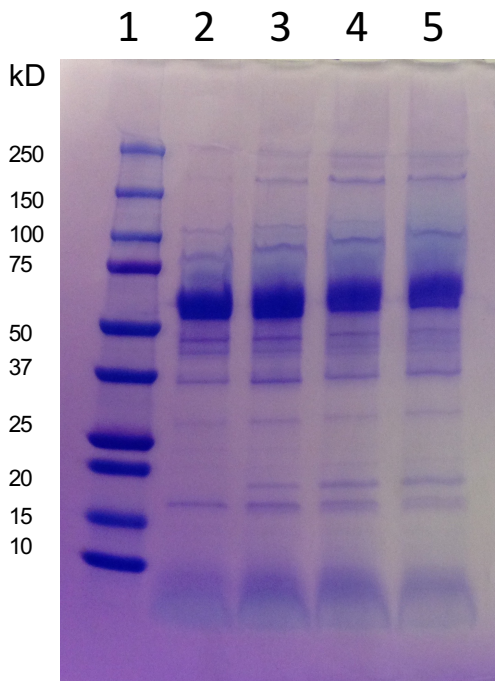
1 2 3 4 5
kD
250
150
100
75
50
37
25
20
15
10

B

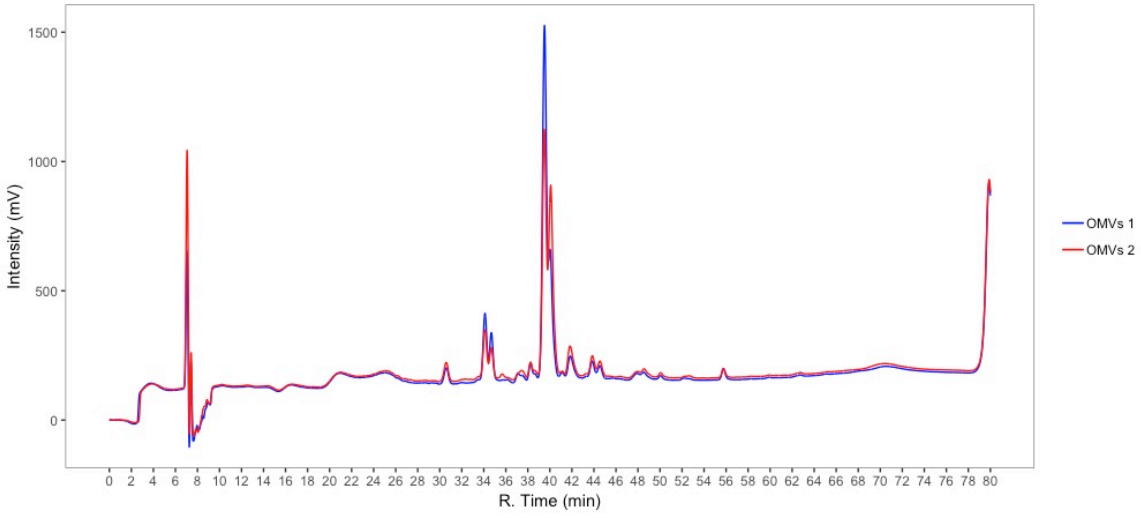
Intensity (mV)
1500
1000
500
0
0 2 4 6 8 10 12 14 16 18 20 22 24 26 28 30 32 34 36 38 40 42 44 46 48 50 52 54 56 58 60 62 64 66 68 70 72 74 76 78 80
R. Time (min)
OMVs 1
OMVs 2

Figure 2-3. OMVs purified with ultracentrifugation method demonstrate consistency in composition

(**A**) Protein composition of OMVs is consistent across four independent preparations as demonstrated by SDS-PAGE and Coomassie stain. Protein molecular weight ladder (lane 1), 5 μg purified OMVs (lanes 2-5). (**B**) Reproducibility of two independent preparations of purified OMVs extracted with organic solvent, subjected to HPLC, and detected at UV 214 nm.

Figure 2-4

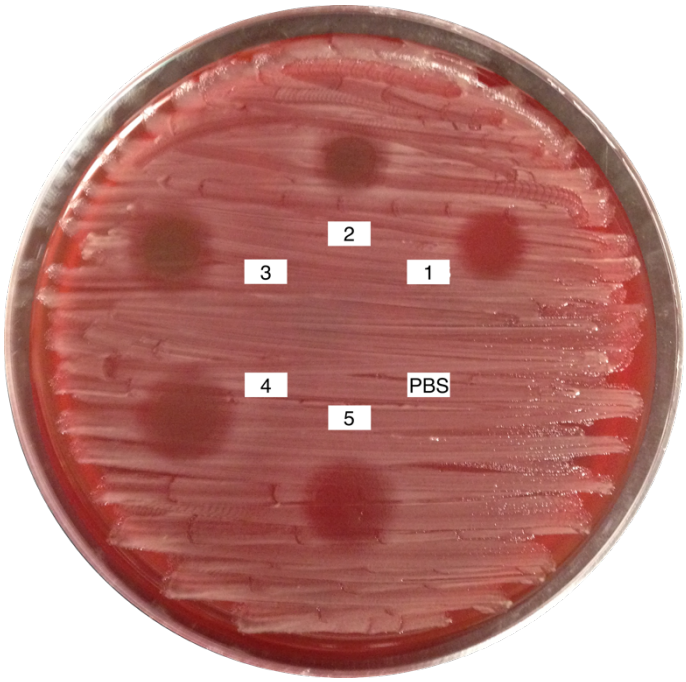

Figure 2-4. OMVs purified with ultracentrifugation method demonstrate consistency in antimicrobial activity

Antimicrobial activity of purified OMVs from four independent preparations was evaluated against MRSA (spots 1-5, 10 μg OMVs in 10 μL PBS) versus negative control, PBS (10 μL).

Figure 2-5

A

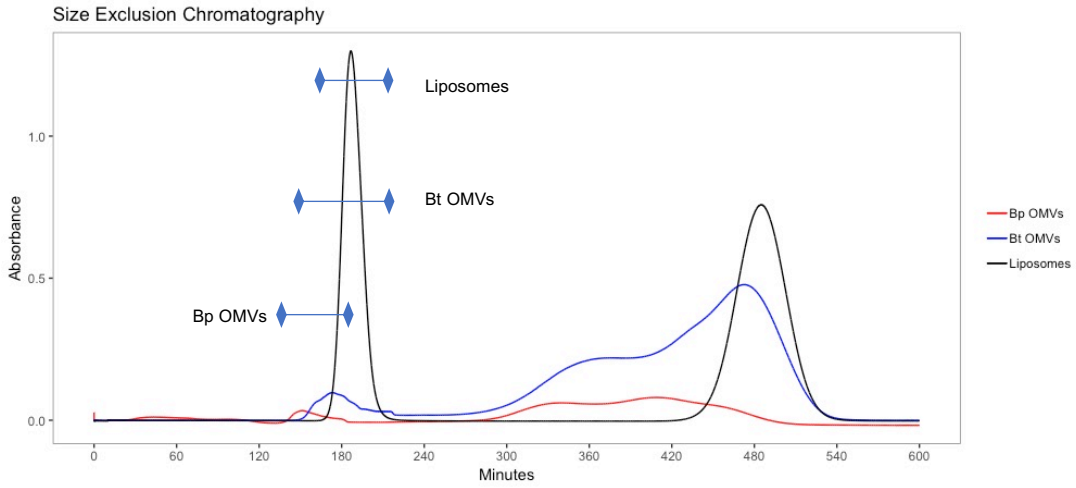
Size Exclusion Chromatography
Liposomes
Bt OMVs
Bp OMVs
Absorbance
Minutes
Bp OMVs
Bt OMVs
Liposomes

B

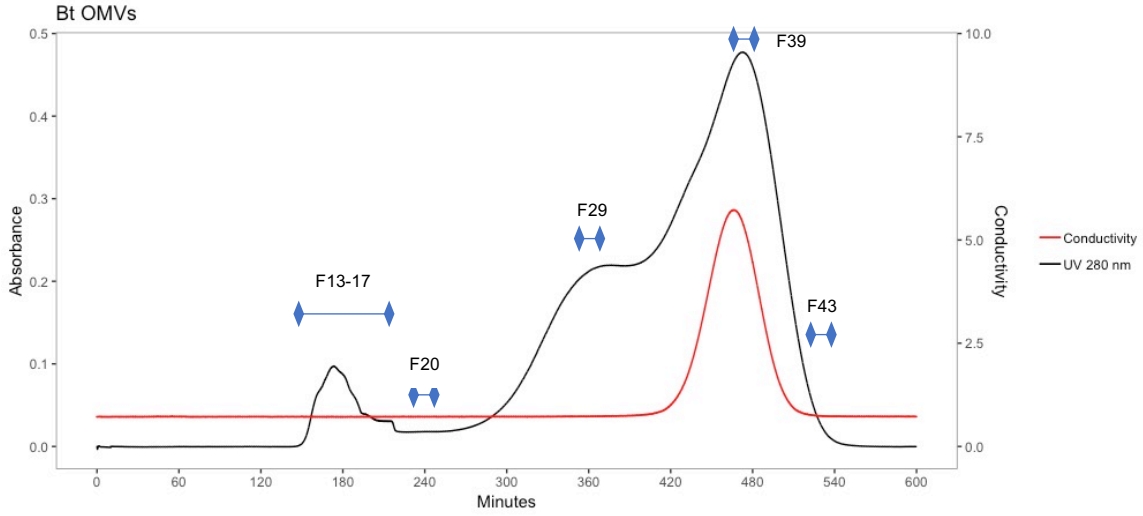
Bt OMVs
F39
F29
F13-17
F20
F43
Absorbance
Conductivity
Minutes
Conductivity
UV 280 nm

Figure 2-5. Representative size exclusion chromatography spectra for liposome and OMV purification

(**A**) Overlapping spectra of liposomes (100 nm), *B. thailandensis* (Bt) OMVs, and *B. pseudomallei* (Bp) OMVs purified with SEC. Bacterial supernatant concentrated with TFF system were centrifuged at 10,000 x g for 15 mins to remove clustered proteins or cell debris before separating on the column packed with Sephadex G-200). Liposomes and OMVs were eluted with 10 mM Tris-HCl buffer (pH 7.5) at a flow rate of 0.4 mL/min. All vesicles were eluted within void volume. Peaks were detected at UV 280 nm for the presence of proteins within OMVs. (**B**) Representative spectrum of Bt OMVs purified with SEC. Five-milliliter fractions were collected for further characterization.

Figure 2-6

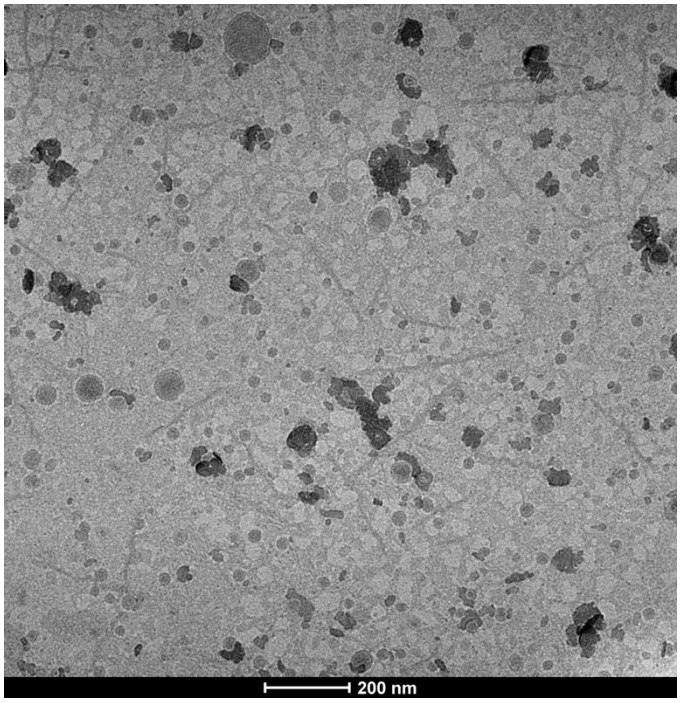

Figure 2-6. TEM image of materials in fraction 13 from size exclusion chromatography

Materials in F13 from SEC OMV purification were stained with 1% uranyl acetate before imaging with transmission electron microscope.

Figure 2-7

A

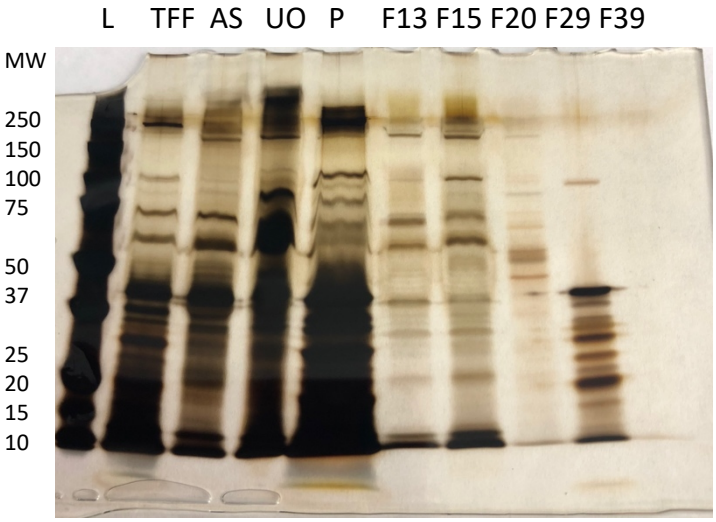
L TFF AS UO P F13 F15 F20 F29 F39
MW
250
150
100
75
50
37
25
20
15
10

B

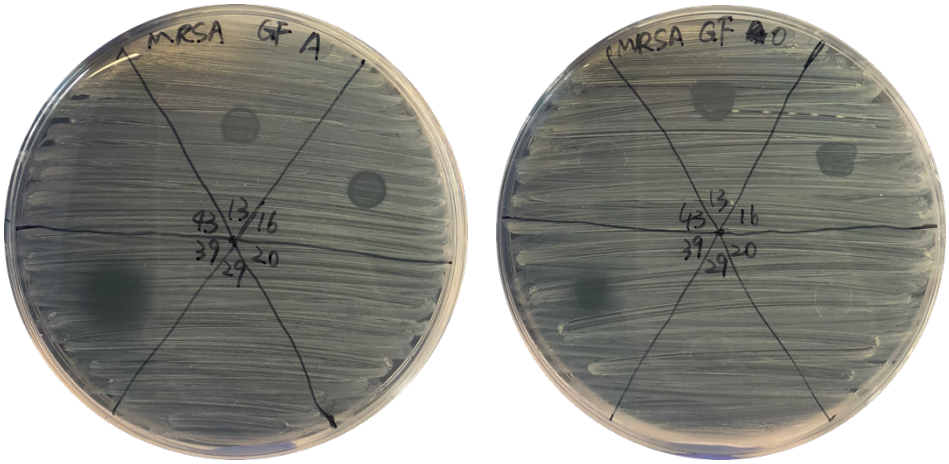
MRSA GF A
MRSA GF

Figure 2-7. Characterization of fractions from size exclusion chromatography for their protein composition and antimicrobial activity

(**A**) Protein composition of fractions eluted from SEC were shown with SDS-PAGE and silver staining. From left to right, L: ladder, TFF: crude OMVs concentrated with TFF system (2.5 μg), AS: crude OMVs purified with ammonium sulfate precipitation (2 μg), UO: OMVs purified with ultracentrifugation method (3 μg), P: pelleted materials from the concentrated TFF crude OMVs (5 μg), F13: 20 μL materials in fraction 13 from the SEC, same for F15, F20, F29, and F39. (**B**) Materials within fractions 13, 16, and 39 showed antimicrobial activity against MRSA. Materials from representative fractions (400 μL) were extracted with MeOH/$CHCl_3$ mix (1:2, v/v). Both aqueous (left) and organic (right) phases were desiccated under vacuum before resuspended with 20% MeOH in H_2O and spotted on plates spread with MRSA. The plates were incubated at room temperature for 24 hours before examining for their antimicrobial activity. Twenty percent MeOH alone did not inhibit MRSA (data not shown).

Figure 2-8

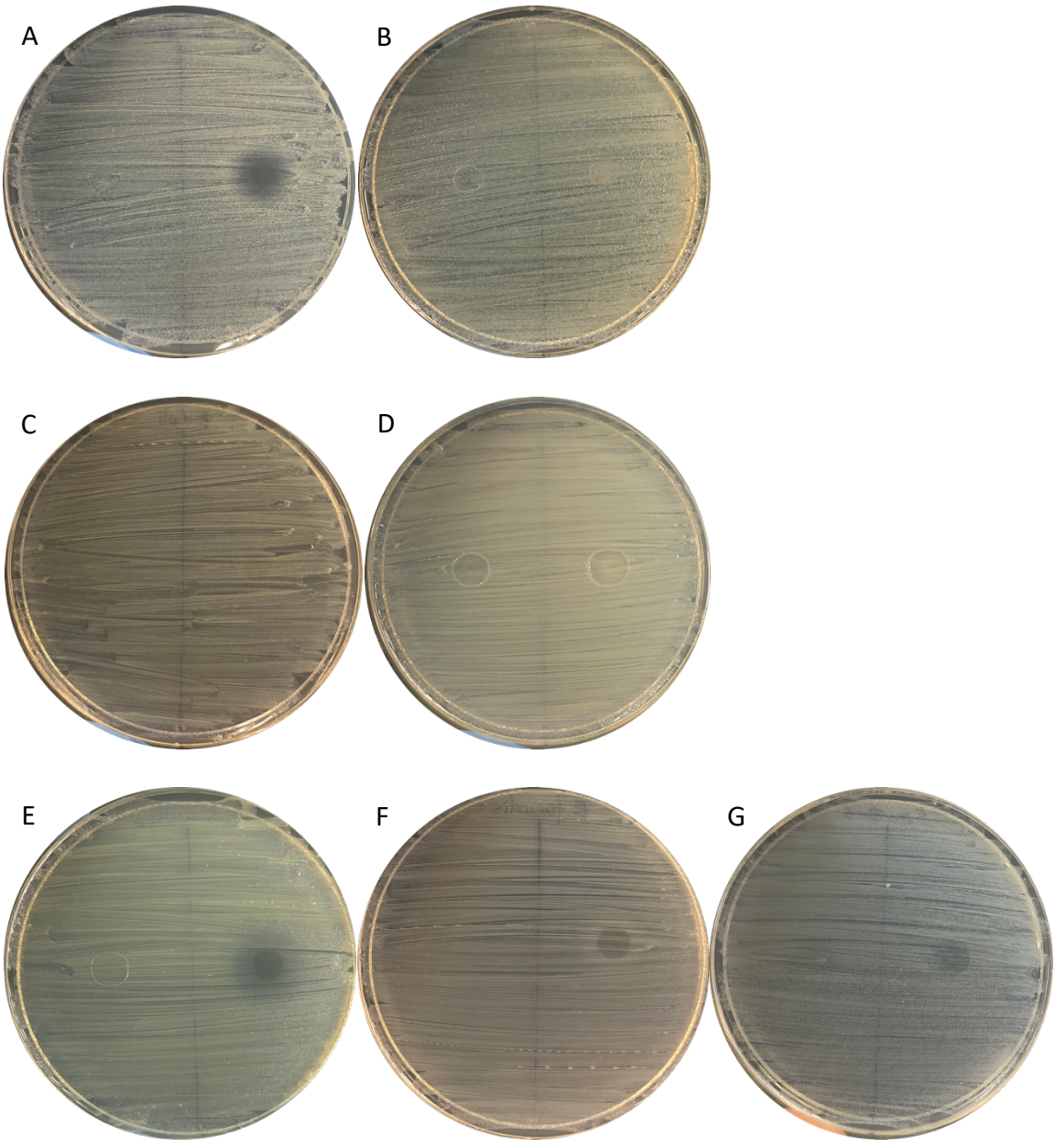

Figure 2-8. The antimicrobial activity of *B. thailandensis* OMVs evaluated against representative Gram-negative and Gram-positive bacteria on agar plates

PBS (left side, 10 μL) or OMVs (right side, 10 μg suspended in 10 μL PBS) were spot plated onto agar streaked with (**A**) *A. baumannii*, (**B**) *P. aeruginosa*, (**C**) *E. coli*, (**D**) *K. pneumoniae*, (**E**) *S. aureus*, (**F**) *E. faecalis*, (**G**) *S. mutans* and incubated for 24 to 48 hours to determine growth inhibition.

Figure 2-9

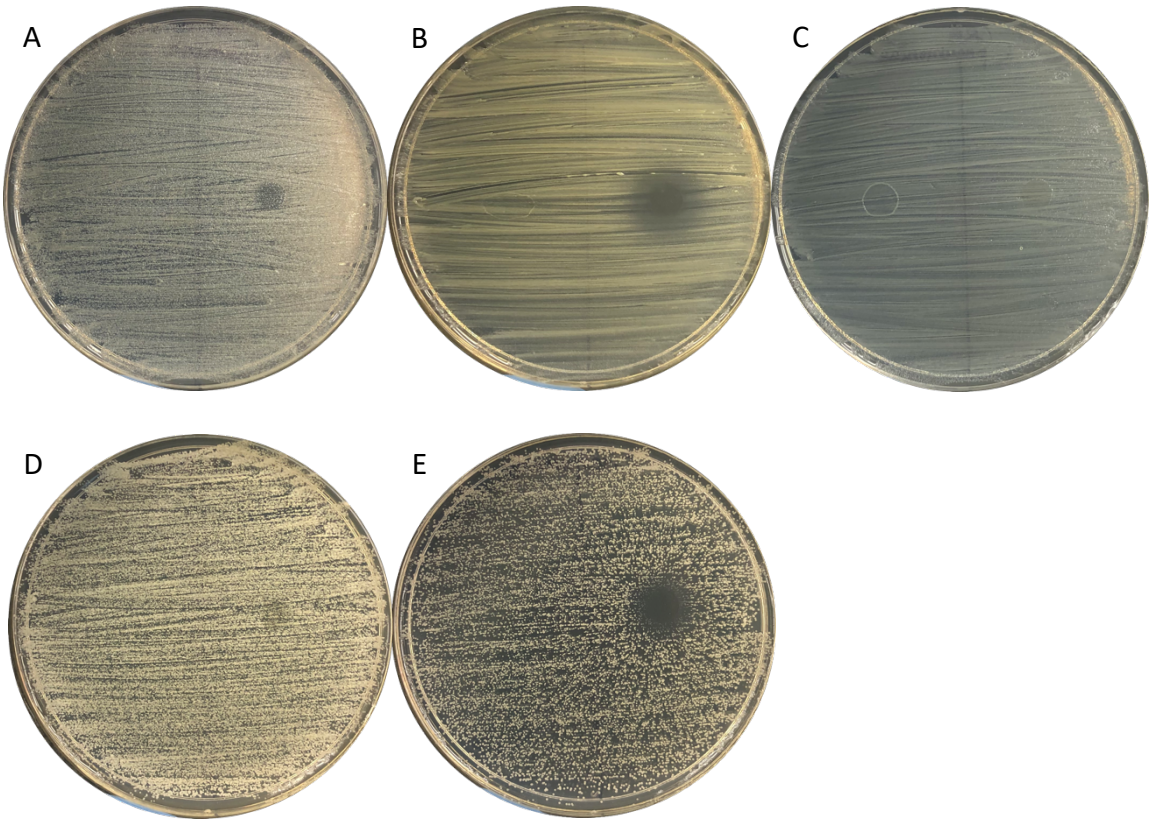

Figure 2-9. The antimicrobial activity of *B. thailandensis* OMVs evaluated against multidrug-resistant bacteria and fungi on agar plates

PBS (left side, 10 μL) or OMVs (right side, 10 μg suspended in 10 μL PBS) were spot plated onto agar streaked with (**A**) MDR *A. baumannii*, (**B**) MRSA, (**C**) carbapenem-resistant *K. pneumoniae*, (**D**) *C. albicans*, (**E**) *C. neoformans* and incubated for 24 to 48 hours to determine growth inhibition.

Figure 2-10

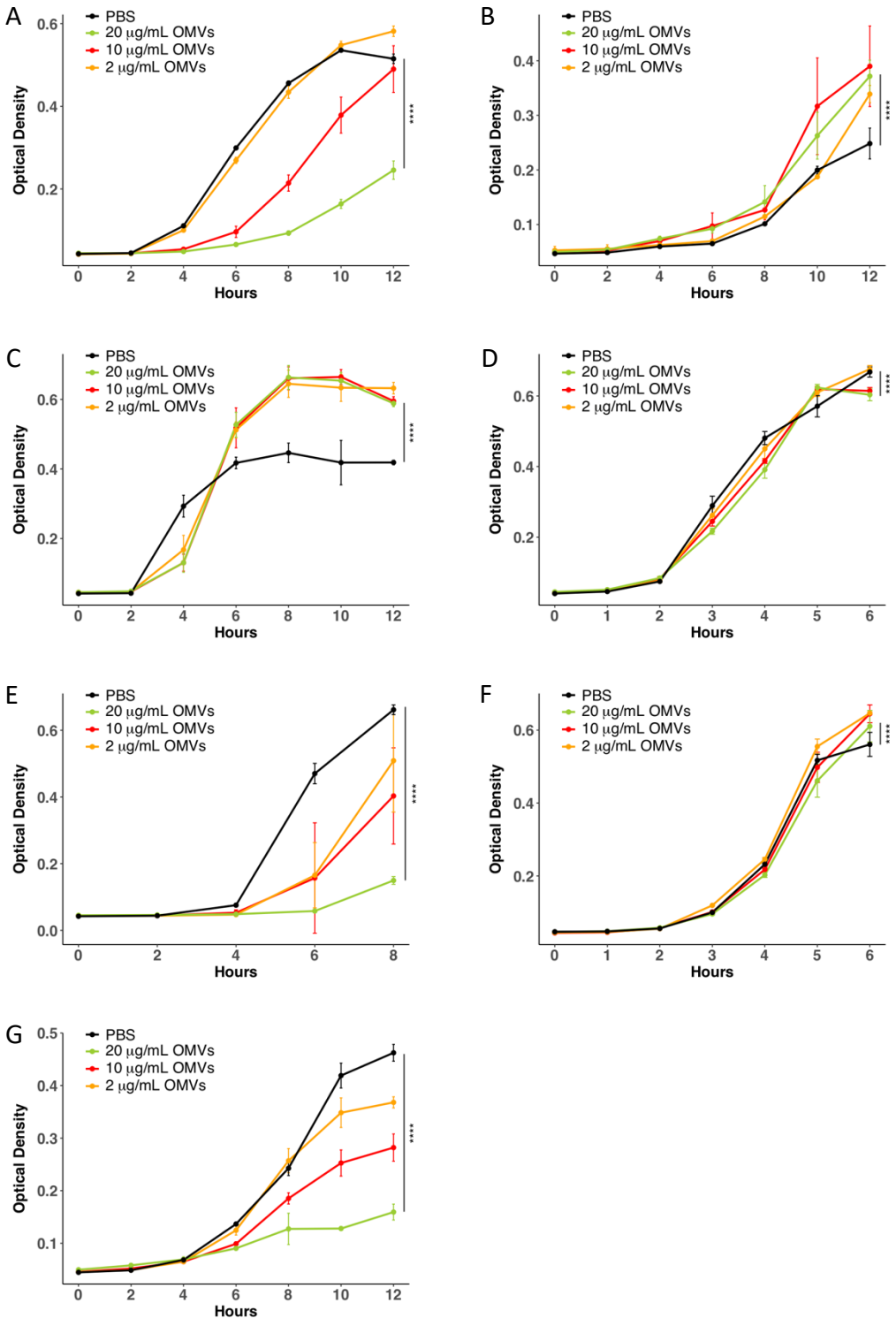
A
B
C
D
E
F
G
PBS
20 μg/mL OMVs
10 μg/mL OMVs
2 μg/mL OMVs
Optical Density
Hours
****

Figure 2-10. Evaluation of *B. thailandensis* OMVs inhibiting microbial growth in planktonic cultures with representative Gram-negative and Gram-positive bacteria

Overnight cultures of (**A**) *A. baumannii*, (**B**) *P. aeruginosa*, (**C**) *E. coli*, (**D**) *K. pneumoniae*, (**E**) *S. aureus*, (**F**) *E. faecalis*, and (**G**) *S. mutans* were diluted 1:1000 in broth and treated with 0.2, 1, or 2 μg OMVs or PBS in a total volume of 100 μL. OD_{600} was monitored for up to 12 hours. The results were analyzed using Chi squared test, **** $p < 0.0001$.

Figure 2-11

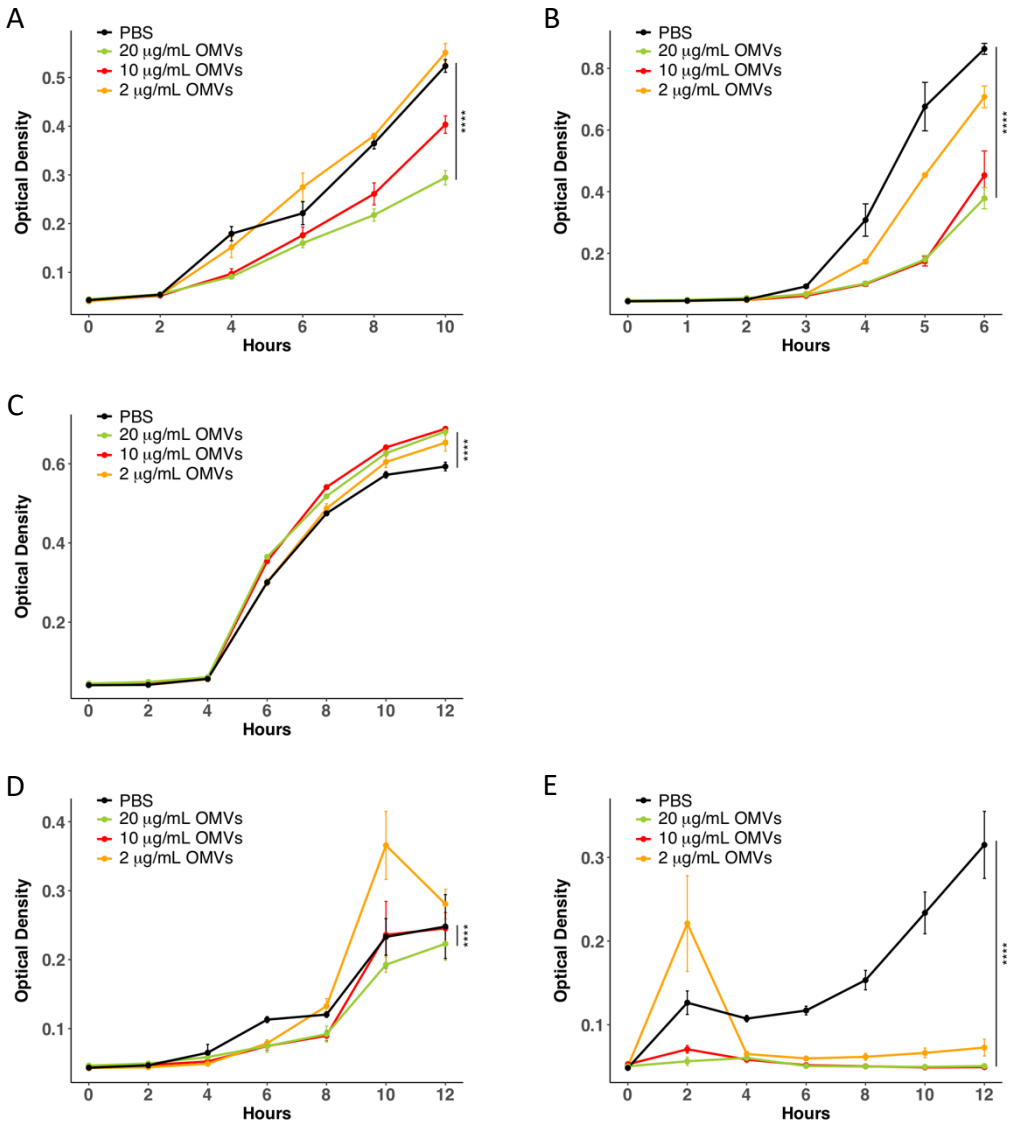
A
PBS
20 μg/mL OMVs
10 μg/mL OMVs
2 μg/mL OMVs
Optical Density
Hours
****
B
PBS
20 μg/mL OMVs
10 μg/mL OMVs
2 μg/mL OMVs
Optical Density
Hours
****
C
PBS
20 μg/mL OMVs
10 μg/mL OMVs
2 μg/mL OMVs
Optical Density
Hours
****
D
PBS
20 μg/mL OMVs
10 μg/mL OMVs
2 μg/mL OMVs
Optical Density
Hours
****
E
PBS
20 μg/mL OMVs
10 μg/mL OMVs
2 μg/mL OMVs
Optical Density
Hours
****

Figure 2-11. Evaluation of *B. thailandensis* OMVs inhibiting microbial growth in planktonic cultures with multidrug-resistant bacteria and fungi

Overnight cultures of (**A**) MDR *A. baumannii*, (**B**) MRSA, (**C**) carbapenem-resistant *K. pneumoniae*, (**D**) *C. albicans*, and (**E**) *C. neoformans* were diluted 1:1000 in broth and treated with 0.2, 1, or 2 μg OMVs or PBS in a total volume of 100 μL. OD_{600} was monitored for up to 12 hours. The results were analyzed using Chi squared test, **** $p < 0.0001$.

Figure 2-12

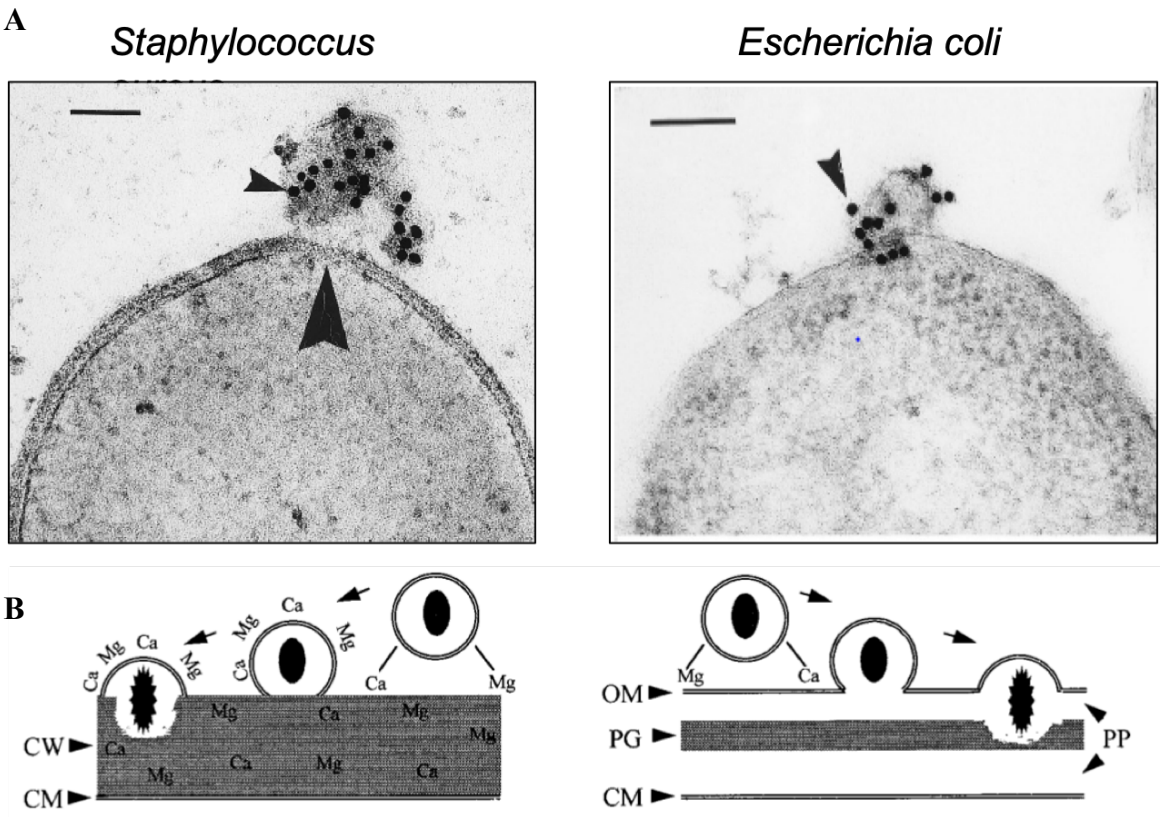

Figure 2-12. Model of OMVs interacting with Gram-positive and Gram-negative surfaces

(**A**) Fusion of *P. aeruginosa* OMVs with *S. aureus* and *E. coli*. Immunogold electron microscopic labelling of thin sections with antibodies to *P. aeruginosa* LPS demonstrates the firm integration of OMVs with bacteria. (**B**) Possible means of OMVs interacting with Gram-positive and -negative bacteria. OMVs initiate the contact with Gram-positive surfaces by forming salt-bridges. OMVs are further broke apart by ion strength followed by releasing contents at the sites of interactions. For Gram-negative bacteria, OMVs would be salt-bridged to the surface and fused into their outer membrane, which will liberate the contents into their periplasm. The image and illustration were originally published by Kadurugamuwa, J. L. *et al*.[129].

Table 2-1

ACINETOBACTER BAUMANNII	M.I.C	RX
AMPICILLIN		
PIPERACILLIN/TAZOBACTAM		
MEROPENEM	>8	R
CEFAZOLIN		
CEFUROXIME		
CETRIAXONE	>32	R
CEFTAZIDIME	>16	R
GENTAMICIN	>8	R
TOBRAMYCIN	>8	R
AMIKACIN	>32	R
CIPROFLOXACIN	>2	R
TRIMETHOPRIM/SULFAMETHOXAOLE	>2/38	R

Table 2-1. Antibiotic susceptibility profile of multidrug-resistant *A. baumannii* isolated from Tulane University Hospital

*Test performed at Tulane University Hospital & Clinic.

CHAPTER 3: The antibiofilm activity of outer membrane vesicles derived from *Burkholderia thailandensis*

Introduction

Biofilms are surface-associated microbial communities surrounded by a complex and highly viscous extracellular polymeric substance (EPS) composed of polysaccharides, proteins, lipids and other microbial-derived materials. The biofilm-forming capacity of microbes greatly contributes to the crisis of antimicrobial resistance. Previous study indicates that bacteria within biofilms are 10- to 1000-fold more resistant to antibiotics making them extremely difficult to eradicate during infections[36]. Biofilms with high microbial density are also natural environments for quorum sensing (QS), cell-to-cell communication processes that enable microbes to modify their behavior within a population according to the changes of the environment[162]. QS involves the production, release, and detection of extracellular signaling molecules. These QS signals play important roles in determining microbial phenotype, regulating virulence, even influencing biofilm constructions and tolerance to antimicrobial treatment[163,164]. OMVs are a ubiquitous and important constituent of Gram-negative and polymicrobial biofilms[131]. Although well documented in cell-to-cell communications, the roles of OMVs in bacterial QS are not well studied. However, it is possible that OMVs play roles in delivering QS signals regulating biofilms formation or dispersal in certain bacterial species. Given the antimicrobial activity of *B. thailandensis* OMVs and their natural occurrence in bacterial biofilms, we hypothesized that OMVs could potentially disrupt biofilms formed by competitor bacteria.

Among the biofilm-forming bacteria we screened OMVs against, *A. baumannii* is notorious for its ability to survive in various environmental conditions[165] and is recognized as a serious problem due to its resistance to almost all known antibiotics[5]. *A. baumannii* is also well known for its ability to form robust biofilms during skin, soft-tissue infections[166] and on most abiotic surfaces during medical-device-associated infections[167].

Enterococci that naturally inhabit the oral cavity, gastrointestinal tract, and female genital tract are common causes of urinary tract infections, endocarditis, catheter-related infections, and surgical wound infections[168]. *E. faecalis* is responsible for over 80 % of human enterococcal infections. It has been reported that 93% of *E. faecalis* strains identified from clinical and fecal isolates produced biofilms[169].

S. aureus is another frequent cause of biofilm-associated infections especially associated with medical devices[170]. In addition, burn or post-operative wounds are also susceptible to biofilm-forming *S. aureus* infections due to its colonization of the skin[171]. Further, previous studies have shown that the biofilm phenotype expressed by *S. aureus* is influenced by acquisition of the methicillin resistance gene *mecA*[170]. While methicillin-sensitive *S. aureus* commonly produce polysaccharide intercellular adhesin (PIA)-dependent biofilms, MRSA mostly form biofilms in a PIA-independent, glucose-dependent manner, releasing extracellular DNA and expressing sortase-anchored proteins and autolysins[170].

Cariogenic plaque is one of the earliest and best-characterized biofilms in the human body. Although well-described in the literature, it is still a neglected topic and major health problem affecting 60-90% of children and most of adults globally[172]. As one of the most cariogenic microorganisms in dental biofilms, *S. mutans* is capable of using dietary

carbohydrates especially sucrose to produce organic acids and generate robust biofilms with glucan-based EPS, which serve as important virulence factors for supporting the microbiologic community on dental surfaces[173,174]. *S. mutans* has been proposed as a novel model Gram-positive organism with the potential to provide a better understanding of the closely related streptococcal and staphylococcal species in terms of biofilm-dependent lifestyle, genetics, and physiological properties[175].

In this chapter, we first screened *B. thailandensis* OMVs against pre-formed biofilms of *A. baumannii, E. faecalis, S. aureus,* and *S. mutans*. The antibiofilm activity of OMVs was then further characterized against the model biofilm-forming pathogens, MRSA and *S. mutans,* in order to further elucidate OMV antibiofilm activities.

Materials and Methods

Bacterial Strains and Growth Conditions

Acinetobacter baumannii clinical isolate, *Enterococcus faecalis* ATCC 29212, *Staphylococcus aureus* ATCC 6538, *Streptococcus mutans* UA159, and methicillin-resistant *Staphylococcus aureus* ATCC 43300 was maintained in lysogeny broth (LB) or brain heart infusion broth (BHI), while solid medium was made by adding 1.5% (wt/vol) agar. Cultures of *A. baumannii*, *S. aureus*, and *E. faecalis* were incubated at 37 °C with 233 rpm oscillation. *S. mutans* cultures were maintained at 37 °C in an aerobic chamber containing 5% CO_2 under static conditions.

96-well Plate Biofilm Assay

Biofilms of *A.* baumannii, *S.* aureus, and *E. faecalis* were cultured in LB or BHI, while *S. mutans* was grown in a semi-defined biofilm medium with glucose (18 mM) and sucrose (2 mM) (BMGS) added as the supplemental carbohydrate sources[176-178]. The biofilm medium contained 58 mM K_2HPO_4, 15 mM KH_2PO_4, 10 mM $(NH_4)_2SO_4$, 35 mM NaCl, 0.0001% (wt/vol) $FeCl_3 \cdot 6H_2O$ and 0.2% (wt/vol) Casamino Acids (pH 7.4), and was supplemented with vitamins (0.04 mM nicotinic acid, 0.1 mM pyridoxine HCl, 0.01 mM pantothenic acid, 1 μM riboflavin, 0.3 μM thiamin HCl, and 0.05 μM D-biotin), amino acids (4 mM L-glutamic acid, 1 mM L-arginine HCl, 1.3 mM L-cysteine HCl, and 0.1 mM L-tryptophan), and 2 mM $MgSO_4 \cdot 7H_2O$. For biofilm formation, flat-bottomed 96-well microtiter plates containing 100 μL culture medium per well were inoculated with individual bacteria and incubated at 37 ºC under static conditions while *S. mutans* was maintained in an aerobic chamber containing 5% CO_2. After 24 hours, the biofilms were treated with 10 μg OMVs or PBS in a total volume of 100 μL for another 24 hours after removing the planktonic cultures from the wells. The biofilms after the treatments were stained with 100 μL 1% crystal violet solution for 15 minutes. Wells were rinsed three times with 200 μL PBS before destained with 30% acetic acid solution. The destained solutions were then transferred to new wells for optical density reading at 550 nm. Experiments were performed in triplicates.

Confocal Laser Scanning Microscopy

MRSA was cultured overnight in BHI and diluted 1:10 in TSB supplemented with 0.5% glucose[179], while *S. mutans* was cultured overnight in BHI and diluted 1:10 in BMGS. Biofilms were cultured on 8-well chambered-slides at 37 °C statically with medium

changed daily. Pre-formed 2-day biofilms of MRSA were then treated with 50, 100 μg/mL OMVs or water for another 4 hours before imaging. Three-day biofilms of *S. mutans* were treated with 10, 50, 100 μg/mL OMVs or PBS for another 24 hours. Biofilms before and after the treatments were stained with LIVE/DEAD *Bac*Light fluorescent dye and imagined. Fluorescent confocal microscopy was performed with a Zeiss LSM 700 microscope. Confocal *z*-stacks and simulated *xyz* three-dimensional images were acquired and generated using Zeiss Zen 10.0 software. More than seven image stacks were acquired from random positions within each well to cover an area of 200,000 μm^2 in order to represent the biofilm[180,181]. Images were acquired at 1.0 μm intervals through the biofilm with an inverted 40x/0.75 oil objective. Images were further analyzed using COMSTAT2.0 software for quantification of biomass, thickness, and roughness coefficient of the biofilms[180,182]. Three independent experiments were performed.

Planktonic and Biofilm Killing Assays

To harvest planktonic cells, *S. mutans* was cultured overnight in 5 mL BHI broth at 37 ºC and 5% CO_2 under static conditions. One-milliliter cell suspensions were centrifuged at 3,500 x g for 10 minutes. The formation of *S. mutans* biofilm was modified from previous studies[183,184]. Biofilms of *S. mutans* were formed on rectangle microscope coverslips in cultures with BMGS for 3 days at 37 ºC and 5% CO_2 under static conditions. The coverslips were vertically submerged in the culture medium that was replaced daily. After 3 days, biofilm cells which had adhered to the microscope coverslip were dispersed into 10 mL PBS. One-milliliter cell suspensions were centrifuged at 3,500 x g for 10 minutes. Cell pellets of planktonic and biofilms cells were resuspended with 300 μL of 50,

100 μg/mL OMVs, 800 μg/mL gentamicin or PBS, respectively, followed by incubation at 37 ºC and 5% CO_2. At 0, 3, 6, and 24 hours, a volume of 70 μL of each cell suspension was dispersed in 630 μL PBS and sonicated at 20 watts for 20 seconds. The sonicated cell suspensions were then serially diluted and plated for colony forming units (CFU) counting.

Field Emission Scanning Electron Microscopy

S. mutans biofilms were grown on hydroxyapatite (HA) discs placed horizontally in 24-well microtiter plates as previously described[185-187]. Briefly, overnight bacterial cultures were grown in BHI and diluted 1:10 in BMGS. Two milliliters of the diluted culture were added to each well with HA disc. After incubating for three days at 37 ºC in a 5% CO_2 aerobic atmosphere with fresh medium changed every 24 hours, the HA discs were transferred into wells with PBS, 50 μg/mL, or 100 μg/mL OMVs for another 24 hours. The HA discs were then washed with PBS and fixed in 2.5% glutaraldehyde overnight at 4 ºC. The fixed samples were dehydrated using increasing concentrations of ethanol, and then desiccated with CO_2 critical point drying. The samples were then coated with carbon before imaging. Scanning electron microscopy (SEM) was performed with a Hitachi S-4800 high-resolution microscope.

Bacterial Susceptibility Assays

Minimum inhibitory concentrations (MIC) of gentamicin cooperatively with or without OMVs for biofilm cells (MIC-B) and planktonic cells (MIC-P) were measured as previously described[188]. For MIC-B, overnight *S. mutans* culture was adjusted to OD_{600} equivalent to 0.5 and then diluted 1:1000 in BMGS. The bacterial suspension was added

into a 96-well plate at 80 μL/well and incubated for 24 hours at 37 ºC and 5% CO_2. Pre-formed biofilms were then washed once with PBS and treated with serially 2-fold diluted gentamicin starting from 800 μg/mL with or without 5, 10, 20 μg/mL OMVs for another 24 hours. The treated biofilms were then washed with PBS to remove the treatments. To allow the detachment of viable cells within biofilms, fresh BHI was added into each well and incubated for 24 hours. OD_{600} was measured before and after the 24-hour incubation. For MIC-P, overnight *S. mutans* culture was adjusted to OD_{600} equivalent to 0.5 and then diluted 1:1000 in BHI. Eighty microliters of cell suspension were added to the wells of the 96-well plates. Twenty microliter of serial 2-fold dilutions of gentamicin (5x) were added in each well with the final concentrations ranges from 0.04 to 40 μg/mL. OD_{600} was measured before and after the 24-hour incubation at 37 ºC and 5% CO_2. All experiments included three biological replicates and were independently repeated for three times.

Statistics

The Chi squared test was applied to compare the over-time killing of biofilm cells and planktonic cells with OMVs. The Chi squared test measures the deviations between a measured and an expected value, divided by the uncertainty. The unpaired two-sample t-test was applied to compare independent samples.

Results

Evaluation of the Antibiofilm Activity of B. thailandensis OMVs against Representative Biofilm-Forming Pathogens

The antibiofilm activity of OMVs was first screened against biofilm-forming pathogens *A. baumannii*, *E. faecalis*, *S. aureus*, and *S. mutans*. Bacterial biofilms were pre-formed in broth before treatment with OMVs or PBS and quantified with crystal violet staining. OMVs significantly reduced the biofilm biomass of all the bacteria tested (**Figure 3-1**). Interestingly, OMVs disrupted the pre-formed biofilms of *E. faecalis* but failed to inhibit its growth on an agar plate and in broth cultures (**Figure 2-8F and Figure 2-10F**).

***B. thailandensis* OMVs disrupted pre-formed MRSA biofilm in a dose-dependent manner**

Next, we investigated the effect of OMVs on pre-formed MRSA biofilms since OMVs significantly inhibit the growth of MRSA on agar plate and in planktonic cultures (**Figure 2-9B and Figure 2-11B**). MRSA biofilms were grown on chamber-slides then treated with water, 50, or 100 μg/mL OMVs. Remarkably, compared to control, treatment with OMVs significantly decreased the total biomass in a dose-dependent manner (**Figure 3-2 and Figure 3-3A**). The decreased ratios of dead cells to all labeled cells with OMV treatments are likely caused by the dispersal of the biofilms with decreased total biomass (**Figure 3-3B**). Treatment with high or low dose of OMVs also reduced the thickness of pre-formed MRSA biofilms compared to control (**Figure 3-3C**). The significant increase in the roughness coefficient in OMV-treated biofilms further indicates an overall decline in biofilm integrity (**Figure 3-3D**).

***B. thailandensis* OMVs kill *S. mutans* planktonic cells and biofilm cells in a time- and dose-dependent manner**

The antibiofilm ability of OMVs was further characterized against the biofilm model pathogen *S. mutans*. In previous chapters, we showed the antimicrobial activity of OMVs against *S. mutans* grown on agar plates and in broth cultures (**Figure 2-8G and Figure 2-10G**). OMVs significantly inhibited the growth of *S. mutans* planktonic cultures in a dose-dependent manner (**Figure 2-10G**). To further illustrate the ability and potency of OMV-mediated disruption of *S. mutans* biofilms, we harvested three-day biofilms cells cultured in biofilm medium supplemented with glucose and sucrose (BMGS) on glass slides (**Figure 3-4A**) and treated them with OMVs, gentamicin, or PBS. These were compared to planktonic cells cultured in BHI that received the same treatments. The killing of *S. mutans* biofilm and planktonic cells started within 3 hours of high-dose OMV treatment with more than 1-log reduction of CFU. After 6 hours, both biofilm and planktonic cells within high-dose OMVs showed 3-log reductions of CFU compared to PBS-treated cells at the same time-point (**Figure 3-4**). Although not as significant as targeting planktonic cells, OMVs showed similar killing ability when applied on biofilm cells. Strikingly, both concentrations of OMVs killed all *S. mutans* planktonic as well as biofilm cells within 24 hours compared to PBS-treated groups with more than 10^7 CFU/ml viable cells remaining. Gentamicin at a concentration of 800 μg/mL failed to clear the bacteria, with more than 10^3 CFU/mL viable planktonic cells and 10^5 CFU/mL viable biofilm cells remaining after treatment (**Figure 3-4**).

Taken together, OMVs showed bactericidal activity on both *S. mutans* planktonic cells and biofilm cells with a time- and dose-dependent manner. Notably, while OMVs and gentamicin were efficient in killing planktonic cells, *S. mutans* biofilm cells were significantly more susceptible to OMVs than gentamicin.

B. thailandensis OMVs reduced total biomass, biofilm integrity, and cell viability in S. mutans biofilms

The roles of OMVs on pre-formed, intact *S. mutans* biofilms was assessed with fluorescent confocal microscopy. Biofilms of *S. mutans* were grown within BMGS on chambered-slides for 3 days then treated with PBS, 10, 50, or 100 μg/mL OMVs for another 24 hours before imaging. Biofilms were stained with SYTO 9 for total biomass and propidium iodide (PI) for dead cell biomass. Representative images showed the biofilms treated with 50 or 100 μg/mL OMVs compared to PBS (**Figure 3-5**). Remarkably, increasing concentrations of OMVs led to a reduction of total biomass (green fluorescence) in *S. mutans* biofilms as well as an increase in the biomass of dead cells (red fluorescence) (**Figure 3-5 and Figure 3-6A**). Side bars in **Figure 3-5** indicate an observable decrease in biofilm thickness after OMVs treatments. Furthermore, the lack of red fluorescence at the bottom of the treated-biofilms demonstrated the difficulty in penetrating biofilms, which is one of the obstacles in developing effective antibiofilm agents. Moreover, COMSTAT analysis demonstrated that OMVs reduced biofilm thickness and integrity in a dose-dependent manner (**Figure 3-6B**). The significant increase in roughness coefficient indicates an overall decline in the healthiness of the biofilms, confirming the decreased biofilm integrity (**Figure 3-5C**).

B. thailandensis OMVs altered S. mutans biofilm structures and bacterial cell morphology

To model dental plaques, *S. mutans* biofilms were grown on hydroxyapatite (HA) discs (which mimic human dentures) within BMGS for 3 days then treated with PBS, 50, or 100 μg/mL OMVs for another 24 hours before imaging. Images revealed complex biofilm structures under the different treatment conditions (**Figure 3-7**). Three-day biofilms on HA discs with control treatment presented net structures with classically-chained *S. mutans* bacterial cells (**Figure 3-7A**). Exopolysaccharides were formed linking the chains of bacteria as indicated by black arrows. *S. mutans* also produced extracellular DNA (eDNA) to support the overall structures (white arrows). Bacteria within PBS-treated biofilms revealed a round-shape and smooth surface (**Figure 3-7A right**). When treated with increased concentrations of OMVs, the linear and elongated chained biofilm structures were less obvious (**Figure 3-7B,C**). No difference was observed in the quality and quantification of EPS and eDNA between PBS and OMVs treated biofilms based on the images. However, *S. mutans* cells in biofilms treated with 100 μg/mL OMVs displayed altered morphology with collapsed cell surfaces, which indicated a decreased bacterial cell integrity (**Fig 3-7C right**). The altered cell morphology may imply direct interactions between OMVs and *S. mutans*.

Synergistic effects of OMVs with gentamicin on S. mutans biofilms

Several strategies have been proposed to target drug-resistant biofilm-related infections including combination therapies. When testing the potency of gentamicin on *S. mutans* planktonic cultures and biofilms, we found that the minimal inhibitory concentrations of gentamicin against *S. mutans* biofilms (MIC-B) increased seven folds compared to targeting the same CFU of planktonic cells (MIC-P) (**Table 3-1**). However,

when supplemented with sub-inhibitory concentrations of OMVs at 5, 10, and 20 μg/mL, MIC-B of gentamicin dramatically decreased by 2, 4, and 14 folds (**Table 2**), respectively, indicating a synergistic effect between gentamicin and OMVs.

Discussion

In this chapter, we first showed the ability of *B. thailandensis* OMVs to disrupt pre-formed biofilms of *A. baumannii*, *E. faecalis*, *S. aureus*, and *S. mutans* in microtiter plates. The antibiofilm activity of OMVs against *A. baumannii*, *S. aureus*, and *S. mutans* may be caused by the direct killing of bacterial cells since we have shown previously OMVs inhibited the growth of these species. However, OMVs significantly disrupted the pre-formed biofilms of *E. faecalis* yet failed to inhibit its growth on agar plates and in planktonic cultures. This suggests there are potential modulatory effects of *B. thailandensis* OMVs on *E. faecalis* biofilms. It is possible that OMVs harbor QS molecules that can modify biofilm formation without affecting cell viability[189].

The antibiofilm activity of OMVs was also evaluated on MRSA biofilms using fluorescent microscopy and COMSTAT analyses. OMVs reduced the biomass, thickness, and integrity of MRSA biofilms in a dose-dependent manner. The roles of OMVs on bacterial biofilms were further investigated with a well-established biofilm model of *S. mutans*, which forms robust biofilms in defined medium. We showed that OMVs are bactericidal against both planktonic and biofilm cells of *S. mutans*. When applied on their biofilms, OMVs potently reduced the biomass, biofilm integrity, cell viability and altered cell morphology of *S. mutans* in a dose-dependent manner. These results suggest the direct killing and disruption of OMVs on *S. mutans* biofilms. However, it remains possible that

materials within OMVs regulate QS and biofilm formation of *S. mutans* independent of killing[189,190].

We observed a synergistic effect between *B. thailandensis* OMVs and gentamicin against *S. mutans* biofilms. In previous studies, Beveridge *et al.* demonstrated the bactericidal effect of gentamicin-induced *P. aeruginosa* OMVs that contained approximately 5.0 ng gentamicin/1 μg OMVs[129,134]. They proposed that the synergistic effect of the trapped gentamicin with *P. aeruginosa* OMVs was the result of the delivery by OMVs to the targeted bacteria cells as well as the combined killing effect of gentamicin and hydrolytic enzymes. In the current study, gentamicin was added along with OMVs to avoid direct delivery by OMVs. However, due to the ability of gentamicin to associate with bacterial cell membrane electrostatically[191,192], we cannot rule out the possibility of accidental carry. Nevertheless, these results indicate that OMVs derived from *B. thailandensis* can be used to enhance combinational therapy with other antibiotics.

In future studies, the antibiofilm activity of *B. thailandensis* OMVs should be evaluated against polymicrobial biofilms. For instance, both *E. faecalis* and *S. mutans* inhabit the oral cavity and play important roles in root canal infections[193]. Given the antibiofilm activity of OMVs evaluated against monocultures, it is important to understand the interactions between OMVs and the dual-species biofilms. It may also be worthwhile to examine the antibiofilm activity of OMVs against fungal species especially *C. albicans*, which is well known for its capacity to form biofilms during infections[194]. Biofilm formation by *C. neoformans* have also been shown to be associated with chronic infections[195] and medical device-related infections[196], especially with the increasing use of

ventriculoperitoneal shunts to manage intracranial hypertension associated with cryptococcal meningoencephalitis.

Figure 3-1

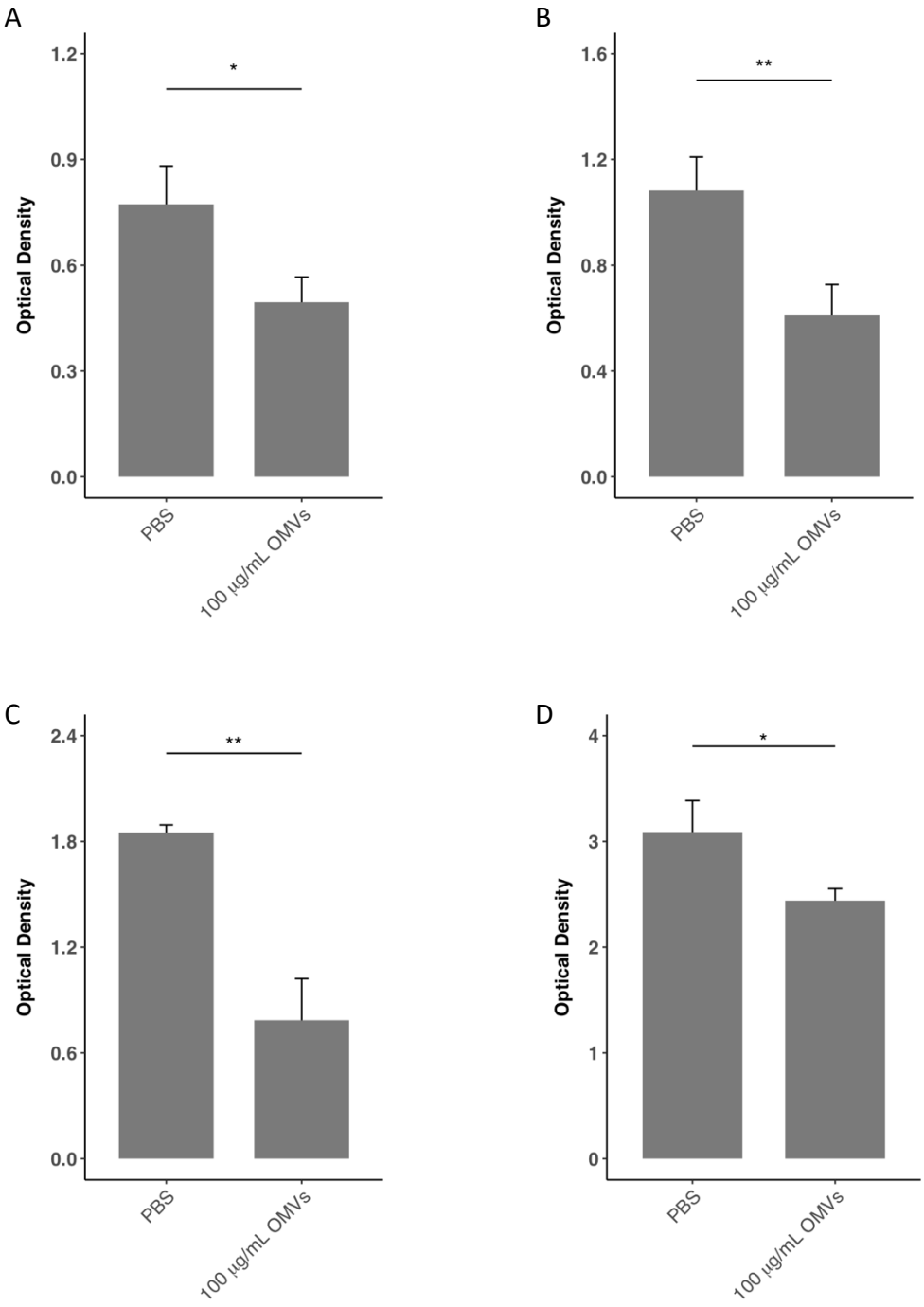

Figure 3-1. Evaluation of *B. thailandensis* OMVs disrupting pre-formed biofilms in microtiter plates

Biofilms of (**A**) *A. baumannii*, (**B**) *E. faecalis*, (**C**) *S. aureus*, (**D**) *S. mutans* were cultured in nutrient-rich broth for 24 hours. After removing the planktonic cultures from the wells, the biofilms were treated with 10 μg OMVs or PBS in a total volume of 100 μL for another 24 hours. The biomasses after the treatments were quantified with crystal violet staining. Experiments were performed in triplicates. The results were analyzed using unpaired two-sample t-test. (* $p < 0.05$, ** $p < 0.01$)

Figure 3-2

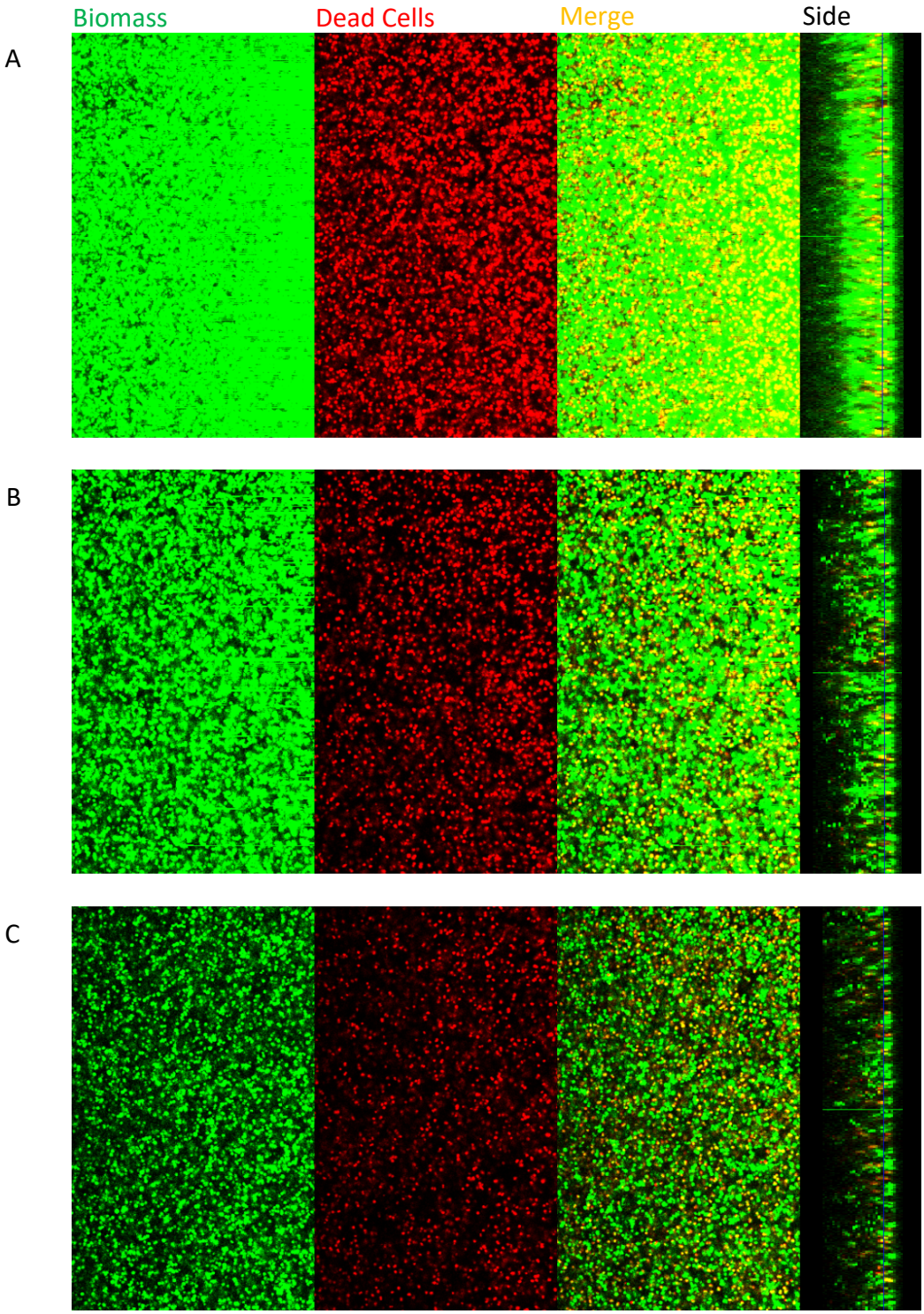

Figure 3-2. The bactericidal and antibiofilm effects of *B. thailandensis* OMVs against MRSA biofilm analyzed by fluorescent confocal microscopy

MRSA biofilms were grown on chamber-slides in TSB supplemented with 0.5% glucose for two days before treated with (**A**) water, (**B**) 50 μg/mL, or (**C**) 100 μg/mL OMVs for another 4 hours. Staining with LIVE/DEAD *Bac*Light fluorescent dye (SYTO 9/propidium iodide), biofilms were subjected to optical dissection using Zeiss LSM 700 laser scanning confocal microscope. At least seven image stacks were acquired at 400 x magnification from each well. Presented layers were 5 μm above the substratum in each image stacks. Green: total biomass. Red: dead cells. Side bars indicate the thickness of the biofilms.

Figure 3-3

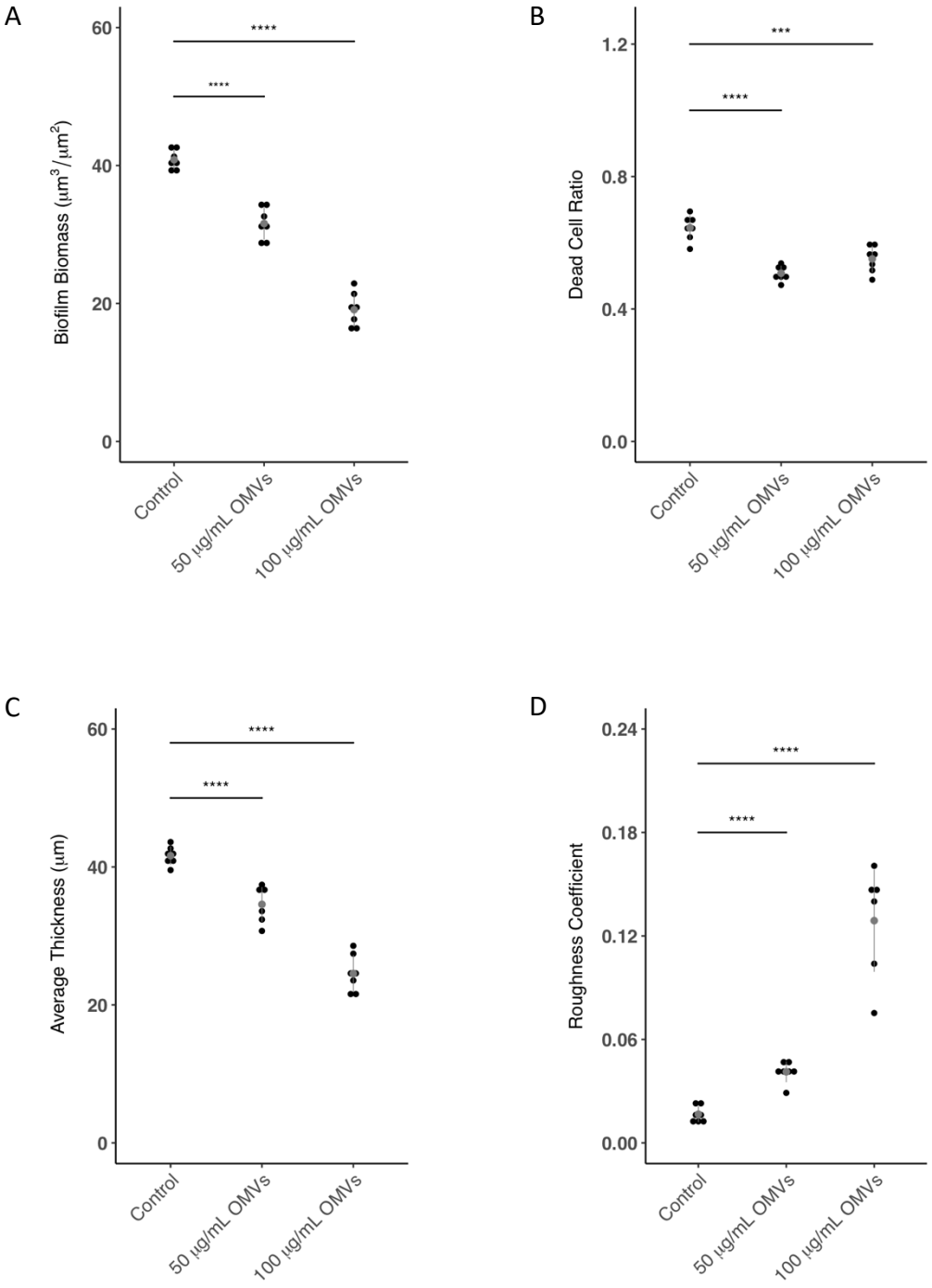
A
Biofilm Biomass (μm³/μm²)
60
40
20
0
****
****
Control
50 μg/mL OMVs
100 μg/mL OMVs
B
Dead Cell Ratio
1.2
0.8
0.4
0.0
***
****
Control
50 μg/mL OMVs
100 μg/mL OMVs
C
Average Thickness (μm)
60
40
20
0
****
****
Control
50 μg/mL OMVs
100 μg/mL OMVs
D
Roughness Coefficient
0.24
0.18
0.12
0.06
0.00
****
****
Control
50 μg/mL OMVs
100 μg/mL OMVs

Figure 3-3. Post-acquisition analyses of fluorescent images of the MRSA biofilms treated with *B. thailandensis* OMVs

Post-acquisition analyses were performed using COMSTAT 2.0. Biofilms treated with OMVs or control were compared in (**A**) biofilm biomass, (**B**) dead cell ratio, (**C**) average thickness, and (**D**) roughness coefficient. Roughness coefficients of the biofilms were calculated with COMSTAT 2.0 as an indication of biofilm healthiness and integrity. The results were analyzed using unpaired two-sample t-test. (**** $p < 0.0001$)

Figure 3-4

A

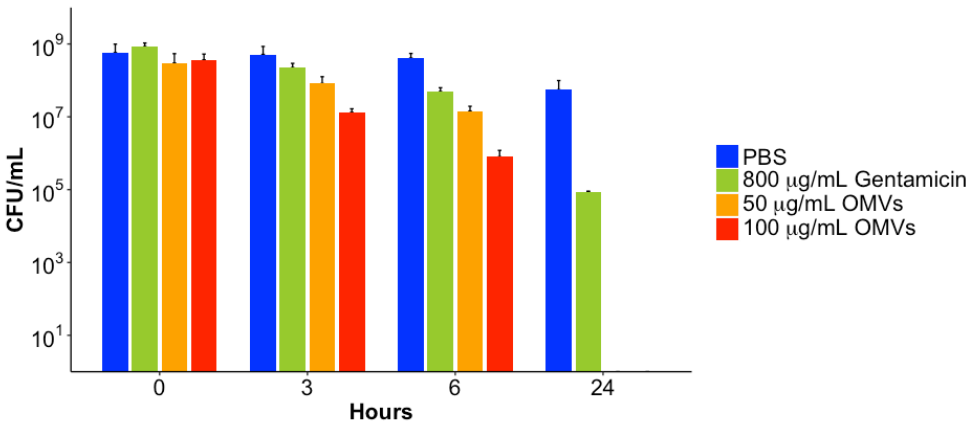

B

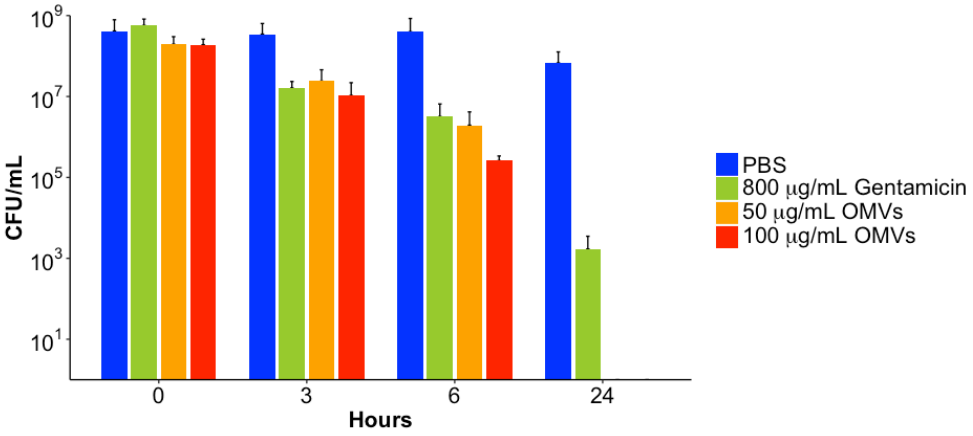

C

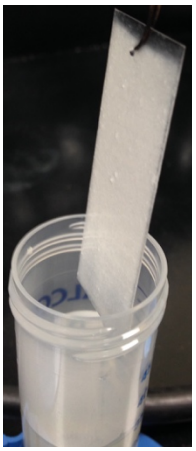

Figure 3-4. *B. thailandensis* OMVs kill *S. mutans* biofilm cells and planktonic cells in a time- and dose-dependent manner

S. mutans (**A**) biofilm cells and (**B**) planktonic cells were treated with OMVs with cell viability monitored over time. Biofilm cells were harvest from three-day biofilms on glass slides cultured with BMGS medium (**C**). Planktonic cells of *S. mutans* were harvest from liquid culture in nutrient rich broth. Both planktonic and biofilm cells were treated with 50, 100 μg/mL Bt OMVs, 800 μg/mL gentamicin or PBS for up to 24 hours. Cell numbers were adjusted to start from the same CFUs. Bacterial cells under different treatments were spread on agar plates for CFU counting at 0, 3, 6, and 24 hours. Experiments were performed independently for three times. Chi square test was applied to compare the intergroup difference. The *p* values were less than 0.0001 for PBS compared to individual experimental groups and for 800 μg/mL gentamicin compared to 50 and 100 μg/mL OMVs, respectively, in (**A**) and (**B**).

Figure 3-5

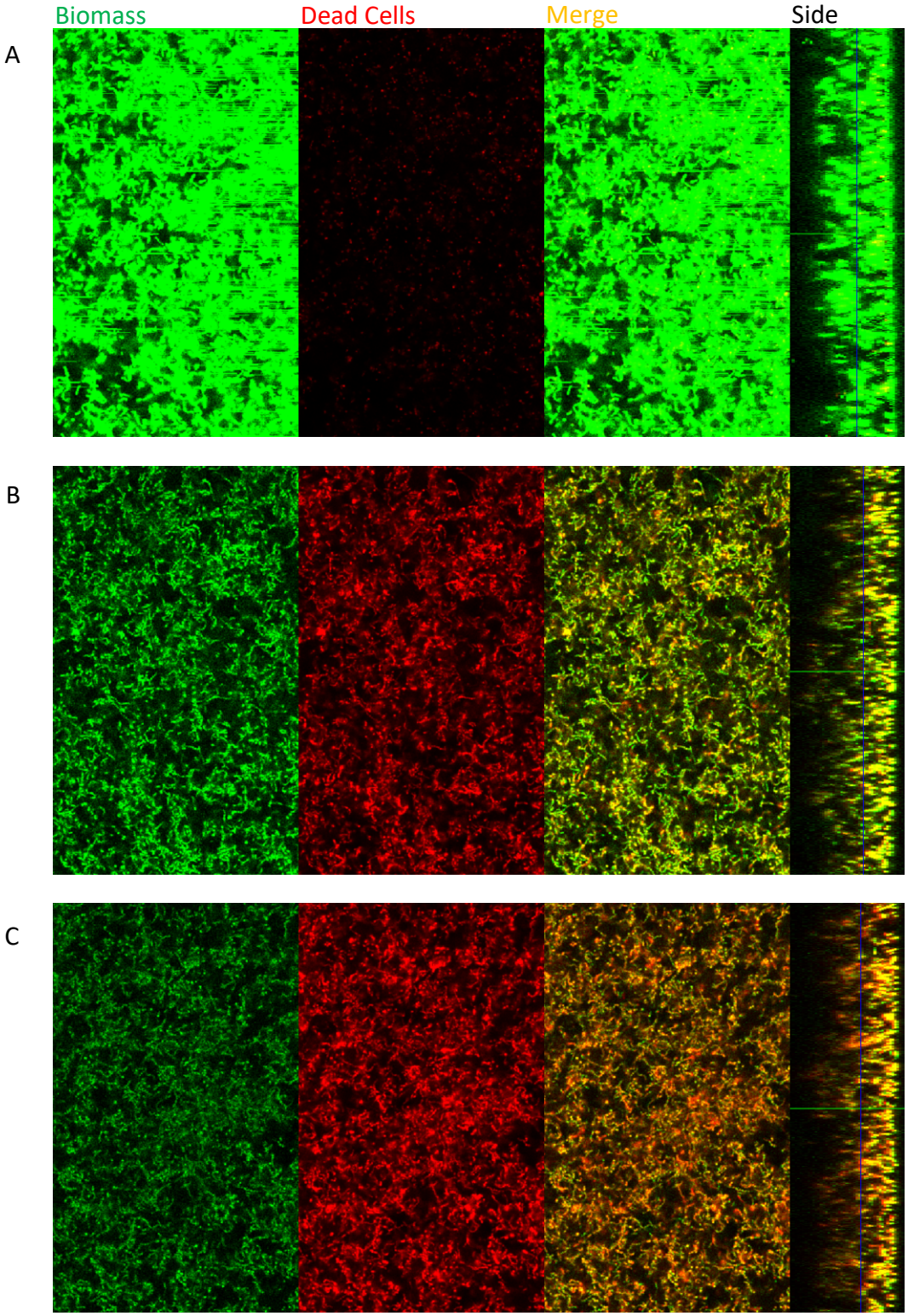

Figure 3-5. The bactericidal and antibiofilm effects of *B. thailandensis* OMVs against *S. mutans* biofilm analyzed by fluorescent confocal microscopy

S. mutans biofilms were grown anaerobically on chamber-slides in BMGS medium for three days before treated with (**A**) PBS, (**B**) 50 μg/mL, or (**C**) 100 μg/mL Bt OMVs for 24 hours. Staining with LIVE/DEAD *Bac*Light fluorescent dye (SYTO 9/propidium iodide), biofilms were subjected to optical dissection using Zeiss LSM 700 laser scanning confocal microscope. At least seven image stacks were acquired at 400 x magnification from each well. Presented layers were 15 μm above the substratum in each image stacks. Green: total biomass. Red: dead cells. Side bars indicate the thickness of the biofilms.

Figure 3-6

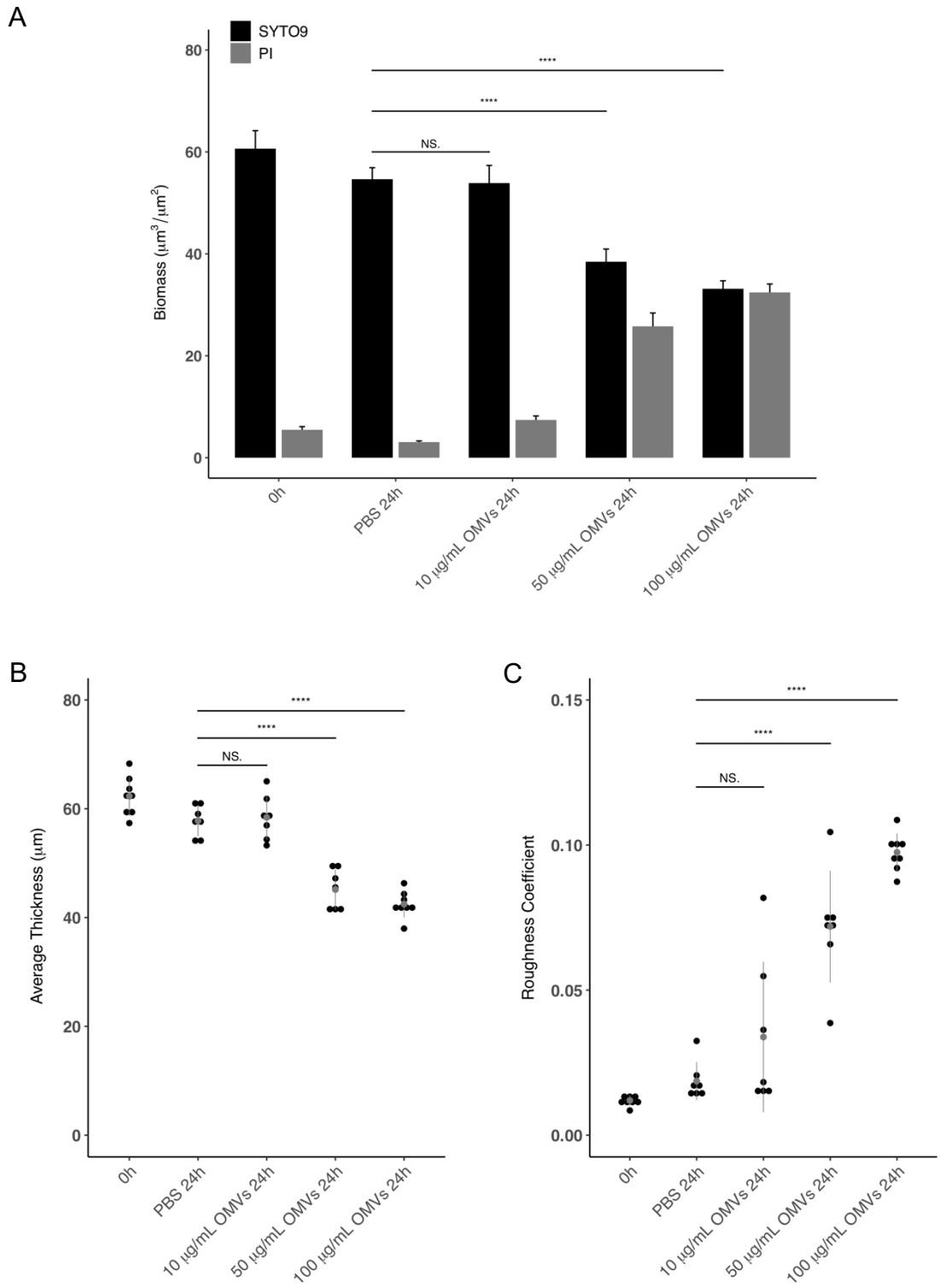
A
SYTO9
PI
Biomass (μm³/μm²)
0
20
40
60
80
NS.
****
****
0h
PBS 24h
10 μg/mL OMVs 24h
50 μg/mL OMVs 24h
100 μg/mL OMVs 24h
B
Average Thickness (μm)
0
20
40
60
80
NS.
****
****
0h
PBS 24h
10 μg/mL OMVs 24h
50 μg/mL OMVs 24h
100 μg/mL OMVs 24h
C
Roughness Coefficient
0.00
0.05
0.10
0.15
NS.
****
****
0h
PBS 24h
10 μg/mL OMVs 24h
50 μg/mL OMVs 24h
100 μg/mL OMVs 24h

Figure 3-6. Post-acquisition analyses of fluorescent images of the *S. mutans* biofilms treated with *B. thailandensis* OMVs

Post-acquisition analyses were performed using COMSTAT 2.0. Treatments with OMVs or PBS were compared in (**A**) total biofilm biomass/dead cell biomass, (**B**) average thickness, and (**C**) roughness coefficient. Roughness coefficients of the biofilms were calculated with COMSTAT 2.0 as an indication of biofilm healthiness and integrity. The results were analyzed using unpaired two-sample t-test. (**** $p < 0.0001$)

Figure 3-7

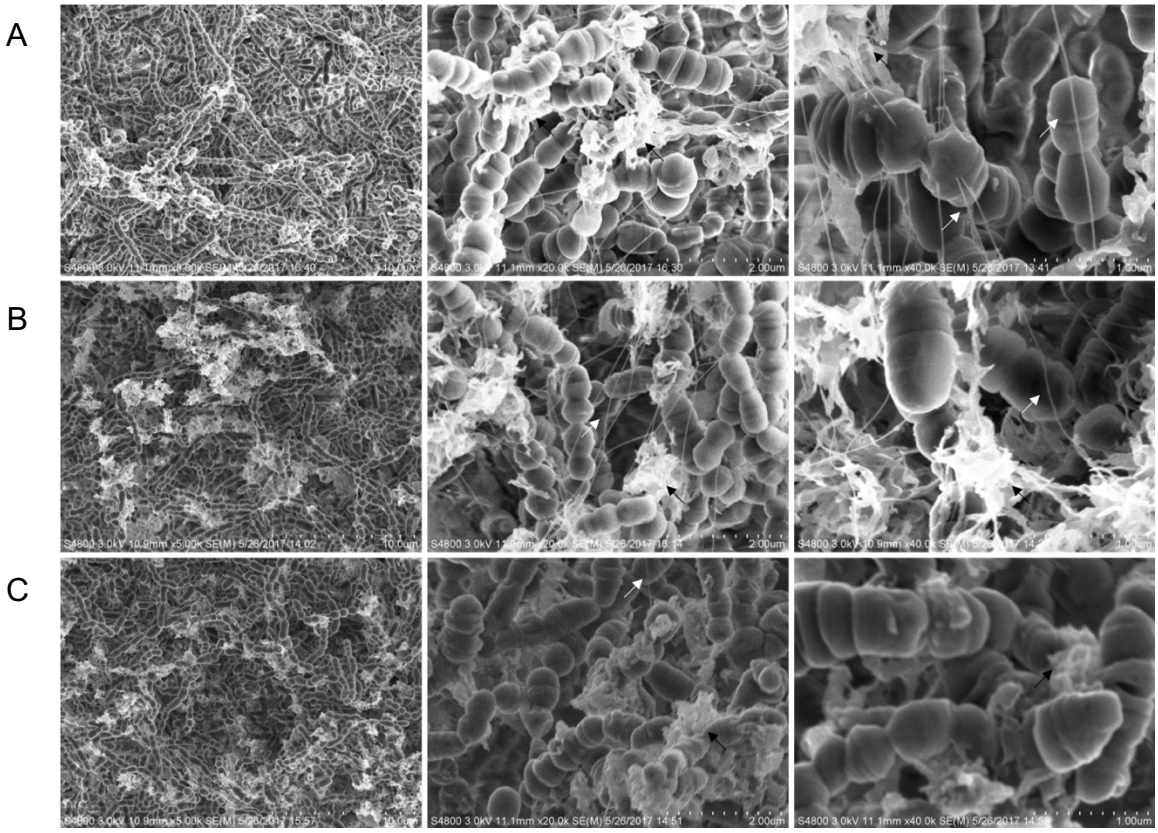

Figure 3-7. *B. thailandensis* OMVs alter *S. mutans* biofilm structure and cell morphology revealed by scanning electron microscopy

S. mutans biofilms were grown on hydroxyapatite discs within BMGS medium for three days before treated with (**A**) PBS, (**B**) 50 μg/mL, or (**C**) 100 μg/mL OMVs for another 24 hours and imaged with SEM. At least 16 images were acquired from each hydroxyapatite discs. Experiment included two biological replicates. Presented images were acquired at 5,000 x (left), 20,000 x (middle), and 40,000 x (right) magnifications. White arrow: extracellular DNA; black arrow: extracellular polysaccharides.

Table 3-1.

Gentamicin	OMVs (μg/mL)			
MIC (μg/mL)	0	5	10	20
Biofilm	141.42	62.98	35.36	9.92
Planktonic	20.00	-	-	-

Table 3-1. Synergistic effect of *B. thailandensis* OMVs with gentamicin on *S. mutans* biofilms

Planktonic cultures and biofilms of *S. mutans* were treated with series 2-fold dilutions of gentamicin alone or gentamicin combined with 5, 10, 20 μg/mL OMVs for 24 hours. Fresh BHI was added and incubated for another 24 hours to allow the detachment of viable cells within biofilms. OD_{600} was measured before and after the incubation to show the inhibition of bacterial growth. MICs were calculated as Start Concentration/$2^{\text{Mean of the powers}}$.

CHAPTER 4: The identification of *Burkholderia thailandensis* outer membrane vesicle components mediating antimicrobial activity

Introduction

The antimicrobial activity of OMVs was first reported in *P. aeruginosa*, and was attributed to the presence of a 26-kDa peptidoglycan hydrolase[129]. A later study revealed that OMVs from *Lysobacter* sp. XL1 contained a bacteriolytic peptidoglycan hydrolase, endopeptidase L5, effective against Gram-positive *Staphylococcus aureus* 209-P and Gram-negative *Erwinia marcescens* EC1[135]. Interestingly, while both homologous enzymes, endopeptidase L1 and L5, were secreted into the culture medium, only endopeptidase L5 was released within the OMVs potentially indicating a selective mechanism of secretion[135]. Moreover, endopeptidase L5 only actively lysed the Gram-negative bacterium *Erwinia marcescens* when inside the vesicles, which was likely facilitated by fusion with the membrane of target cells by the vesicles[135]. Similarly, *Myxococcus xanthus* was reported to produce OMVs with lethal cargos[136]. Proteomic analysis of *M. xanthus* OMVs indicated a number of OMV-specific or OMV-enriched proteins, including several with putative hydrolytic function[136]. Specifically, metalloprotease, MepA, was identified as contributing to the bacteriolytic activity of *M. xanthus* OMVs[136]. Further, secondary metabolite profiling identified 16 molecules, many associated with antimicrobial activities[136]. Myxochelines are iron chelating siderophores with antibacterial properties against several Gram-positive bacteria including *S. aureus* and *Bacillus*[197]. Myxalamids have been shown to possess antimicrobial activity by inhibiting the cytochrome I NADH:ubiquinone oxidoreductase[198]. Myxovirescin A has a macrocyclic

structure with antibiotic activity inhibiting type II signal peptidases during protein secretion[199]. Another peptide antibiotic identified from *M. xanthus* OMVs was cittilin A with a structure derived from three tyrosine residues and an isoleucine residue[136]. These findings suggest the possible types of antimicrobial components contained within *B. thailandensis* OMVs.

In recent years, studies have revealed the roles of *P. aeruginosa* OMVs in interspecies interactions with cargo involved in bacterial quorum sensing[200,201]. Specifically, *Pseudomonas* quinolone signal (PQS) packaged in OMVs has been well studied for its ability to regulate virulence factors including elastase, rhamnolipids, and pyocyanin[201]. It also influences OMV production by inserting into the membrane, which leads to asymmetric growth of the outer leaflet of the lipid bilayer membrane[201,202]. Besides its function as a signaling molecule, PQS has been shown to chelate iron and regulate redox homeostasis[201]. Although it has not been directly linked to bacterial killing, the influence of PQS on the growth rate of many bacteria was observed[203]. Moreover, studies showed that PQS modulates various phenotypes including motility and biofilm formation in Gram-positive and Gram-negative bacteria as well as yeasts[189]. For instance, PQS inhibited biofilm formation by *S. mutans* without affecting its cell growth[190].

Many bacterial species are capable of producing biosurfactants with the ability to reduce surface tension and display emulsifying activity while having other biological properties[111]. Biosurfactants usually have low critical micelle concentration and toxicity as well as high biodegradability and thermostability and have been considered as a promising alternative to synthetic surfactants[111]. These amphiphilic compounds can be further classified into glycolipids, lipoproteins, phospholipids, and polymers. Among them,

glycolipids including rhamnolipids, sophorolipids, trehalolipids, and mannosylerythritol lipids are the most widely studied biosurfactants[111]. *P. aeruginosa* is a prominent producer of rhamnolipids which have been well characterized for their antimicrobial and antibiofilm activities[113,115].

Given the fact that *B. thailandensis* is closely related to *P. aeruginosa*, we hypothesized that the antimicrobial activity of *B. thailandensis* OMVs could be mediated by one or more hydrolytic enzymes, quorum sensing molecules, or biosurfactants.

Materials and Methods

Purification of bacterial peptidoglycan

Preparation of peptidoglycan from Gram-positive bacteria was modified from previous publications[204,205]. Lawns of bacteria were grown on agar plates overnight and washed off with 1 mL PBS. Bacterial cell suspension was boiled for 20 minutes before centrifuged at 2,000 x g, 4 ºC for 15 minutes. The bacterial pellets were then washed twice with PBS, once with acetone followed by desiccation at 37 ºC. To disrupt the cells, the dry bacterial powder was suspended in 750 μL 10% TCA and boiled for 30 minutes. The cell walls were then pelleted by centrifugation at 10,000 x g for 15 minutes and washed three times with water. To remove nucleic acids and proteins, the pelleted cell walls were suspended at a concentration of 10 mg/mL in 50 mM phosphate buffer pH 7.6 with 0.2% toluene. RNase A and DNase I were added to the suspension at a final concentration of 100 and 50 μg/mL, respectively. The incubation took for 18 hours at 37 ºC with slow or occasional mixing. Trypsin was further added to the suspension to a concentration of 3 mg/mL. The suspension was incubated for another 3 hours at 37 ºC. Then, the trypsin

treated suspension was centrifuged at 10,000 x g for 15 minutes to sediment the crude peptidoglycan. After removing the supernatant, the pellets were washed three times with sterile water and three times with diethyl ether followed by desiccating on a heat block at 45 ºC. The purified peptidoglycan was stored at -20 ºC until use.

Another method was used to purify the peptidoglycan from *S. mutans*. Bacteria was cultured in 100 mL BHI till mid-log phase. Bacterial cells were harvested by centrifugation 2,000 x g for 10 minutes at 4 ºC and washed once in 10 mL of 50 mM Tris-HCl buffer (pH 7.5). Cells were then pelleted again and resuspended in 20 mL of 50 mM Tris-HCl buffer (pH 7.5) containing 4% SDS and boiled for 30 minutes followed by washing with Tris-HCl buffer for five times. The cells were then bead-beat for four times, 30 seconds each, with intermittent rest on ice for 1 minute. After removing the beads, the lysed cells were transferred into a clean tube and centrifuged at 10,000 x g for 10 minutes to obtain the cell envelope. The pellet was then washed once with Tris-HCl buffer and resuspended in 50 mM Tris-HCl buffer containing 10 mM $CaCl_2$, 20 mM $MgCl_2$ and 10 μg/mL DNase followed by incubation at 37 ºC for 2 hours. To remove proteins, the buffer containing cell envelope was centrifuged at 10,000 x g for 10 minutes and the pellet was treated with 50 μg/mL Proteinase K in 50 mM Tris-HCl buffer with 1% SDS at 37 ºC overnight. On the second day, the purified peptidoglycan was washed twice in 1 mL of 50 mM Tris-HCl buffer and desiccated after removing the supernatant.

Peptidoglycan Degradation Assay

Enzymatic digestion of peptidoglycan was modified based on previous methods[206,207]. Briefly, insoluble peptidoglycan from *S. aureus* and *S. mutans* was

suspended in PBS and solubilized by sonicating for 3 minutes at 300 watts (Sonifier). The suspensions were further diluted in PBS to yield a reading of between 0.5 and 1.0 at OD_{450} before treatments. The same amount of peptidoglycan was treated with 0.5, 5, 50 μg/mL native OMVs, 50 μg/mL heat inactivated OMVs (80 ºC for 2 hours), 200 μg/mL lysozyme (Sigma-Aldrich) and PBS, respectively. The experiments were performed in triplicate in a 96-well plate. The plates were incubated at 37 ºC and the OD_{450} was read every 30 minutes for 4 hours. Additionally, the plates were shaked before each reading to resuspend any peptidoglycan that had fallen out of solution during the incubation.

Bacterial strains and growth conditions

Acinetobacter baumannii, multidrug-resistant *Acinetobacter baumannii, Pseudomonas aeruginosa* PAO1, *Staphylococcus aureus* ATCC 6538*,* methicillin-resistant *Staphylococcus aureus* ATCC 43300, *Enterococcus faecalis* ATCC 29212*, Escherichia coli* ATCC 25922*, Klebsiella pneumoniae* ATCC 1706, carbapenem-resistant *Klebsiella pneumoniae* ATCC 1705, *Streptococcus mutans* UA159, *Cryptococcus neoformans* and *Candida albicans* ATCC 14053 were maintained in lysogeny broth (LB) or brain heart infusion broth (BHI), while solid medium was made by adding 1.5% (wt/vol) agar. All bacterial cultures were incubated at 37 ºC with 233 rpm oscillation. *S. mutans* cultures and plates were maintained at 37 °C in an aerobic chamber containing 5% CO_2 under static conditions. Drug-sensitive and multidrug-resistant (MDR) *A. baumannii* strains and *C. neoformans* we used for current study were isolated from Tulane hospital.

Growth inhibition assay

The ability of OMVs and purified fractions to inhibit the growth of representative microorganisms was examined using a growth inhibition assay. For testing OMVs, microorganisms were cultured overnight in 5 mL LB or BHI broth at 37 ºC. The suspension was further diluted 1:1000 in nutrient broth and added into a 96-well plate (Costar) at 80 μL/well followed by treatments with 20 μL of PBS, native, or heat-inactivated OMVs. Heat inactivation of OMVs was achieved by incubation on a heat block at 80 ºC for 2 hours. For HPLC fractions, fractions were pooled and desiccated (F1: 6-11 mins, F2: 12-17 mins, F3: 18-23 mins, F4: 24-29 mins, F5: 30-35 mins, F6: 36-41 mins, F7: 42-44 mins, F8: 45-46 mins, F9: 47-48 mins, F10: 49-50 mins, F11: 51-53 mins, F12: 54-59 mins, F13: 60-65 mins). Material in each fraction were dissolved in MeOH and added into a 96-well plate. The overnight culture of microorganisms was diluted 1:1000 in Mueller Hinton II Broth and added at 100 μL/well into a 96-well plate after evaporating the MeOH. Optical density at 600 nm was monitored until the culture reached plateau.

Confocal laser scanning microscopy

MRSA was cultured overnight in BHI and diluted 1:10 in TSB supplemented with 0.5% glucose[179], while *S. mutans* was cultured overnight in BHI and diluted 1:10 in BMGS. Biofilms were cultured on 8-well chambered-slides at 37 °C statically with medium changed daily. Pre-formed 2-day biofilms of MRSA were then treated with water, 100 μg/mL heat-inactivated OMVs or native OMVs for another 4 hours before imaging. One-day biofilms of *S. mutans* were treated with PBS, 100 μg/mL heat-inactivated OMVs or native OMVs for another 24 hours. Biofilms after the treatments were stained with LIVE/DEAD *Bac*Light fluorescent dye and imagined. Fluorescent confocal microscopy

was performed with a Zeiss LSM 700 microscope. Confocal *z*-stacks and simulated *xyz* three-dimensional images were acquired and generated using Zeiss 10.0 software. More than seven image stacks were acquired from random positions within each well to cover an area of 200,000 μm^2 in order to represent the biofilm[180,181]. Images were acquired at 1.0 μm intervals down through the biofilm with an inverted 40x/0.75 oil objective. Images were further analyzed using COMSTAT2.0 software for quantification of biomass, thickness, and roughness coefficient of the biofilms[180,182].

Characterization of heat-stable antimicrobial components within OMVs

To determine the chemical property of the antimicrobial components, OMVs were separately treated with 40 mM CHAPS (detergent), 2 mg/mL proteinase K, 0.1 u/μL DNase, 1 mg/mL RNase, or the combination before heat-inactivation and spot plated onto agar streaked with MRSA. Their antimicrobial activity was compared to the non-treated heat-inactivated and native OMVs. The sizes of the heat-stable antimicrobial components against MRSA and *C. neoformans* were characterized by size exclusion filtration. Heat-inactivated OMVs were extracted with MeOH/$CHCl_3$ mix (1:2, v/v). The organic extracts were desiccated followed by resuspension in 70% MeOH. This solution was then loaded onto the centrifugal filters (compatible with MeOH) with 3 kDa and 100 kDa cutoff and centrifuged at 14,000 x g. Materials with different size cutoffs were collected and desiccated in vacuo followed by resuspension in 20 μL of 20% MeOH before screening for antimicrobial activity against MRSA and *C. neoformans*.

Purification of hydroxyalkylquinoline and rhamnolipid

Heat inactivated OMVs were extracted with MeOH/$CHCl_3$ mix (1:2, v/v) at 45 ºC until complete separation and the process was repeated three times. Both aqueous and organic phases were concentrated and tested for antimicrobial activities. The extracts from organic phase was then resuspended with 20% MeOH in H_2O and separated on a SPE Sep-Pak C18 Cartridge (Waters) with a gradient of MeOH (20%, 40%, 60%, 80% and 100% MeOH in H_2O, 2 mL each). Each eluted fraction was tested for antimicrobial activity. The active fractions eluted with 80% and 100% MeOH were further concentrated in vacuo and subjected to HPLC separation. The HPLC (Shimadzu) was carried out on with a UV-Fluorescence detector and an automated fraction collector. A C2 column (250/4.6 Nucleosil 100-7, Macherey-Nagel) was used with a flow of 0.5 mL/min and a gradient of 5% MeOH in H_2O to 100% MeOH (with 50 mM NH_4OAc, pH 5.6) over 80 mins. The injection volume was 70 uL. The elution started with 5% MeOH isocratic for 5 min, from 5 to 10 min a linear increase from 5 to 45% MeOH was applied, followed by a second linear increase from 45% to 100% MeOH (10 to 55 min). An isocratic step (100% MeOH) was then maintained for 10 min and ended with a return to 5% MeOH in 2 min. The re-equilibration was done with 5% MeOH isocratic for 13 min. The HPLC run was collected every minute from 5 to 65 mins. The active HPLC fractions were tested by growth inhibition assay and a Kirby Bauer-like method against MRSA. Fractions showing activity were collected and concentrated for LC/MS, ^1H NMR and other analyses.

Mass spectrometry and proteomics

For identification of HMNQ, rhamnolipid, a Thermo-Fisher Orbitrap Elite mass spectrometer (Waltham, MA) in the Proteomics and Mass Spectrometry Facility at the

University of Georgia was used for high-resolution accurate mass analyses. The LC fractions collected at Tulane University were introduced into the ESI source by loop injection. The mass spectra shown were acquired at positive ion mode with a spray voltage of +4.5 KV. Selected precursor ions found in MS were subjected to further analyses by collisional induced dissociation (CID) and higher-energy collisional dissociation (HCD) MS/MS analysis.

For proteomic analysis of OMVs, 100 μg of OMV were separated by SDS-PAGE. Bands were excised from the gel and incubated for 20 minutes with 25 mM ammonium bicarbonate in 50% acentonitrile. Proteins were then digested with 1 μg/sample Trypsin in 25 mM ammonium bicarbonate for 16 hours at 37 °C. Peptides were extracted by incubating the samples with 100 μL extraction buffer, comprised of 0.1% formic acid in 50% acentronitrile, for 20 minutes, briefly spun and supernatant collected. This was then followed by an additional incubation for 20 minutes in 100% acetonitrile. Samples were then dehydrated by Eppendorf Vacufuge and resuspended in 10 μL 0.1% formic acid with 2% acetonitrile. Samples were run on a ThermoScientific Orbitrap Elite mass spectrometer for high resolution and high mass accuracy analysis. This was coupled with a nano HPLC. Results were provided as raw data, which was searched against the *B. thailandensis* proteome through the Basic Local Alignment Search Tool (BLAST) search engine.

Nuclear magnetic resonance spectroscopy

NMR spectra were acquired at the Tulane University Department of Chemistry NMR facilities. HMNQ was dissolved in deuterated methanol for nuclear magnetic resonance analysis with a Bruker 500 MHz NMR spectrometer.

Fluorescence measurement

Purified HMNQ was dissolved in MeOH before fluorescence measurement with a fluorometer. Fluorescence emission spectrum after excitation at 370 nm was recorded from 400 to 700 nm, while excitation spectrum for emission at 480 nm was recorded from 240 to 450 nm.

Statistical analysis

The Chi squared test was applied to compare two curves, which measures the deviations between a measured and an expected value, divided by the uncertainty. The unpaired two-sample t-test was applied to compare independent samples.

Results

B. thailandensis OMVs contain peptidoglycan hydrolases

OMVs from *P. aeruginosa* were previously reported to possess antimicrobial activity mediated by peptidoglycan hydrolases that were effective against *S. aureus* and *E. coli*[129]. Proteomic analysis of *B. thailandensis* OMV preparations identified the presence of several classes of peptidoglycan hydrolases (**Table 4-1**). To determine whether the antimicrobial activity of *B. thailandensis* OMVs could be attributed to one or more hydrolases, we performed peptidoglycan degradation assays using lysozyme as a positive control. As expected, *B. thailandensis* OMVs degraded *S. aureus* peptidoglycan in a dose-dependent manner (**Figure 4-1A**). After 4 hours, 50 μg/mL OMVs degraded *S. aureus* peptidoglycan to the same degree as 200 μg/mL lysozyme (**Figure 4-1A**). Upon heat-

inactivation of OMVs, no degradation of peptidoglycan was observed (**Figure 4-1A**). These results indicate that *B. thailandensis* OMVs contain heat-labile peptidoglycan hydrolases that contribute to their antimicrobial activity against *S. aureus*. However, when applied on *S. mutans* peptidoglycan, OMVs as well as lysozyme failed to degrade the peptidoglycan (**Figure 4-1B**). To exclude the possible peptidoglycan purification discrepancy between *S. aureus* and *S. mutans*, we employed another *Streptococci* peptidoglycan purification method. Even so, those *S. mutans* peptidoglycan preparations still could not be degraded by OMVs (**Figure 4-1B**).

Heat-inactivated OMVs still possess antimicrobial activity

Since heat-inactivated *B. thailandensis* OMVs failed to degrade *S. aureus* peptidoglycan, we tested whether heat-inactivated OMVs still exhibited antimicrobial activity against *S. aureus*. Surprisingly, heat-inactivated OMVs still significantly inhibited *S. aureus* growth (**Figure 4-2E**). Heat-inactivated OMVs also maintained antimicrobial activity against *A. baumannii*, MDR *A. baumannii*, *S. mutans*, MRSA, *C. albicans*, and *C. neoformans*. (**Figure 4-2 and Figure 4-3**). These results indicate that OMVs must contain heat-stable antimicrobial molecule(s) that mediate antibacterial and antifungal activities.

Heat-inactivated OMVs possess antibiofilm activity

Next, we investigated the antibiofilm activity of heat-inactivated OMVs on pre-formed MRSA or *S. mutans* biofilms compared to native OMVs. MRSA and *S. mutans* biofilms were grown on chamber-slides then treated with vehicle control, 100 μg/mL heat-inactivated OMVs, or 100 μg/mL native OMVs. Compared to control, treatment with heat-

inactivated OMVs significantly decreased the total biomass and average thickness of pre-formed MRSA biofilm while increasing the dead cell ratio (**Figure 4-4A,B and Figure 4-5A,B,C**). The significant increase in the roughness coefficient in the biofilms treated with heat-inactivated OMVs indicates an overall decline in biofilm integrity (**Figure 4-5D**). When applied on *S. mutans* biofilms, heat-inactivated OMVs significantly decreased the average thickness and increased the dead cell ratio without affecting the total biomass and roughness coefficient (**Figure 4-6A,B and Figure 4-7**). However, compared to native OMVs at the same concentration, heat-inactivation partially abolished their antibiofilm activity against both MRSA and *S. mutans* (**Figure 4-4B,C and Figure 4-6B,C**). Thus, the heat-labile components of OMVs partially contribute to the decreased biomass, thickness, cell viability, and integrity of the biofilms (**Figure 4-5 and Figure 4-7**).

B. thailandensis OMVs contain antimicrobial 4-hydroxy-3-methyl-2-(2-non-enyl)-quinoline and long chain rhamnolipid

To determine the identity of the antimicrobial molecules, heat-inactivated *B. thailandensis* OMVs were separately treated with proteinase, DNase, and RNase and tested for activity. None of the treatments impacted OMV antimicrobial activity (**Figure 4-8A**). In order to identify the heat-stable antimicrobial molecules, heat-inactivated OMVs were extracted with a mix of methanol and chloroform (1:2, v/v). Both aqueous and organic phases were concentrated and tested for antimicrobial activities. The majority of the antimicrobial activity was retained in the organic phase, suggesting molecules with relative lipophilic property (**Figure 4-8B,C**). Size exclusion filtration indicated the compounds were less than 3 kDa in size (**Figure 4-9A,B**). The isolated organic extracts were then

separated with solid phase extraction (**Figure 4-9C**) followed by HPLC. The HPLC fractions were collected every minute from 5 to 65 mins and detected at UV 214 nm (**Figure 4-10**).

Next, broth cultures of each organism were treated with pooled HPLC fractions. Optical density readings were obtained every 2 hours for a total of 12 hours and compared with control-treated cultures. The difference in the optical density between treated and control-treated cultures at each time point was plotted as a heatmap in **Figure 4-11.** Notably, materials from fractions (F) F5 to F9 and F11 significantly inhibited the growth of *S. aureus*, MRSA, *S. mutans*, *C. albicans* and *C. neoformans*. Materials from F5 to F9 inhibited the growth of *A. baumannii* with F7 and F8 having the most significant effect against MDR *A. baumannii*. Not surprisingly, materials from all fractions failed to inhibit the growth of *P. aeruginosa* (**Figure 4-11C**). To further examine the isolated compounds from each fraction, individual 1-minute fractions were tested by spot-plating against MRSA. Materials from 42-44 mins showed significant antimicrobial activity against MRSA, whereas materials from 51-53 mins slightly inhibited MRSA growth (**Figure 4-10**).

To elucidate the structures of the materials from 42-44 mins and 51-53 mins, fractions were collected and desiccated then analyzed by tandem MS. The tandem MS spectrum of materials from 42-44 mins revealed a predominant molecule with m/z 284.2005 which suggested the existence of 4-hydroxy-3-methyl-2-nonenylquinoline (HMNQ), the structure of which was further confirmed by NMR analysis (**Figure 4-12 and Figure 4-13**). MS/MS fragmentation patterns of HMNQ used to elucidate the structure are shown in **Figure 4-12B** and **Table 4-2**. For proper detection during purification process,

HMNQ was characterized for fluorescence with excitation at 370 nm and emission at 480 nm (**Figure 4-14**). The presence of HMNQ in *B. thailandensis* OMVs purified with equilibrium density-gradient ultracentrifugation was confirmed with HPLC and detected for fluorescence with excitation at 370 nm and emission at 480 nm (**Figure 4-15**). We observed other HAQ derivatives in adjacent fractions (data not shown). One of them with m/z 300.1960 which is very likely to be the N-oxide form of HMNQ that is tailing from fractions before. The predominant molecule in the materials from 51-53 mins was determined to be a long-chain di-rhamnolipid (Rha-Rha-C_{14}-C_{14}) sodium salt as shown by the tandem MS spectrum of predominant m/z 785.5027 (**Figure 4-16 and Table 4-3**). *B. thailandensis* has been previously characterized for its ability to produce rhamnolipids with predominantly longer fatty acid chains (Rha-Rha-C_{14}-C_{14})[102,112].

Discussion

In this chapter, we first confirmed the presence of peptidoglycan hydrolases within *B. thailandensis* OMVs that were effective against *S. aureus* but not *S. mutans.* Peptidoglycan structures are well studied in *S. aureus* and possess a conserved disaccharide (*N*-acetylglucosamine and *N*-acetylmuramic acid), a pentapeptide stem (L-alanine-D-*iso*-glutamine-L-lysine-D-alanine-D-alanine), and a pentaglycyl bridge[142]. Our proteomic analysis of *B. thailandensis* OMVs showed the presence of transglycosylases, peptidases, and amidases, which potentially cleave glycosidic bonds between *N*-acetylglucosamine and *N*-acetylmuramic acid, peptide bonds, and amide groups linking L-alanine and *N*-acetylmuramic acid, respectively (**Table 4-1**). The distal difference in peptide stems and

bridges cross-linking glycan strands within *S. mutans* could potentially explain the inability of peptidoglycan hydrolases from *B. thailandensis* OMVs.

The antimicrobial and antibiofilm activities of heat-inactivated OMVs were further evaluated. We showed that heat-inactivated OMVs partially retained the ability to inhibit the growth of microbes susceptible to native OMVs. While still able to disrupt MRSA and *S. mutans* biofilms, their antibiofilm activity was also reduced compared with native OMVs. This implies the presence of other heat-labile component(s) other than peptidoglycan hydrolases contributing to the disruption of *S. mutans* biofilms.

The initial characterization of the heat-stable antimicrobial molecules showed that they were small molecules less than 3 kDa and resistant to the treatments of proteinase, DNase, and RNase. To identify these molecules, crude OMVs from ammonium sulfate precipitation were extracted with organic solvent before separating with solid phase extraction and HPLC (**Figure 4-17**). The antimicrobial activity was monitored during each step of the purification. We identified two molecules from the HPLC fractions with antimicrobial activity, 4-hydroxy-3- methyl-2-nonenylquinoline (HMNQ) and long-chain di-rhamnolipid (Rha-Rha-C_{14}-C_{14}). In next the chapter, their antimicrobial and antibiofilm activities will be characterized, separately and independent of OMVs, against representative microbes. The efficacy and toxicity of these molecules will also be evaluated in cell cultures and in a murine wound infection model.

Figure 4-1

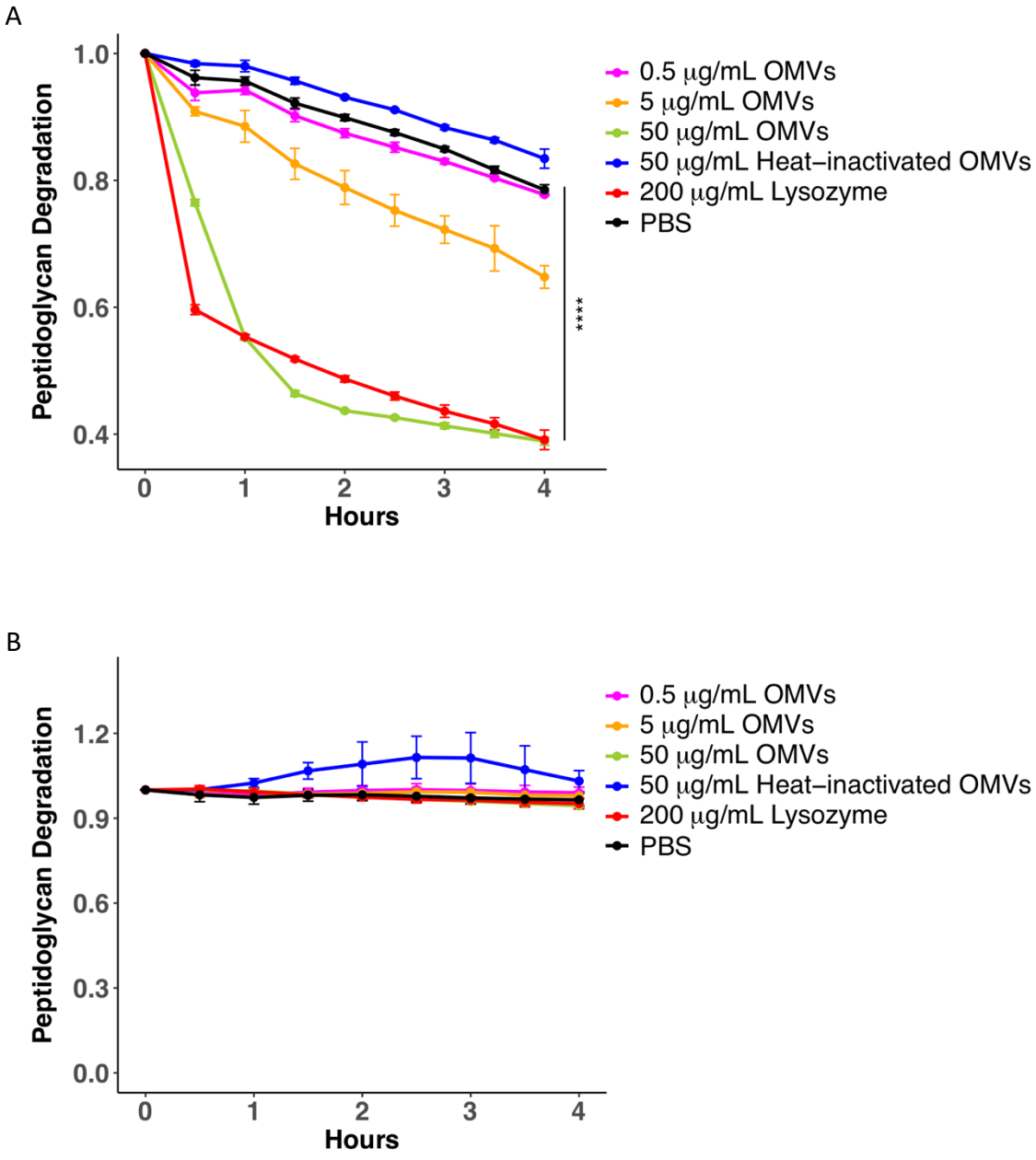
A
Peptidoglycan Degradation
1.0
0.8
0.6
0.4
0
1
2
3
4
Hours
****
0.5 μg/mL OMVs
5 μg/mL OMVs
50 μg/mL OMVs
50 μg/mL Heat−inactivated OMVs
200 μg/mL Lysozyme
PBS
B
Peptidoglycan Degradation
1.2
0.9
0.6
0.3
0.0
0
1
2
3
4
Hours
0.5 μg/mL OMVs
5 μg/mL OMVs
50 μg/mL OMVs
50 μg/mL Heat−inactivated OMVs
200 μg/mL Lysozyme
PBS

Figure 4-1. Evaluation of peptidoglycan degradation by *B. thailandensis* OMVs

Peptidoglycan purified from (**A**) *S. aureus* and (**B**) *S. mutans* was incubated with 0.5, 5, or 50 μg/mL OMVs, 50 μg/mL heat-inactivated OMVs, 200 μg/mL lysozyme (positive control), or PBS (negative control). OD_{450} was read every 30 minutes for 4 hours. Peptidoglycan degradation was indicated by the decrease of OD_{450} and normalized by $1 - (OD_{start} - OD_{time\ point})/OD_{start}$. The results were analyzed using Chi squared test when comparing OMV to control and lysozyme to control, **** $p < 0.0001$.

Figure 4-2

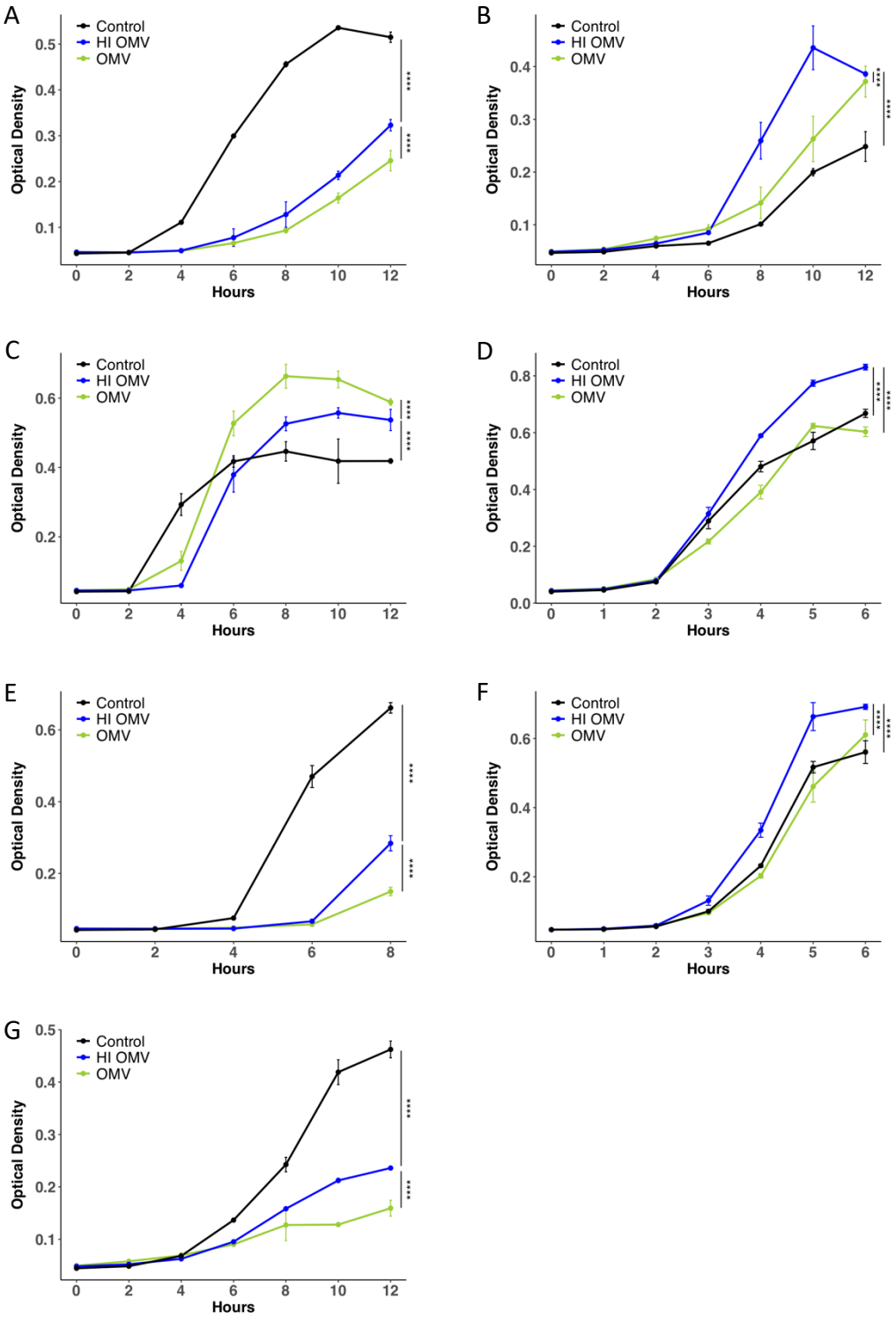

Figure 4-2. Evaluation of heat-inactivated *B. thailandensis* OMVs inhibiting microbial growth in planktonic cultures with representative Gram-negative and Gram-positive bacteria

Overnight cultures of (**A**) *A. baumannii*, (**B**) *P. aeruginosa*, (**C**) *E. coli*, (**D**) *K. pneumoniae*, (**E**) *S. aureus*, (**F**) *E. faecalis*, and (**G**) *S. mutans* were diluted 1:1000 in broth and treated with PBS, 2 μg OMVs, or 2 μg heat-inactivated OMVs in a total volume of 100 μL. OD_{600} was monitored for up to 12 hours. The results were analyzed using Chi squared test, **** $p < 0.0001$.

Figure 4-3

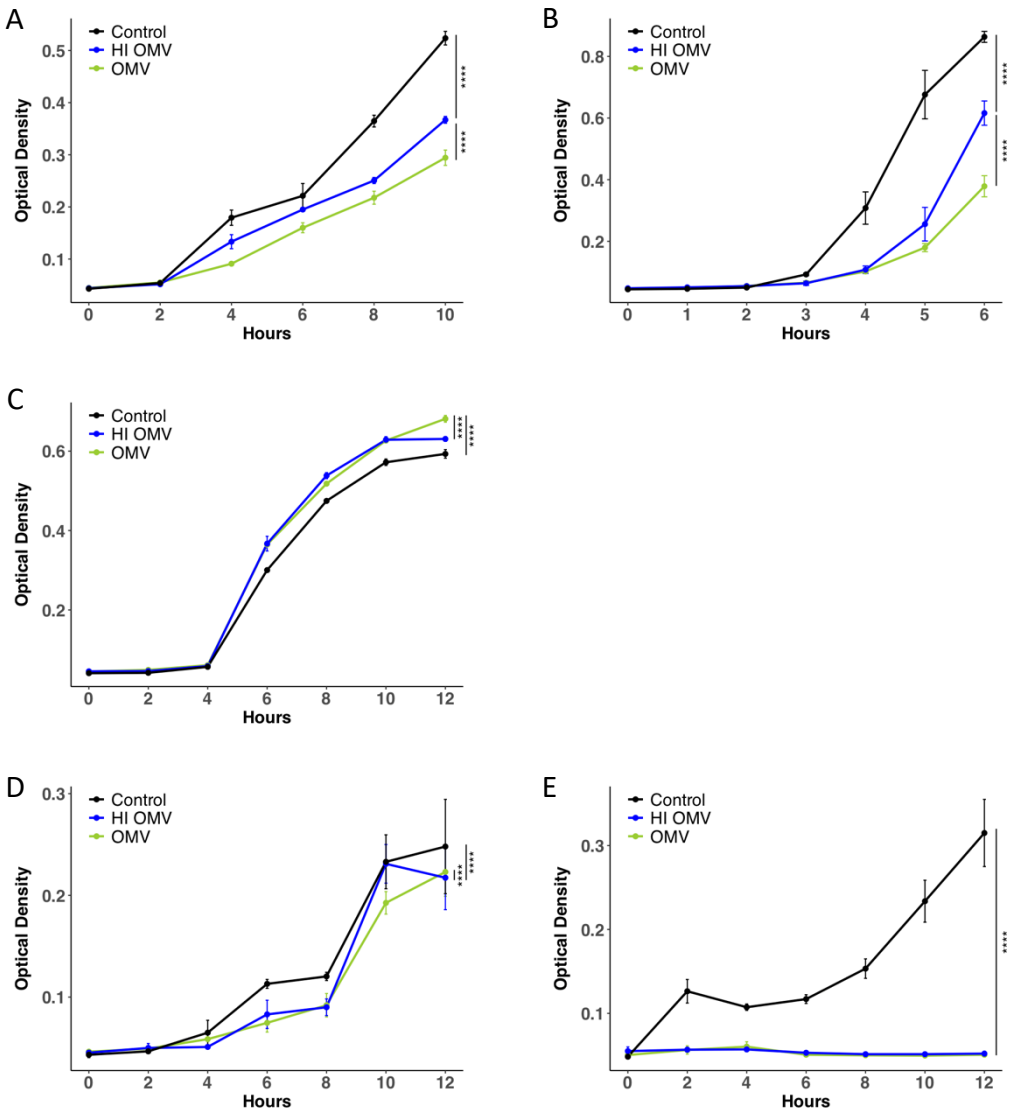
A
Control
HI OMV
OMV
Optical Density
Hours
****
****
B
Control
HI OMV
OMV
Optical Density
Hours
****
****
C
Control
HI OMV
OMV
Optical Density
Hours
****
****
D
Control
HI OMV
OMV
Optical Density
Hours
****
****
E
Control
HI OMV
OMV
Optical Density
Hours
****

Figure 4-3. Evaluation of heat-inactivated *B. thailandensis* OMVs inhibiting microbial growth in planktonic cultures with multidrug-resistant bacteria and fungi

Overnight cultures of (**A**) MDR *A. baumannii*, (**B**) MRSA, (**C**) carbapenem-resistant *K. pneumoniae*, (**D**) *C. albicans*, and (**E**) *C. neoformans* were diluted 1:1000 in broth and treated with PBS, 2 μg OMVs, or 2 μg heat-inactivated OMVs in a total volume of 100 μL. OD_{600} was monitored for up to 12 hours. The results were analyzed using Chi squared test, **** $p < 0.0001$.

Figure 4-4

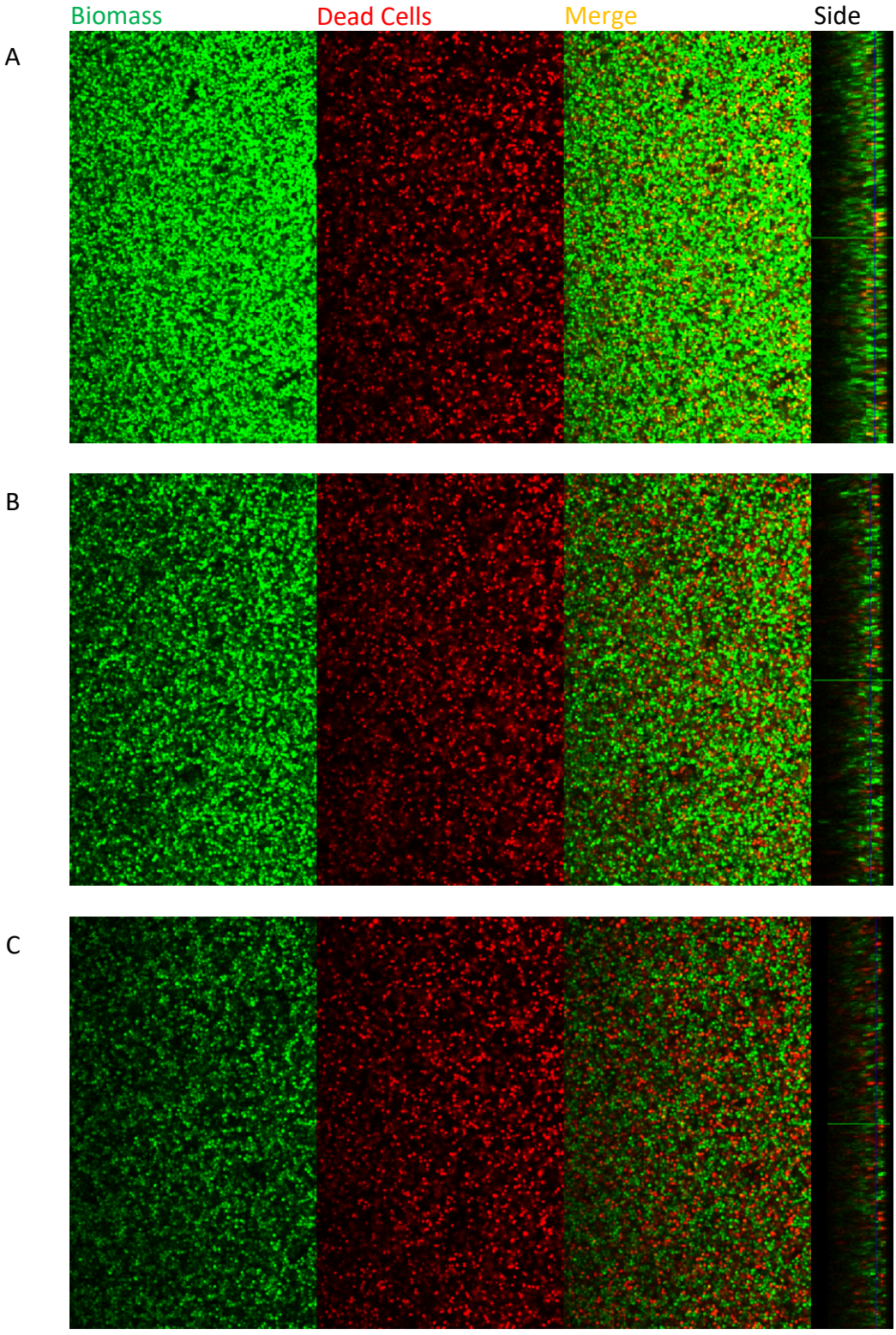

Figure 4-4. The bactericidal and antibiofilm effects of heat-inactivated *B. thailandensis* OMVs against MRSA biofilm analyzed by fluorescent confocal microscopy

MRSA biofilms were grown on chamber-slides in TSB supplemented with 0.5% glucose for two days before treated with (**A**) water, (**B**) 100 μg/mL heat-inactivated OMVs, or (**C**) 100 μg/mL native OMVs for another 4 hours. Staining with LIVE/DEAD *Bac*Light fluorescent dye (SYTO 9/propidium iodide), biofilms were subjected to optical dissection using Zeiss LSM 700 laser scanning confocal microscope. At least seven image stacks were acquired at 400 x magnification from each well. Presented layers were 5 μm above the substratum in each image stacks. Green: total biomass. Red: dead cells. Side bars indicate the thickness of the biofilms.

Figure 4-5

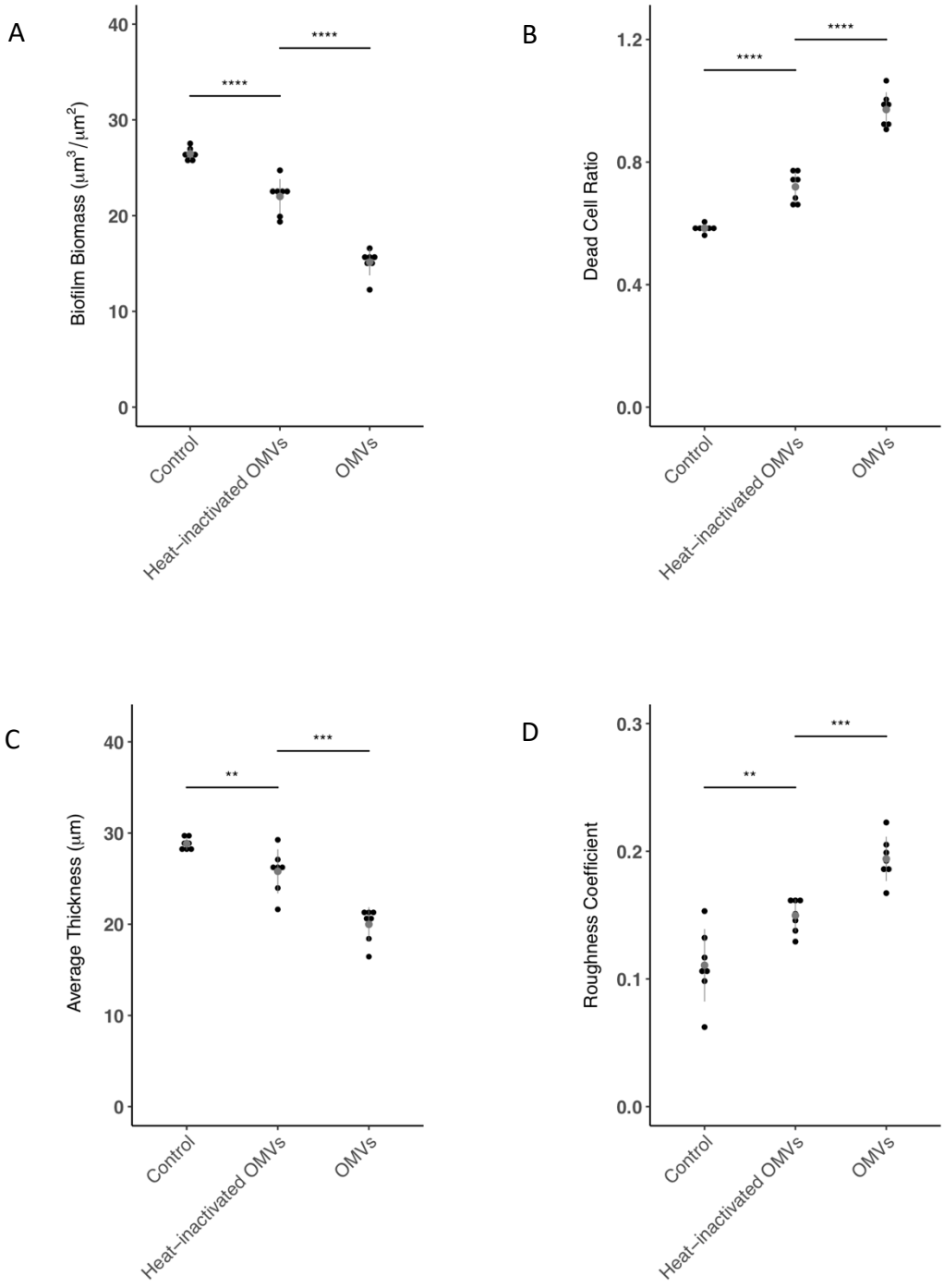
A
Biofilm Biomass (μm³/μm²)
40
30
20
10
0
****
****
Control
Heat−inactivated OMVs
OMVs
B
Dead Cell Ratio
1.2
0.8
0.4
0.0
****
****
Control
Heat−inactivated OMVs
OMVs
C
Average Thickness (μm)
40
30
20
10
0
**
***
Control
Heat−inactivated OMVs
OMVs
D
Roughness Coefficient
0.3
0.2
0.1
0.0
**
***
Control
Heat−inactivated OMVs
OMVs

Figure 4-5. Post-acquisition analyses of fluorescent images of the MRSA biofilms treated with heat-inactivated *B. thailandensis* OMVs

Post-acquisition analyses were performed using COMSTAT 2.0. Biofilms treated with heat-inactivated OMVs, native OMVs, or control were compared in (**A**) biofilm biomass, (**B**) dead cell ratio, (**C**) average thickness, and (**D**) roughness coefficient. Roughness coefficients of the biofilms were calculated with COMSTAT 2.0 as an indication of biofilm healthiness and integrity. The results were analyzed using unpaired two-sample t-test. (** $p < 0.01$, *** $p < 0.001$, **** $p < 0.0001$)

Figure 4-6

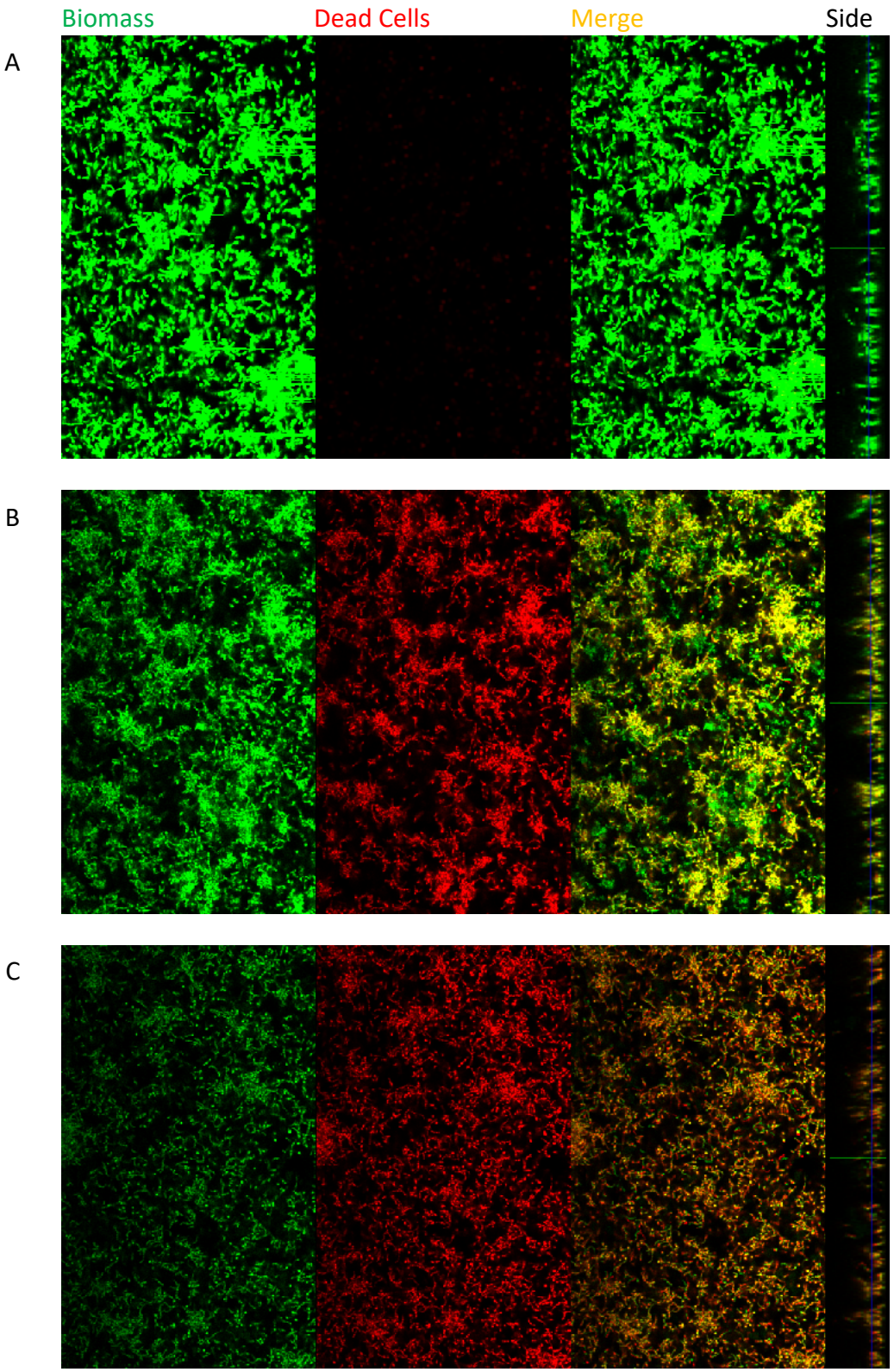

Figure 4-6. The bactericidal and antibiofilm effects of heat-inactivated *B. thailandensis* OMVs against *S. mutans* biofilm analyzed by fluorescent confocal microscopy

S. mutans biofilms were grown anaerobically on chamber-slides in BMGS medium for 24 hours before treated with (**A**) PBS, (**B**) 100 μg/mL heat-inactivated OMVs, or (**C**) 100 μg/mL native OMVs for another 24 hours. Staining with LIVE/DEAD *Bac*Light fluorescent dye (SYTO 9/propidium iodide), biofilms were subjected to optical dissection using Zeiss LSM 700 laser scanning confocal microscope. At least seven image stacks were acquired at 400 x magnification from each well. Presented layers were 5 μm above the substratum in each image stacks. Green: total biomass. Red: dead cells. Side bars indicate the thickness of the biofilms.

Figure 4-7

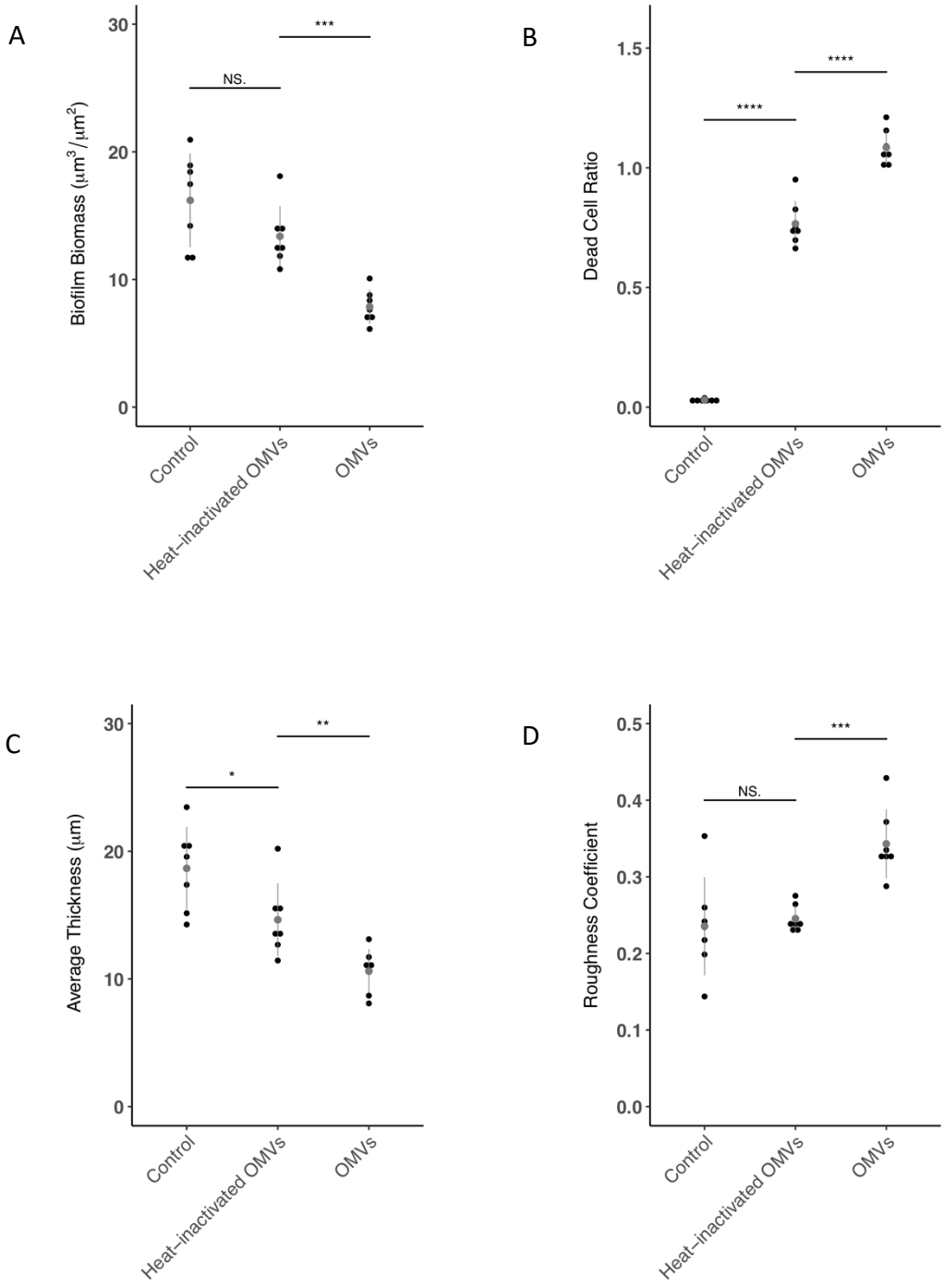
A
Biofilm Biomass (μm³/μm²)
30
20
10
0
NS.
***
Control
Heat–inactivated OMVs
OMVs
B
Dead Cell Ratio
1.5
1.0
0.5
0.0
****
****
Control
Heat–inactivated OMVs
OMVs
C
Average Thickness (μm)
30
20
10
0
*
**
Control
Heat–inactivated OMVs
OMVs
D
Roughness Coefficient
0.5
0.4
0.3
0.2
0.1
0.0
NS.
***
Control
Heat–inactivated OMVs
OMVs

Figure 4-7. Post-acquisition analyses of fluorescent images of the *S. mutans* biofilms treated with heat-inactivated *B. thailandensis* OMVs

Post-acquisition analyses were performed using COMSTAT 2.0. Biofilms treated with heat-inactivated OMVs, native OMVs, or control were compared in (**A**) biofilm biomass, (**B**) dead cell ratio, (**C**) average thickness, and (**D**) roughness coefficient. Roughness coefficients of the biofilms were calculated with COMSTAT 2.0 as an indication of biofilm healthiness and integrity. The results were analyzed using unpaired two-sample t-test. (* $p < 0.05$, ** $p < 0.01$, *** $p < 0.001$, **** $p < 0.0001$)

Figure 4-8

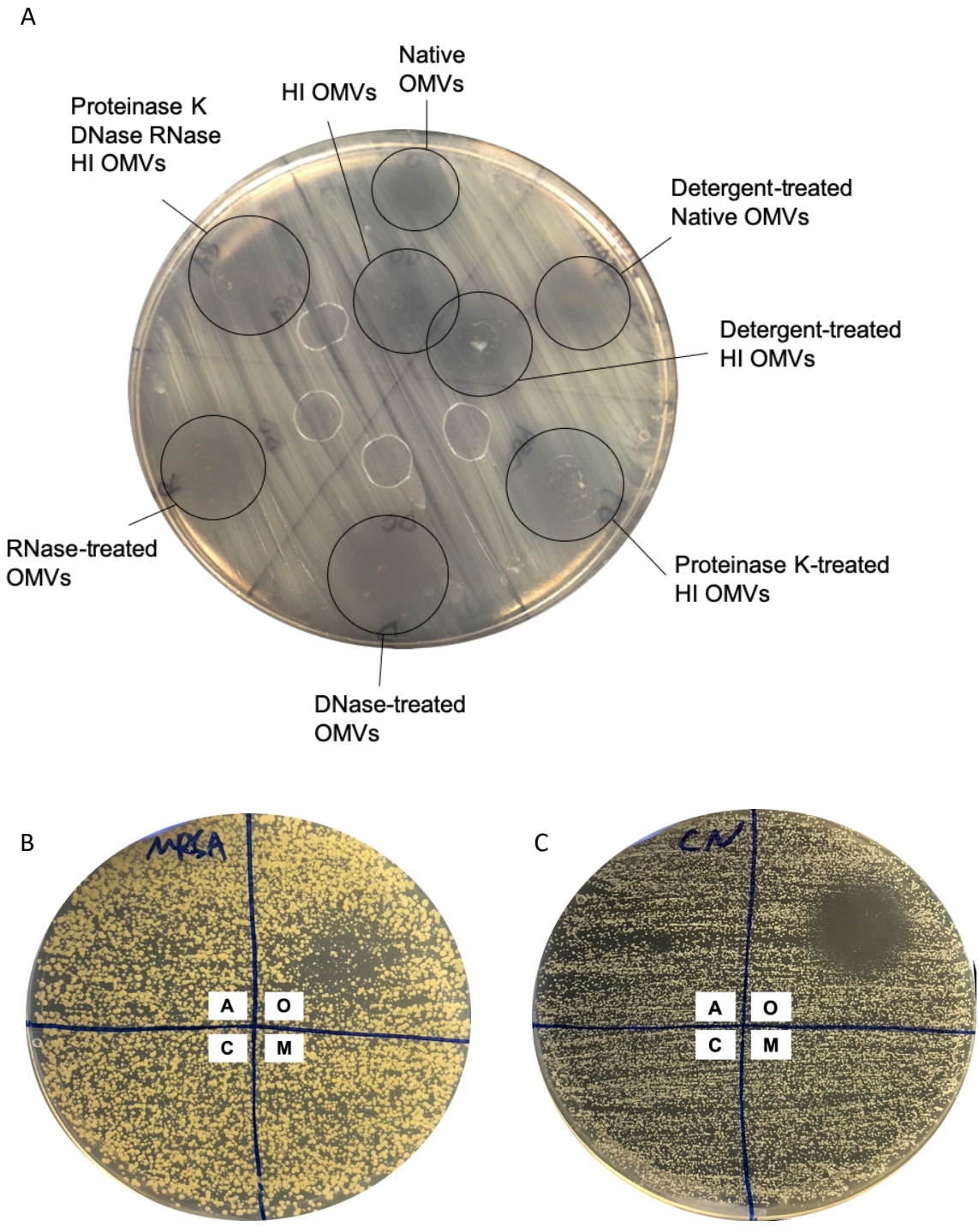
A
Native OMVs
HI OMVs
Proteinase K DNase RNase HI OMVs
Detergent-treated Native OMVs
Detergent-treated HI OMVs
RNase-treated OMVs
Proteinase K-treated HI OMVs
DNase-treated OMVs
B
MRSA
A
O
C
M
C
CN
A
O
C
M

Figure 4-8. Chemical characterization of the heat-stable antimicrobial components within *B. thailandensis* OMVs

The heat-stable antimicrobial components were characterized for their chemical properties. (**A**) Native OMVs were separately treated with 40 mM CHAPS (detergent), 2 mg/mL proteinase K, 0.1 u/μL DNase, 1 mg/mL RNase, or the combination before heat-inactivation and spot plated onto agar streaked with MRSA. Their antimicrobial activity was compared to the non-treated heat-inactivated and native OMVs. The treatments alone did not inhibit MRSA. (**B**) Heat-inactivated OMVs were extracted with MeOH/$CHCl_3$ mix (1:2, v/v). Aqueous phase (A), organic phase (O), and middle phase (M) with incomplete separation were desiccated in vacuo followed by resuspension in 20 μL of 20% MeOH. Ten microliters from each suspension was spot-plated against (**B**) MRSA and (**C**) *C. neoformans* to test for antimicrobial activity. Twenty percent MeOH alone (C) did not inhibit MRSA or *C. neoformans*.

Figure 4-9

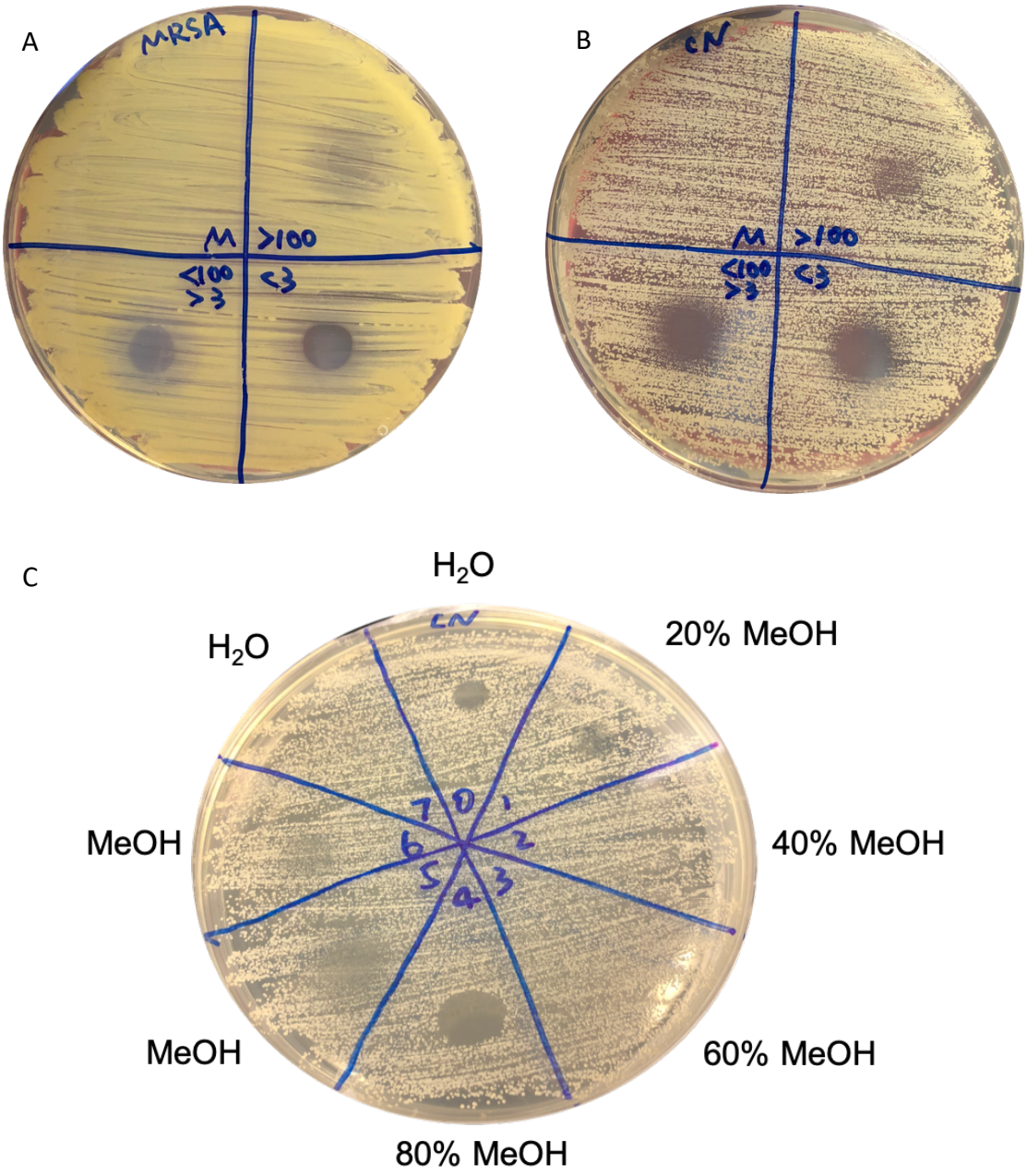
A
MRSA
M
>100
<100
>3
<3
B
CN
M
>100
<100
>3
<3
C
H2O
H2O
20% MeOH
MeOH
40% MeOH
MeOH
60% MeOH
80% MeOH
CN
0
1
2
3
4
5
6
7

Figure 4-9. Characterization of the heat-stable antimicrobial components within *B. thailandensis* OMVs for their sizes and hydrophobicity

The sizes of the heat-stable antimicrobial components against (**A**) MRSA and (**B**) *C. neoformans* were characterized by size exclusion filtration with 3 kDa and 100 kDa cutoff. M: solvent control. (**C**) The organic extracts of OMVs were separated with solid phase extraction. Fractions eluted from C18 cartridge with increased concentrations of MeOH in water were collected and desiccated in vacuo followed by resuspension in 20 μL of 20% MeOH before screening for antimicrobial activity against *C. neoformans*.

Figure 4-10

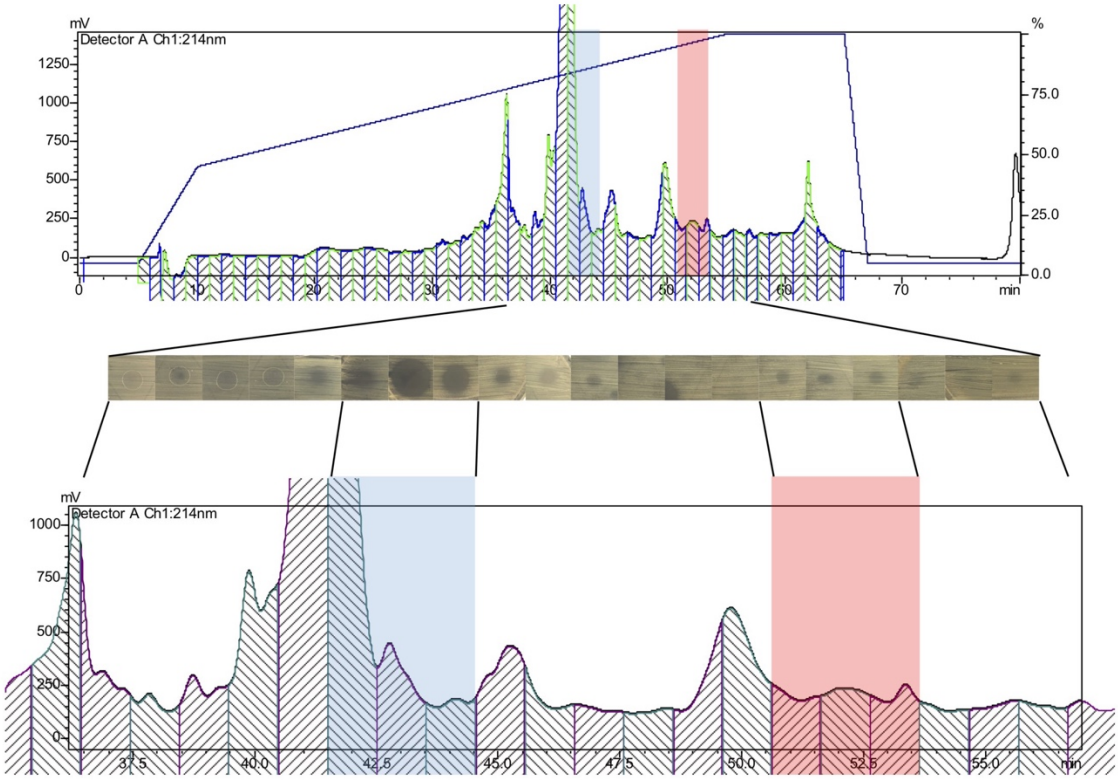
mV
Detector A Ch1:214nm
%
1250
1000
750
500
250
0
75.0
50.0
25.0
0.0
0
10
20
30
40
50
60
70
min
mV
Detector A Ch1:214nm
1000
750
500
250
0
37.5
40.0
42.5
45.0
47.5
50.0
52.5
55.0
min

Figure 4-10. Identification of HPLC fractions with antimicrobial activity

Individual 1-minute fractions from HPLC were screened for antimicrobial activity against MRSA using a Kirby Bauer-like method. Fractions were collected and desiccated in vacuo followed by resuspension in 20 μL of 20% MeOH. Ten microliters from each suspension was spot-plated against MRSA to screen for antimicrobial activity. Twenty percent MeOH alone did not inhibit MRSA shown in **Figure 4-8B**.

Figure 4-11

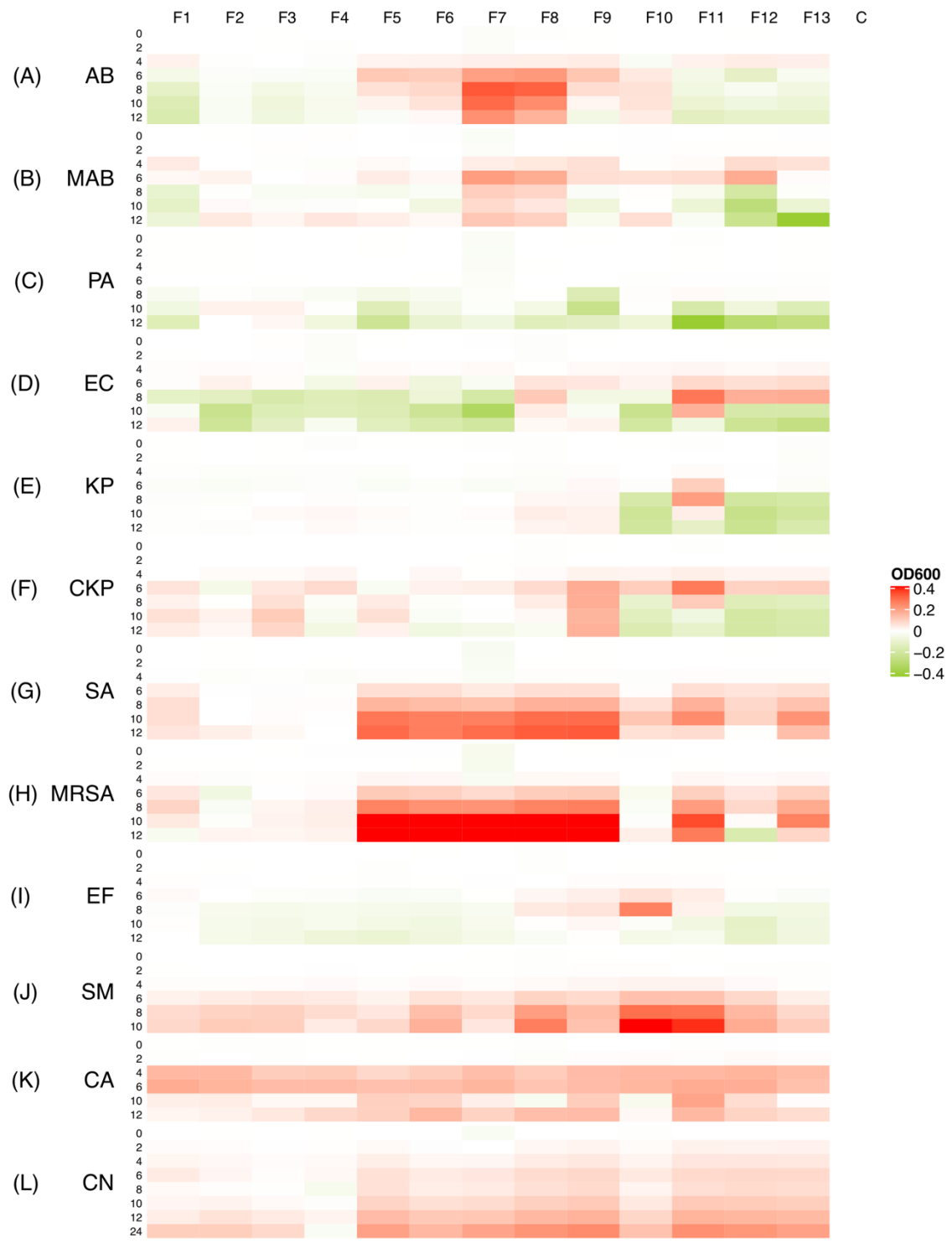
F1
F2
F3
F4
F5
F6
F7
F8
F9
F10
F11
F12
F13
C
(A) AB
(B) MAB
(C) PA
(D) EC
(E) KP
(F) CKP
(G) SA
(H) MRSA
(I) EF
(J) SM
(K) CA
(L) CN
OD600
0.4
0.2
0
−0.2
−0.4

Figure 4-11. Evaluation of HPLC fractions for broad-spectrum antimicrobial activity

Broth cultures of (**A**) *A. baumannii*, (**B**) MDR *A. baumannii*, (**C**) *P. aeruginosa*, (**D**) *E. coli*, (**E**) *K. pneumoniae*, (**F**) carbapenem-resistant *K. pneumoniae*, (**G**) *S. aureus*, (**H**) MRSA, (**I**) *E. faecalis*, (**J**) *S. mutans*, (**K**) *C. albicans*, and (**L**) *C. neoformans* were inoculated with HPLC fractions. OD_{600} measurements were performed every 2 hours for 12 hours. The difference in OD_{600} between fraction-treated cultures and non-treated cultures at each time point was plotted as a heat map ($OD_{control}$ - $OD_{treated}$). F1: 6-11 mins, F2: 12-17 mins, F3: 18-23 mins, F4: 24-29 mins, F5: 30-35 mins, F6: 36-41 mins, F7: 42-44 mins, F8: 45-46 mins, F9: 47-48 mins, F10: 49-50 mins, F11: 51-53 mins, F12: 54-59 mins, F13: 60-65 mins, C: control.

Figure 4-12

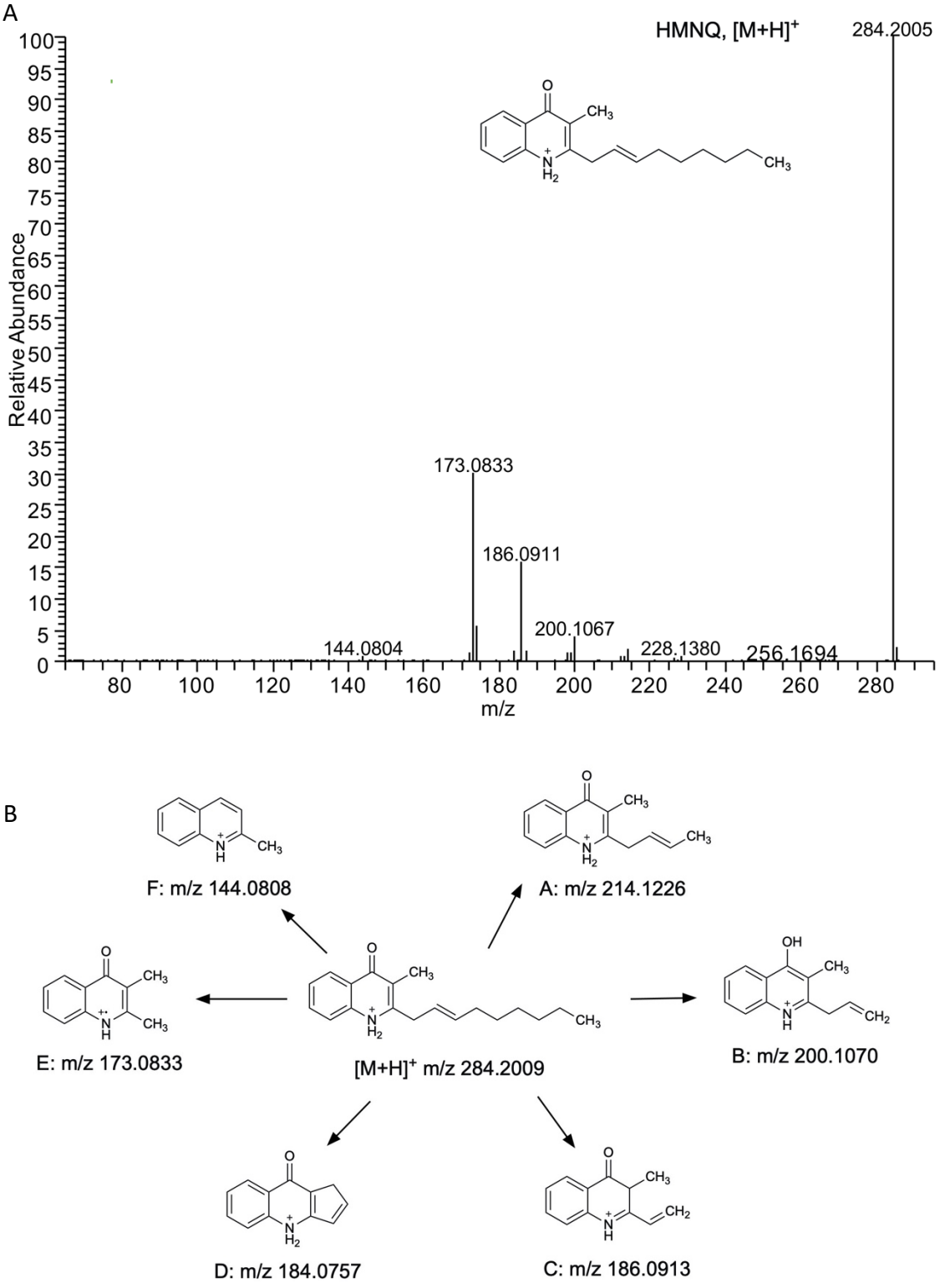
A
HMNQ, [M+H]+
284.2005
Relative Abundance
173.0833
186.0911
200.1067
144.0804
228.1380
256.1694
m/z
B
F: m/z 144.0808
A: m/z 214.1226
E: m/z 173.0833
[M+H]+ m/z 284.2009
B: m/z 200.1070
D: m/z 184.0757
C: m/z 186.0913

Figure 4-12. HMNQ (4-hydroxy-3-methyl-2-(2-non-enyl)-quinoline) identified with mass spectrometry

(**A**) CID spectrum of HMNQ. (**B**) MS/MS fragmentation patterns of HMNQ used to elucidate the structure.

Figure 4-13

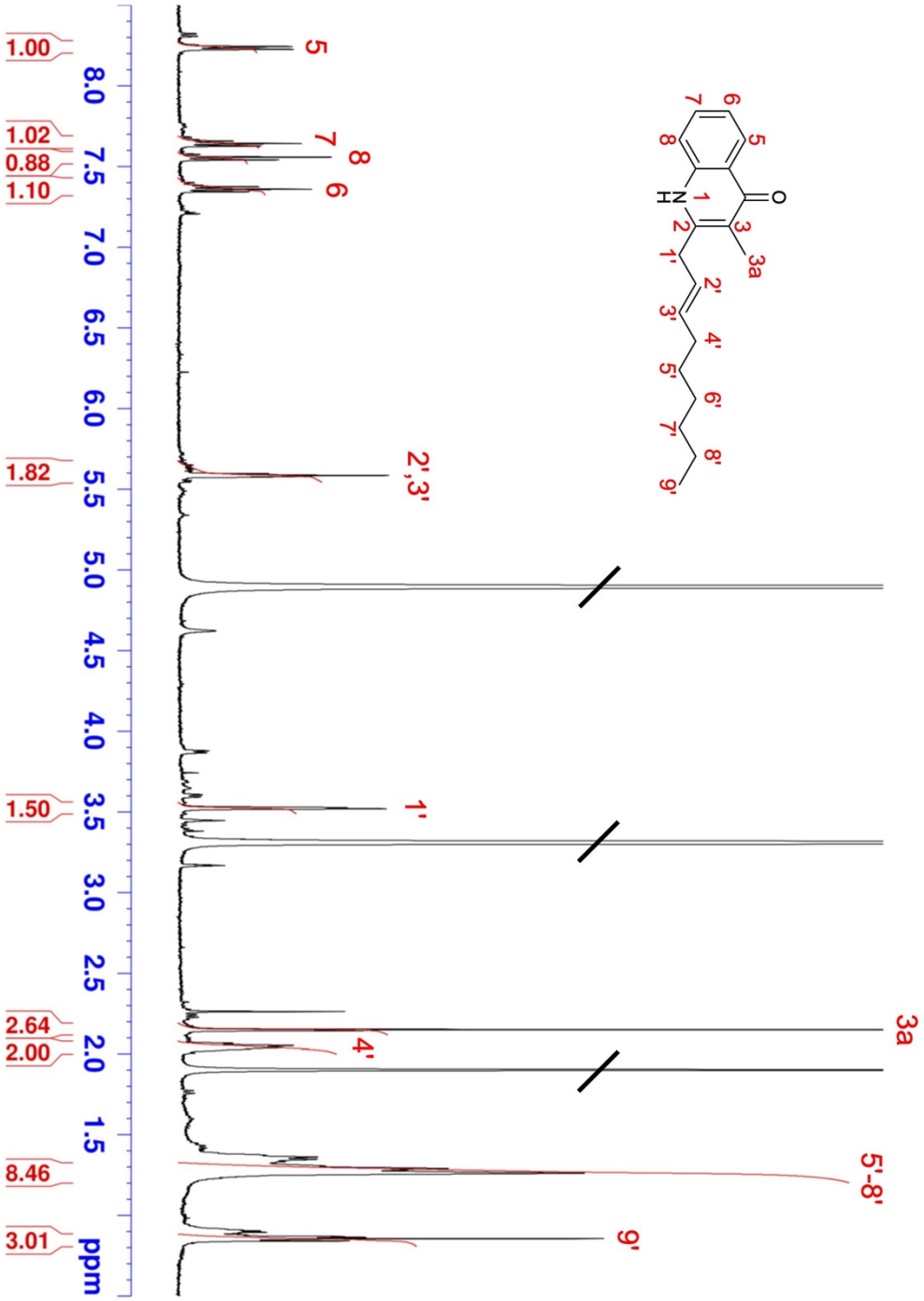
1.00
1.02
0.88
1.10
1.82
1.50
2.64
2.00
8.46
3.01
ppm
8.0
7.5
7.0
6.5
6.0
5.5
5.0
4.5
4.0
3.5
3.0
2.5
2.0
1.5
5
7
8
6
2',3'
1'
4'
3a
5'-8'
9'
N
H
O

Figure 4-13. ^{1}H NMR spectrum of HMNQ

HMNQ was dissolved in deuterated methanol for NMR analysis. The number scheme for HMNQ and the assignment for each proton are shown.

Figure 4-14

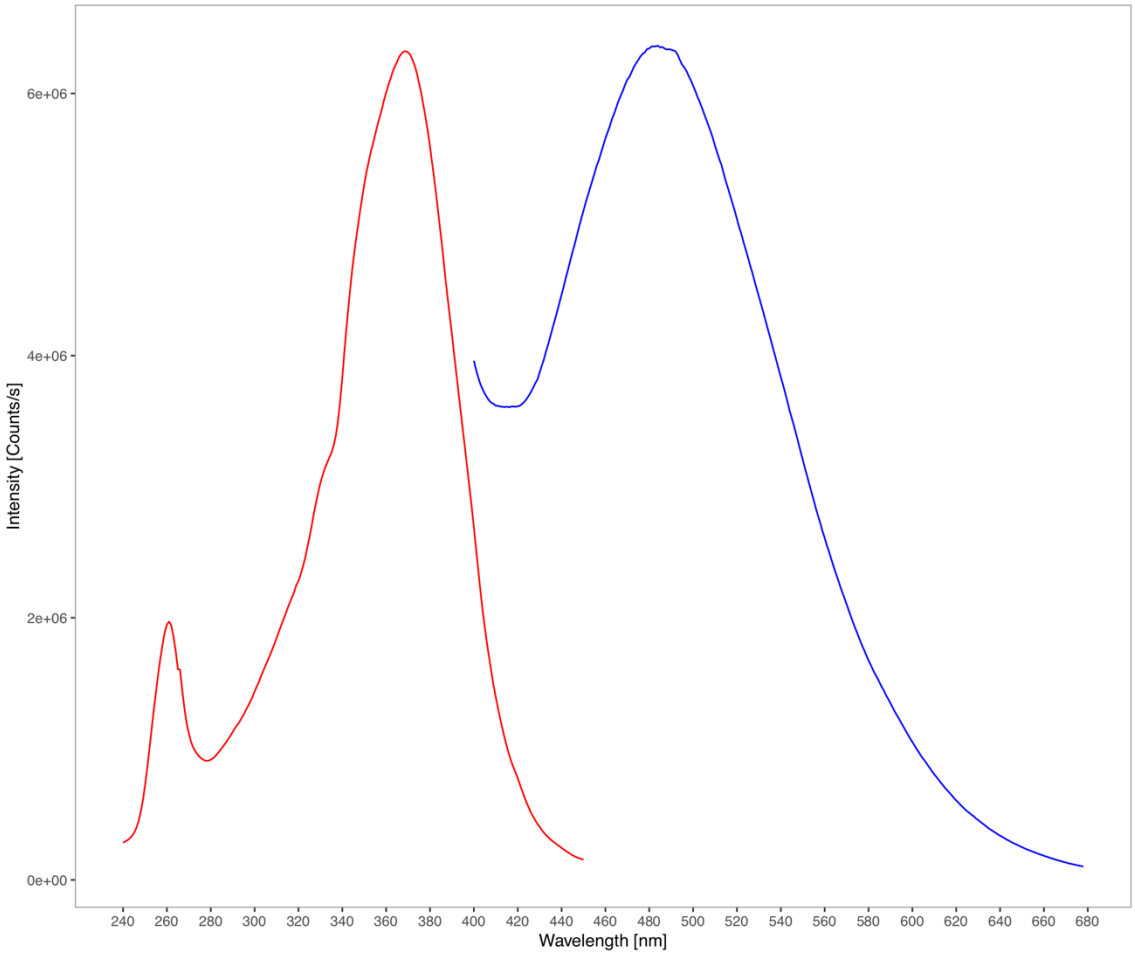
6e+06
4e+06
2e+06
0e+00
Intensity [Counts/s]
240 260 280 300 320 340 360 380 400 420 440 460 480 500 520 540 560 580 600 620 640 660 680
Wavelength [nm]

Figure 4-14. Fluorescence excitation and emission spectra of HMNQ

Purified HMNQ was dissolved in MeOH for fluorescence measurements. Red: excitation spectrum peaked around 370 nm. Blue: emission spectrum peaked around 480 nm.

Figure 4-15

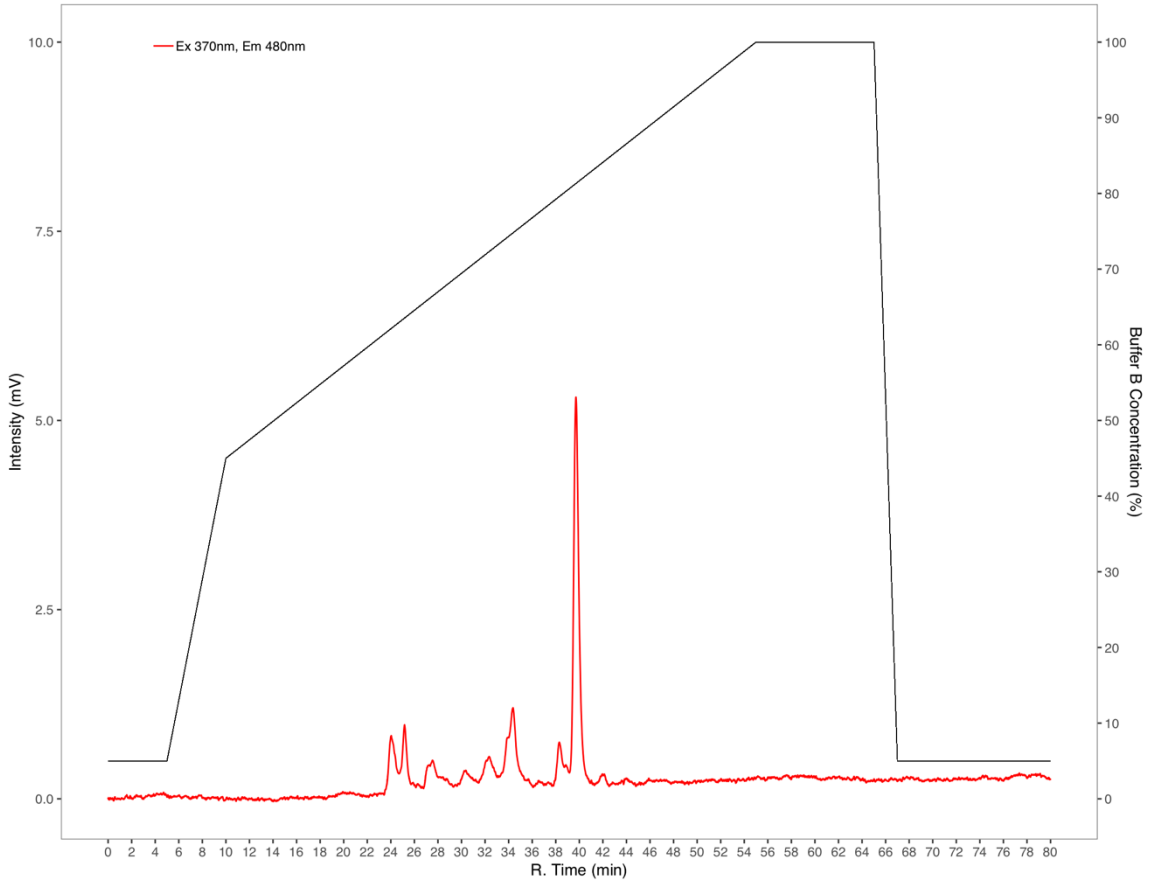
Ex 370nm, Em 480nm
Intensity (μV)
Buffer B Concentration (%)
R. Time (min)
10.0
7.5
5.0
2.5
0.0
100
90
80
70
60
50
40
30
20
10
0
0 2 4 6 8 10 12 14 16 18 20 22 24 26 28 30 32 34 36 38 40 42 44 46 48 50 52 54 56 58 60 62 64 66 68 70 72 74 76 78 80

Figure 4-15. Representative HPLC spectrum of purified *B. thailandensis* OMVs for HMNQ detected at excitation 370 nm, emission 480 nm

Purified OMVs (100 μg) were first extracted with MeOH/$CHCl_3$ mix (1:2, v/v). The organic extracts were separated with solid phase extraction. Fractions with antimicrobial activity eluted from C18 cartridge with increased concentrations of MeOH in water were collected and concentrated before HPLC. The HPLC was carried out with a C2 column and a fluorescence detector. Materials were eluted with a flow of 0.5 mL/min and a gradient of 5% MeOH in H_2O to 100% MeOH (with 50 mM HN_4OAc, pH 5.6) over 80 mins.

Figure 4-16

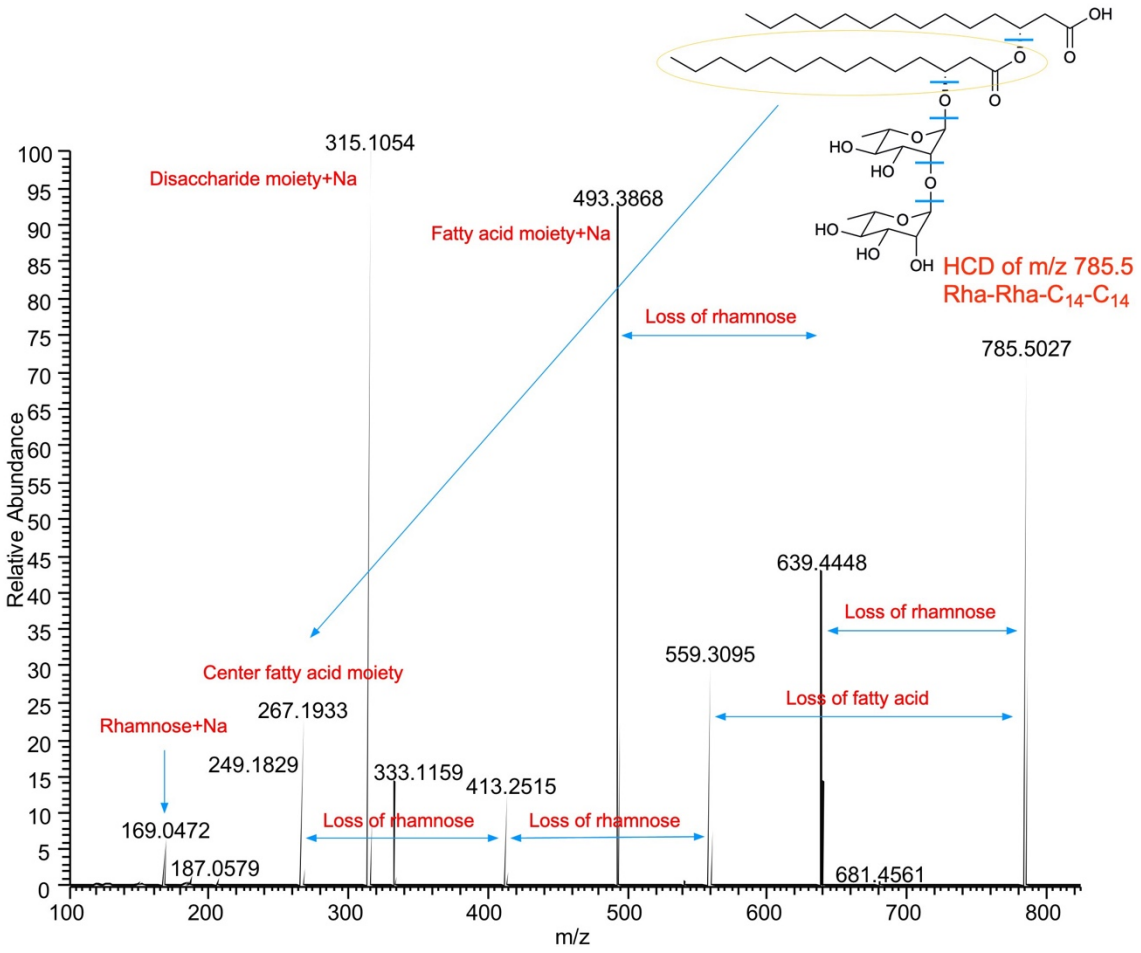
315.1054
Disaccharide moiety+Na
493.3868
Fatty acid moiety+Na
Loss of rhamnose
785.5027
639.4448
Loss of rhamnose
559.3095
Loss of fatty acid
Center fatty acid moiety
267.1933
Rhamnose+Na
249.1829
333.1159
413.2515
169.0472
Loss of rhamnose
Loss of rhamnose
187.0579
681.4561
Relative Abundance
m/z
HCD of m/z 785.5
Rha-Rha-C14-C14

Figure 4-16. CID spectrum of rhamnolipid (Rha-Rha-C_{14}-C_{14})

Di-rhamnolipids identified from *B. thailandensis* OMVs are glycolipidic surfactants with two rhamnoses linked through a β-glycosidic bond to two 3-hydroxyfatty acids with C_{14} acyl chain. Fragmentations of di-rhamnolipids were shown in the MS/MS spectrum.

Figure 4-17

A

Crude OMVs
$(NH_4)_2SO_4$

Organic extraction: MeOH:$CHCl_3$
(1:2, v/v, 45C)

SPE C18, 80-100% MeOH
Concentrate in pure MeOH

C2 HPLC
Injection: 70 ul MeOH
A: H_2O, 50 mM NH_4OAc
B: 100% MeOH, 50 mM NH_4OAc

42-44 min: 84-87%, 0.6 mg
51-53 min: 95-98%, 3.3 mg
LCMS-GU

HMNQ: m/z 283
Rhamnolipid: m/z 763.5

B

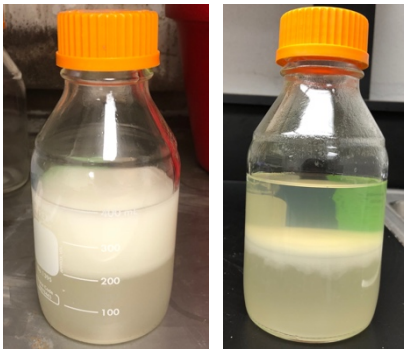

C

D

Figure 4-17. Illustration of HMNQ and rhamnolipid purification from *B. thailandensis* OMVs

(**A**) Purification and identification process of HMNQ and rhamnolipid. To increase the yield, crude OMVs from ammonium sulfate precipitation instead of purified OMVs were used as starting material. OMVs in water were first extracted with organic solvent (**B**). The bottom organic phase was concentrated (**C**) and further separated with solid phase extraction. Fractions eluted from C18 cartridge with 80%, and 100 % MeOH in water were collected and concentrated (**D**) before C2 HPLC with a flow of 0.5 mL/min and a gradient of 5% MeOH in H_2O to 100% MeOH (with 50 mM HN_4OAc, pH 5.6) over 80 mins. Materials eluted from 42-44 mins and 51-53 mins were collected for MS/MS analysis which revealed the identities of HMNQ with m/z 283, and rhamnolipid with m/z 763.5.

Table 4-1

Accession Number	Protein	kDa	Description
685746792	LysM domain protein	25.8	Protein domain associated with the binding of peptidoglycan[208]
644994812	N-acetylmuramoyl-L-alanine amidase	55.6	Soluble N-acetylmuramoyl-L-Ala amidase (AmiC)[140]
685744463	Transglycosylase SLT domain protein	72.3	Soluble lytic transglycosylase[209]
497592087	Murein transglycosylase (mltA)	40.1	Membrane-bound lytic transglycosylase (mltA)[210]
685745036	Lytic murein transglycosylase B	44.5	Transglycosylase (mltB) that has both a soluble and membrane bound form[211]
584094633	N-acetylmuramoyl-L-alanine amidase AmiD	32.7	Membrane bound N-acetylmuramoyl-L-alanine amidase (AmiD)[212]
DM82_RS07650 gi	β-lytic endopeptidase	30.0	β-lytic endopeptidase in the M23 family[213]
BTL_RS12275 gi	β-lytic endopeptidase	24.1	β-lytic endopeptidase in the M23 family[213]
BTH_I2668 gi	β-N-acetylglucosaminidase	74.9	Potential β-N-acetylglucosaminidase[214]

Table 4-1. Peptidoglycan hydrolases identified with LCMS that are present in *B. thailandensis* OMVs

Table 4-2

Ion	Formula	m/z (obs)	m/z (calc)	Δppm	Relative intensity
F	$[C10\ H9\ N + H]^+$	144.0805	144.0808	1.9	0.78
	$[C11\ H9\ O\ N + H]^+$	172.0756	172.0757	0.5	1.42
E	$[C11\ H11\ O\ N]^+$	173.0833	173.0835	1.2	30.39
	$[C11\ H11\ O\ N + H]^+$	174.0910	174.0913	2.0	5.47
D	$[C12\ H9\ O\ N + H]^+$	184.0754	184.0757	1.6	1.59
C	$[C12\ H11\ O\ N + H]^+$	186.0911	186.0913	1.3	15.85
	$[C13\ H11\ O\ N + H]^+$	198.0911	198.0913	1.2	1.34
B	$[C13\ H13\ O\ N + H]^+$	200.1067	200.1070	1.5	3.96
A	$[C14\ H15\ O\ N + H]^+$	214.1225	214.1226	0.7	1.74
	$[C15\ H17\ O\ N + H]^+$	228.1382	228.1383	0.4	0.82
	$[C16\ H19\ O\ N + H]^+$	242.1534	242.1539	2.2	0.27
$[M+H]^+$	$[C19\ H25\ O\ N + H]^+$	284.2005	284.2009	1.4	100

Table 4-2. MS/MS data for HMNQ identified in this study

Table 4-3

Ion	Formula	m/z (obs)	m/z (calc)	Δppm	Relative intensity
Rha (b ion)	$[C6\ H10\ O4 + Na]^+$	169.0472	169.0471	-0.41	8.2
Rha (c ion)	$[C6\ H12\ O5 + Na]^+$	187.0579	187.0577	-1.10	1.38
C_{14} lipid	$[C14\ H28\ O3 + Na]^+$	267.1932	267.1931	-0.50	25.66
Rha-Rha (b ion)	$[C12\ H20\ O8 + Na]^+$	315.1052	315.1050	-0.51	100
Rha-Rha (c ion)	$[C12\ H22\ O9 + Na]^+$	333.1158	333.1156	-0.59	14.35
Internal fragment of Rha-C_{14} lipid	$[C20\ H38\ O7 + Na]^+$	413.2513	413.2510	-0.79	9.58
Loss of Rha-Rha	$[C28\ H54\ O5 + Na]^+$	493.3867	493.3863	-0.72	68.94
M-C_{14}	$[C26\ H48\ O11+Na]^+$	559.3091	559.3089	-0.39	17.69
M-Rha	$[C34\ H64\ O9 + Na]^+$	639.4447	639.4443	-0.70	16.35
$[M+Na]^+$	$[C40\ H74\ O13 + Na]^+$	785.5027	785.5022	-0.68	13.1

Table 4-3. MS/MS data for rhamnolipid identified in this study

CHAPTER 5: The antimicrobial efficacy, safety, and wound healing capacity of HMNQ and rhamnolipid assessed *in vitro* and *in vivo*

Introduction

4-Hydroxy-2-alkylquinolines (HAQs), especially 3,4-dihydroxy-2-heptylquinoline (PQS), were originally characterized in *P. aeruginosa* and recognized as a class of quorum sensing molecules that exhibit numerous functions[109]. Besides regulating virulence factors, PQS has been shown to modulate biofilm formation in bacteria and yeast[189]. In addition, PQS may have direct immunomodulatory effects on host cells[215]. Specifically, PQS has been shown to reduce the NFκB binding to its binding sites and the expression of downstream genes, suppressing host innate immune responses[216]. It also inhibited cell proliferation and the release of interleukin-2 in human peripheral blood mononuclear cells following mitogen stimulation[217]. In another study, PQS decreased the production of interleukin-12 by LPS-stimulated bone marrow-derived dendritic cells and changed the maturation pattern of stimulated dendritic cells away from a proinflammatory Th1 response, therefore decreasing the antibacterial adaptive immune response[218].

P. aeruginosa produces various HAQs, which are synthesized and regulated by the *pqsABCDE* operon. They are characterized by the presence of a hydrogen or hydroxyl group at the 3 position, an *N*-oxide group in place of the quinoline nitrogen, and an unsaturation on the alkyl side chain[219]. The presence of a homologous operon, *hmqABCDEFG*, was reported in *Burkholderia* species, including *B. thailandensis*, *B. pseudomallei*, and *B. ambifaria*[103]. Twenty-nine different HAQ derivatives have been shown to be produced by 3 out of 11 related *Burkholderia* species tested[103]. Different from

P. aeruginosa, *Burkholderia* HAQs are mostly methylated at the 3 position with an unsaturated aliphatic side chain[103]. It has been recently reported that *B. thailandensis* HAQ derivatives are quorum sensing signals with synergistic effects that could inhibit *E. coli* growth in planktonic cultures[103,107]. HMNQ, the dominant form of HAQs produced by *B. thailandensis*, was shown to function as an ionophore and to disrupt proton motive force and inhibit pyrimidine biosynthesis of other bacteria[107]. In the current study, we examined the spectrum of HMNQ antimicrobial activity by screening for growth inhibition of various microbial species. Considering the similarity of HMNQ to PQS, the antibiofilm activity of HMNQ was also evaluated. Additionally, we characterized the immunomodulatory effects of HMNQ using a NFκB reporter macrophage cell line.

Rhamnolipids are glycolipidic surfactants with up to two rhamnoses (mono or di-rhamnolipids) linked through a β-glycosidic bond to up to two 3-hydroxyfatty acids with various acyl chain lengths[110]. Rhamnolipids are well studied in *P. aeruginosa*, which predominantly produces short chain rhamnolipids (Rha-Rha-C_{10}-C_{10}), for their applications in pharmaceutical, agricultural, chemical, cosmetic and food industries[111]. Notably, a previous study showed that the addition of rhamnolipids increased the solubility and bioactivity of PQS implying the role of rhamnolipids as a PQS solubilizing factor in *P. aeruginosa*[220]. Recent studies revealed that rhamnolipids are also produced by the non-pathogenic *B. thailandensis,* predominantly in a form with longer fatty acid chains (Rha-Rha-C_{14}-C_{14}), which may provide additional industrial applications[102,112]. The antimicrobial activities of rhamnolipids have also been previously characterized against a variety of microbes including *Serratia, Enterobacter, Klebsiella, Bacillus, Staphylococcus,* and *Mycobacterium* and a range of fungal species, but not any yeast[221,222]. Rhamnolipids

promote the swarming motility and dispersion of *P. aeruginosa* cells from the biofilm[115,223]. Their antibiofilm activities have been shown against many bacterial species including *Bacillus subtilis, Salmonella typhimurium*, *Bordetella bronchiseptica*, and *S. mutans*[113,224-226]. Interestingly, a previous study showed that a specific form of rhamnolipid, di-rhamnolipid BAC-3, accelerated wound closure in mice when applied to full-thickness burn wounds[227]. Histologic comparisons revealed that rhamnolipid significantly decreased collagen content, which led to less scar tissue formation, in rat burn wounds compared to the vehicle control[227]. Moreover, a recent study demonstrated that rhamnolipid reduced scar tissue by targeting pathological myofibroblasts in rabbits[228]. Another study reported that application of rhamnolipid promoted healing of a chronic decubitus ulcer in an elderly, debilitated patient[229].

In this chapter, we characterized the safety, antimicrobial efficacy, and wound healing capacity of HMNQ and rhamnolipid in a murine wound infection model. This full-thickness splinted punch wound model approximates wound healing in humans by integration of a wound splinted using sutured silicon torus to prevent skin contraction during rodent wound healing[230] This forces re-epithelialization and the formation of granulation tissue, which are similar to what occurs in humans[231,232]. Full-thickness wounds are infected with bioluminescent bacteria, which allows tracking both infection progression and wound healing in each mouse over time and decreases the number of mice needed for a particular study. Results from these experiments may elucidate novel clinical or industrial applications for HMNQ and rhamnolipid.

Materials and Methods

Bacterial strains and growth conditions

Acinetobacter baumannii, multidrug-resistant *Acinetobacter baumannii, Pseudomonas aeruginosa* PAO1, *Staphylococcus aureus* ATCC 6538*,* methicillin-resistant *Staphylococcus aureus* ATCC 43300, *Enterococcus faecalis* ATCC 29212*, Escherichia coli* ATCC 25922*, Klebsiella pneumoniae* ATCC 1706, carbapenem-resistant *Klebsiella pneumoniae* ATCC 1705, *Streptococcus mutans* UA159, *Cryptococcus neoformans*, *Candida albicans* ATCC 14053, and bioluminescent CA-MRSA SAP227 were maintained in lysogeny broth (LB) or brain heart infusion broth (BHI), while solid medium was made by adding 1.5% (wt/vol) agar. All bacterial cultures were incubated at 37 ºC with 233 rpm oscillation. *S. mutans* cultures and plates were maintained at 37 °C in an aerobic chamber containing 5% CO_2 under static conditions. Drug-sensitive and multidrug-resistant (MDR) *A. baumannii* strains and *C. neoformans* we used for current study were isolated from Tulane hospital.

For all topically treated wound experiments, mice were infected with a bioluminescent MRSA SAP227. The recombinant bacteria was previously described and consists of the clinically relevant community acquired MRSA (CA-MRSA) strain MW2 with the pRP1195 plasmid containing Lux genes to confer bioluminescence[233]. CA-MRSA was cultured overnight in 5 mL LB before diluted 1:100 and incubated at 37 °C and shaken at 233 rpm for 4 hours until the culture reached early to mid-exponential growth phase. Cells were collected at an optical density of ≈ 0.7 at 600 nm and washed with sterile PBS twice before resuspended in PBS at 1 x 10^6 CFU/mL, ensuring that 10 μL applied to each wound delivered 1 x 10^4 CFU dose.

Growth inhibition assay

The ability of HMNQ and rhamnolipid to inhibit the growth of representative microorganisms was examined using a growth inhibition assay. HMNQ and rhamnolipid were dissolved in MeOH and added into a 96-well plate for a final concentration of 100 μM HMNQ, or 64 μg/mL rhamnolipid. The overnight culture of microorganisms was diluted 1:1000 in Mueller Hinton II Broth and added at 100 μL/well into a 96-well plate after evaporating the MeOH. Optical density at 600 nm was monitored until the culture reached plateau.

Confocal laser scanning microscopy

MRSA was cultured overnight in BHI and diluted 1:10 in TSB supplemented with 0.5% glucose[179], while *S. mutans* was cultured overnight in BHI and diluted 1:10 in BMGS. Biofilms were cultured on 8-well chambered-slides at 37 °C statically with medium changed daily. Pre-formed 2-day biofilms of MRSA were then treated with water, 200 μg/mL rhamnolipid, 300 μM HMNQ, or a combination of 200 μg/mL rhamnolipid with 300 μM HMNQ for another 1.5 hours before imaging. One-day biofilms of *S. mutans* were treated with PBS, 200 μg/mL rhamnolipid, 300 μM HMNQ, or a combination of 200 μg/mL rhamnolipid with 300 μM HMNQ for another 1.5 hours. Biofilms after the treatments were stained with LIVE/DEAD *Bac*Light fluorescent dye and imagined. Fluorescent confocal microscopy was performed with a Zeiss LSM 700 microscope. Confocal *z*-stacks and simulated *xyz* three-dimensional images were acquired and generated using Zeiss 10.0 software. More than seven image stacks were acquired from random positions within each well to cover an area of 200,000 μm^2 in order to represent

the biofilm[180,181]. Images were acquired at 1.0 μm intervals down through the biofilm with an inverted 40x/0.75 oil objective. Images were further analyzed using COMSTAT2.0 software for quantification of biomass, thickness, and roughness coefficient of the biofilms[180,182].

Cell culture

NFκB reporter macrophage cell line (RAW-Blue, invivogen) was maintained in DMEM with 4.5 g/L glucose, 2 mM L-glutamine, 10% heat-inactivated FBS, and 200 μg/mL Zeocin. Serial dilutions of HMNQ and rhamnolipid in MeOH were added into wells of a 96-well plate. After evaporating the MeOH, cells were seeded at 1.25 x 10^5 cells/well. Heat-killed MRSA (10^9 CFUs) was added into the each well 0 or 2 hours after seeding the cells. After incubation for 18 hours, supernatant was collected from each well and diluted 1:10 with QUANTI-Blue reagent. After 6-hour incubation at 37°C, secreted embryonic alkaline phosphatase (SEAP) levels were detected as an indication of NFκB activation using a spectrophotometer at 620 nm.

Full thickness splinted punch wound model

All animal experiments used female CD1 mice (Charles River Laboratories, Boston, MA). Animals were acquired at 7-10 weeks of age at 24-34 g and kept on an alfalfa-free diet prior to and throughout the experimental period to minimize autofluorescent signal [234]. All experimental procedures performed on animals were previously approved by the Tulane University Institutional Animal Care and Use Committee (P0131). On day 0, mice were wounded. Animals were anesthetized by an

intraperitoneal (IP) injection of ketamine (90 mg/kg) and xylazine (10 mg/kg) mixture. A separate IP injection of buprenorphine (0.05 mg/kg) was also administered to prophylactically accommodate for pain. Once fully anesthetized, the dorsum was shaved, and the exposed skin was scrubbed with chlorhexidine to sanitize the surface. Then, a full-thickness wound was generated using a 5 mm biopsy punch (Integra Miltex) by application of pressure on the dorsum below the base of the skull and between the solar plexus, generating a 5 mm circular wound outline. The light perforation was then excised, and the skin was cut through the epidermis, dermis, and panniculus carnosis exposing the muscle beneath. Thereafter, a 10 mm silicone torus coated in surgical adhesive was placed over the wound. Tegaderm (3M Healthcare) was placed over the silicone torus covering the exposed wound bed and the torus was secured in place using 4-0 braided silk interrupted sutures (Ethicon) fortified with additional surgical adhesive. An insulin syringe (BD Biosciences) was used to experimentally infect or treat the wound by penetrating the tegaderm and expressing directly onto the wound bed if needed. Animals were allowed to recover for four hours post wounding surgery and then anesthetized via inhalation (2.5%, isoflurane, VetOne) before treatments. Mice were singly housed post-procedure and monitored daily to access clinical status, bacterial burdens, wound closure, and weight change for the duration of the experiments until sacrifice.

To test the safety of HMNQ and rhamnolipid when applied to the wound bed, mice were given increased doses of a combination of HMNQ and rhamnolipid daily (Day 0: 40 μM HMNQ, 25.6 μg/mL rhamnolipid; Day 1: 200 μM HMNQ, 128 μg/mL rhamnolipid; Day 2: 1000 μM HMNQ, 640 μg/mL rhamnolipid; Day 3: 5000 μM HMNQ, 3200 μg/mL

rhamnolipid). On day 4, mice from both control and treated groups were sacrificed. Their wound tissues were excised for histological analysis.

To test the efficacy of HMNQ and rhamnolipid against CA-MRSA in the wound model, mice post wounding surgery were infected with 10^5 CFUs of bioluminescent CA-MRSA and given a combination of 2 mM HMNQ and 1.28 mg/mL rhamnolipid (n = 3), or 1.28 mg/mL rhamnolipid alone (n = 3) in a volume of 20 μL on the wound bed via injection through the tegaderm. Treatments were provided every eight hours for the first three days (total of 9 treatments). To determine bacterial burdens within the wound over time and examine the rate at which the wound was healing, mice were imaged daily using an *in vivo* imaging system (IVIS)-XMRS (PerkinElmer). The IVIS is capable of detecting and quantifying bioluminescent signals used to track the infection progression of the bioluminescent bacteria within the wound. During use, mice were anesthetized via inhalation of 2.5% isoflurane and imaged individually for 60 s. Resulting images were analyzed using the IVIS Lumina Living Image Software (PerkinElmer). A circular region of interest (RoI) was electronically captured over each wound bed to quantify bioluminescence as an indicator of bacterial burdens, which was recorded for every mouse daily. Relative luminescence within the RoI in units of radiance (photons/centemeter^2/steradian/second) is interpolated by a companion system software. The wound area was measured at day 4 after removing the tegaderm covering using custom RoIs traced along the epithelial lip of each wound that generated. After imaging on day 4, animals were humanely euthanized via CO_2 asphyxiation. The wound tissues were excised and mechanically disrupted in 1 mL PBS before serially diluted and plated on LB agar to

further quantify bacterial burdens. Resulting bacterial colonies were imaged to verify the presence of CA-MRSA.

Histology

Wounds were excised from the animals after euthanized with roughly 5 mm beyond the wound edge and fixed in 4% formaldehyde in PBS at 4 °C overnight. On the next day, the samples were washed with PBS and 20% (wt/vol) sucrose before embedded in OCT compound and froze immediately in liquid nitrogen. The tissue was then cut into 10-μm-thick cryostat sections on a cryosectioning machine and mounted onto SuperFrost Plus slides. Sections were stained with Hematoxylin and Eosin and examined using a Evos FL Auto microscope (Life Technologies).

Statistical analysis

The Chi squared test was applied to compare two curves, which measures the deviations between a measured and an expected value, divided by the uncertainty. The unpaired two-sample t-test was applied to compare independent samples.

Results

Evaluation of the antimicrobial activity of HMNQ and rhamnolipid against representative microbes

To test the isolated compounds for antimicrobial activity, HMNQ and rhamnolipid were added to broth cultures of representative Gram-negative and -positive bacteria, MDR bacteria and fungi. Initial pilot experiments were performed to identify effective

antimicrobial concentrations (data not shown). HMNQ at a concentration of 100 μM significantly inhibited the growth of *A. baumannii,* MDR *A. baumannii, E. coli, S. aureus,* MRSA, *S. mutans, C. albicans*, and *C. neoformans* (**Figure 5-1 and Figure 5-2**). Similarly, rhamnolipid at a concentration of 64 μg/mL significantly inhibited the growth of these microorganisms as well as *K. pneumoniae,* and carbapenem-resistant *K. pneumoniae* (**Figure 5-1 and Figure 5-2**). Not surprisingly, both HMNQ and rhamnolipid failed to inhibit the growth of *P. aeruginosa* (**Figure 5-1B**).

Evaluation of the antibiofilm activity of HMNQ and rhamnolipid against MRSA and S. mutans

Next, we investigated the effect of HMNQ and rhamnolipid on pre-formed bacterial biofilms since HMNQ is a QS regulator[103] and rhamnolipids have been shown to disrupt biofilm structures[113,115]. MRSA biofilms were grown on chamber-slides then treated with water, 200 μg/mL rhamnolipid, 300 μM HMNQ, or a combination of rhamnolipid and HMNQ. HMNQ is relatively insoluble in aqueous solutions similar to PQS, its analog in *P. aeruginosa*. Interestingly, previous studies have shown that the addition of rhamnolipids increased the solubility and bioactivity of the PQS[220]. Remarkably, compared to vehicle alone (**Figure 5-3A**), treatment with rhamnolipid or HMNQ significantly decreased the total biomass (**Figure 5-3B,C and Figure 5-4A**) and increased the ratio of dead cells to all labeled cells (**Figure 5-3B,C and Figure 5-4B**). Treatment with either rhamnolipid or HMNQ also reduced the thickness of pre-formed MRSA biofilms compared to control (**Figure 5-4C**). The significant increase in the roughness coefficient in rhamnolipid- or HMNQ-treated biofilms further indicates an overall decline in biofilm integrity (**Figure 5-**

4D). There were no synergistic effects noted when biofilms were treated with a mixture of HMNQ and rhamnolipid (**Figure 5-3D and Figure 5-4**).

When applied on pre-formed *S. mutans* biofilms, treatments with rhamnolipid, HMNQ, or combination significantly decreased the total biomass, biofilm thickness (**Figure 5-5B,C,D and Figure 5-6A,C**), and increased the ratio of dead cells to all labeled cells as well as the roughness coefficient (**Figure 5-5B,C,D and Figure 5-6B,D**). No synergistic effects were observed when treating *S. mutans* biofilms with a mixture of HMNQ and rhamnolipid (**Figure 5-5D and Figure 5-6**).

Evaluation of HMNQ and rhamnolipid on NFκB activation in vitro

PQS at 1 μM has been shown to suppress host innate immune responses by reducing the NFκB binding to its binding sites and the expression of downstream pro-inflammatory genes[216]. To investigate if HMNQ has similar activity, we cultured NFκB reporter macrophages in the presence of increased concentrations of HMNQ or rhamnolipid, then stimulated the cells with heat-killed MRSA. The reporter cells stably express a secreted embryonic alkaline phosphatase (SEAP) gene inducible by NFκB and AP-1 transcription factors. HMNQ less than 40 μM failed to induce NFκB activation compared to solvent control (0 μM) when incubated with cells 0 or 2 hours prior to stimulation (**Figure 5-7A**). Surprisingly, HMNQ at 200 μM increased NFκB activation regardless of the incubation time (**Figure 5-7A**). Rhamnolipid when applied less than 25 μg/mL failed to induce NFκB activation at both time points (**Figure 5-7B**). At 125 μg/mL, it was cytotoxic to macrophages as confirmed by light microscopy (data not shown).

The safety assessment of HMNQ and rhamnolipid in vivo

The safety of HMNQ and rhamnolipid for topical application was characterized in a full-thickness wound model. Mice post wounding surgery were given increased doses of a combination of HMNQ and rhamnolipid daily for three days before sacrificed. Light inflammation was observed initially in the wound beds at day 0 post-surgery in both mixture-treated and PBS-treated mice. No different observation was noticed in the following days when examining the wounds (data not shown). One of the mixture-treated mice scratched the sutured silicon torus completely off its wound, which rarely happens in the model at day 4 in control mice. Histological analysis of the excised wounds from mixture-treated mice showed no difference in neutrophil invasion and inflammation compared to wounds from PBS-treated mouse, but implied a decreased collagen level in mixture-treated mice compared to control (**Figure 5-8**). However, the collagen secretion should be monitored over time and confirmed with Masson trichrome staining or Verhoeff's staining in future experiments[228].

The antimicrobial efficacy and wound healing capacity of HMNQ and rhamnolipid assessed in vivo

Finally, we evaluated the antimicrobial efficacy and wound healing capacity of HMNQ and rhamnolipid in a murine wound infection model. We first confirmed the antimicrobial activity of HMNQ and rhamnolipid on bioluminescent CA-MRSA grown on an agar plate (**Figure 5-9**). The killing of HMNQ and rhamnolipid started immediately when applied on CA-MRSA (**Figure 5-9A**). At day 3, expanded zones of inhibition were observed with the treatment of rhamnolipid, or the mixture of HMNQ and rhamnolipid

(**Figure 5-9B**). To assess their efficacy *in vivo*, mice post wounding surgery were infected with 10^5 CFU of bioluminescent CA-MRSA and treated with a mixture of HMNQ (2 mM) and rhamnolipid (1.28 mg/mL) compared to rhamnolipid (1.28 mg/mL) alone. We observed no difference in bacterial luminescence within the wounds between the two groups when recorded daily by IVIS (**Figure 5-10A**). However, at the experimental end point (day 4), excised wounds from the mixture-treated mice contained significantly less CFU compared to wounds from rhamnolipid-treated mice (**Figure 5-10B**). No significant difference in weight loss was observed between the two groups (**Figure 5-10C**). After removing the tegaderm from the wounds at day 4, there was no difference in wound area measurements in both groups compared to PBS treated wounds in previous experiment (**Figure 5-10D**).

Discussion

In this chapter, we showed that HMNQ at a concentration of 100 μM inhibited the growth of *A. baumannii,* MDR *A. baumannii, E. coli, S. aureus,* MRSA, *S. mutans, C. albicans*, and *C. neoformans*, whereas rhamnolipid showed broader spectrum at 64 μg/mL working against these microorganisms as well as *K. pneumoniae* and carbapenem-resistant *K. pneumoniae*. Both HMNQ and rhamnolipid showed antibiofilm activity against MRSA and *S. mutans*. Rhamnolipid is superior at reducing the integrity of biofilms while HMNQ displays greater bactericidal activity.

HMNQ at 200 μM induced NFκB activation in a macrophage cell line in the presence of heat-killed bacteria stimulation compared to control, opposite to what has been reported with PQS[216]. Not surprisingly, rhamnolipid failed to activate NFκB *in vitro* and

lysed macrophages at the highest concentration tested. These results implied that HMNQ may be proinflammatory when applied at high concentrations on open wounds. However, HMNQ and rhamnolipid did not induce inflammation in a full-thickness wound model characterized with histology. When applied on the infected wounds, HMNQ and rhamnolipid failed to reduce the bacterial burden compared to rhamnolipid alone according to luminescence data. However, wound tissue from the mixture-treated mice contained significantly less bacteria compared to wounds from rhamnolipid-treated mice. Interestingly, a previous study showed that the bioluminescence produced by *Lux* containing bacteria is regulated by bacterial respiration and electron transport chain[235]. HMNQ has been shown to function as an ionophore and to disrupt proton motive force along the electron transport chain[107], which could potentially promote bioluminescence production while inhibiting bacterial growth. Notably, HMNQ induced bioluminescence at the edge of the zone of inhibition (**Figure 5-9A**), where the bacteria were eventually killed at day 3 (**Figure 5-9B**). Thus, bioluminescent bacteria and IVIS imaging may not be suitable for the characterization of HMNQ and alternative models should be explored in the future.

Besides its antimicrobial and antibiofilm activities, rhamnolipid has been previously shown to accelerate the wound closure and decreased collagen secretion by targeting pathological myofibroblasts[227,228]. Histological analysis of wound tissue treated with the combination of HMNQ and rhamnolipid implied a decreased collagen level compared to PBS-treated wound. Further characterization with collagen specific staining and the measurement of myofibroblast markers is necessary for the assessment of rhamnolipid on scar tissue formation and wound healing. Although treatment with the

combination of HMNQ and rhamnolipid or rhamnolipid alone failed to decrease the wound area at 4 days post wounding surgery compared to PBS control, the rate of wound healing should be monitored over longer period of time in future work.

Figure 5-1

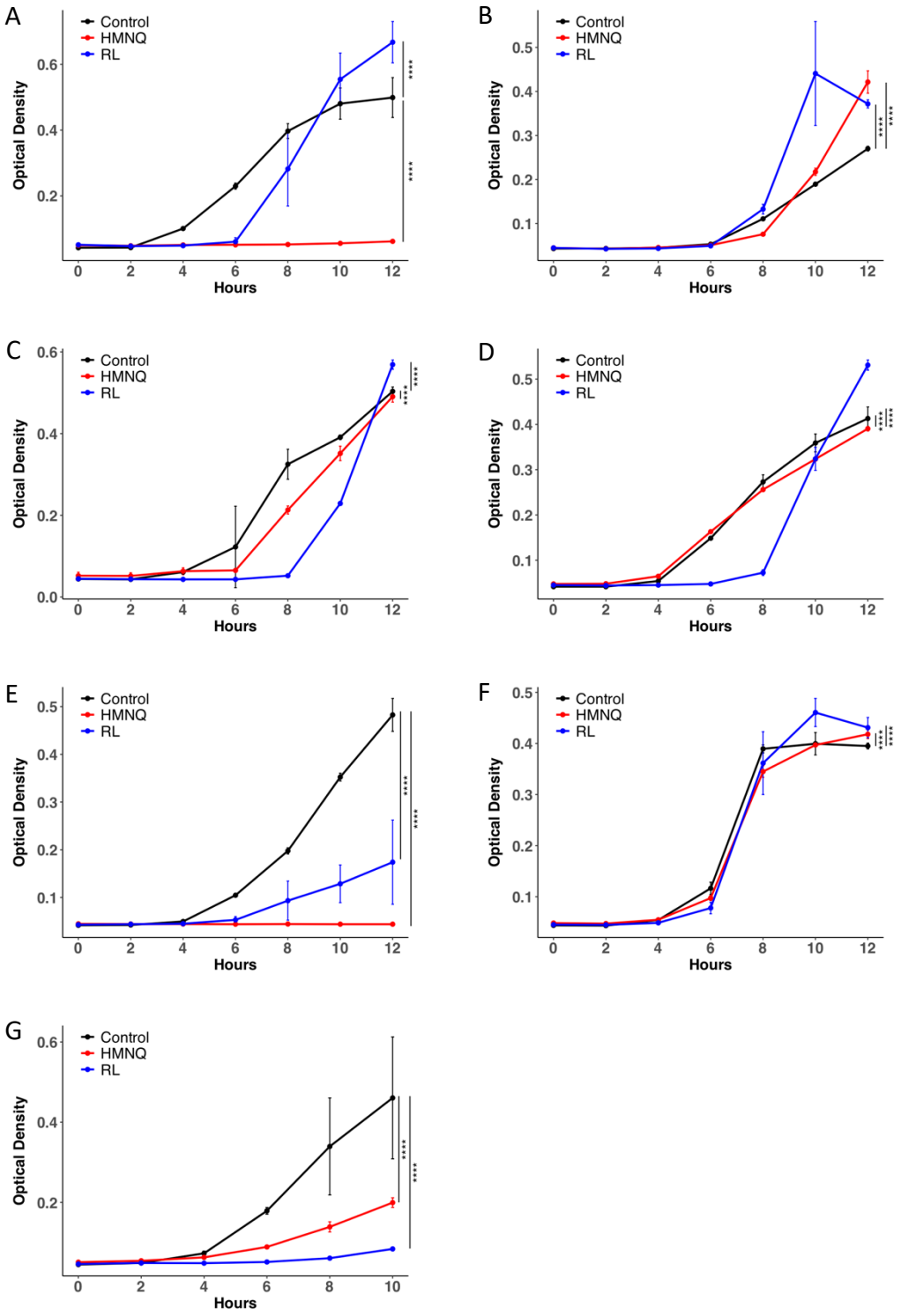

Figure 5-1. Evaluation of HMNQ and rhamnolipid inhibiting microbial growth in planktonic cultures with representative Gram-negative and Gram-positive bacteria

Overnight cultures of with (**A**) *A. baumannii*, (**B**) *P. aeruginosa*, (**C**) *E. coli*, (**D**) *K. pneumoniae*, (**E**) *S. aureus*, (**F**) *E. faecalis*, and (**G**) *S. mutans* were diluted 1:1000 in broth and treated with PBS, 100 μM HMNQ, or 64 μg/mL rhamnolipid in a total volume of 100 μL. OD_{600} was monitored for 12 hours. The results were analyzed using Chi squared test, **** $p < 0.0001$.

Figure 5-2

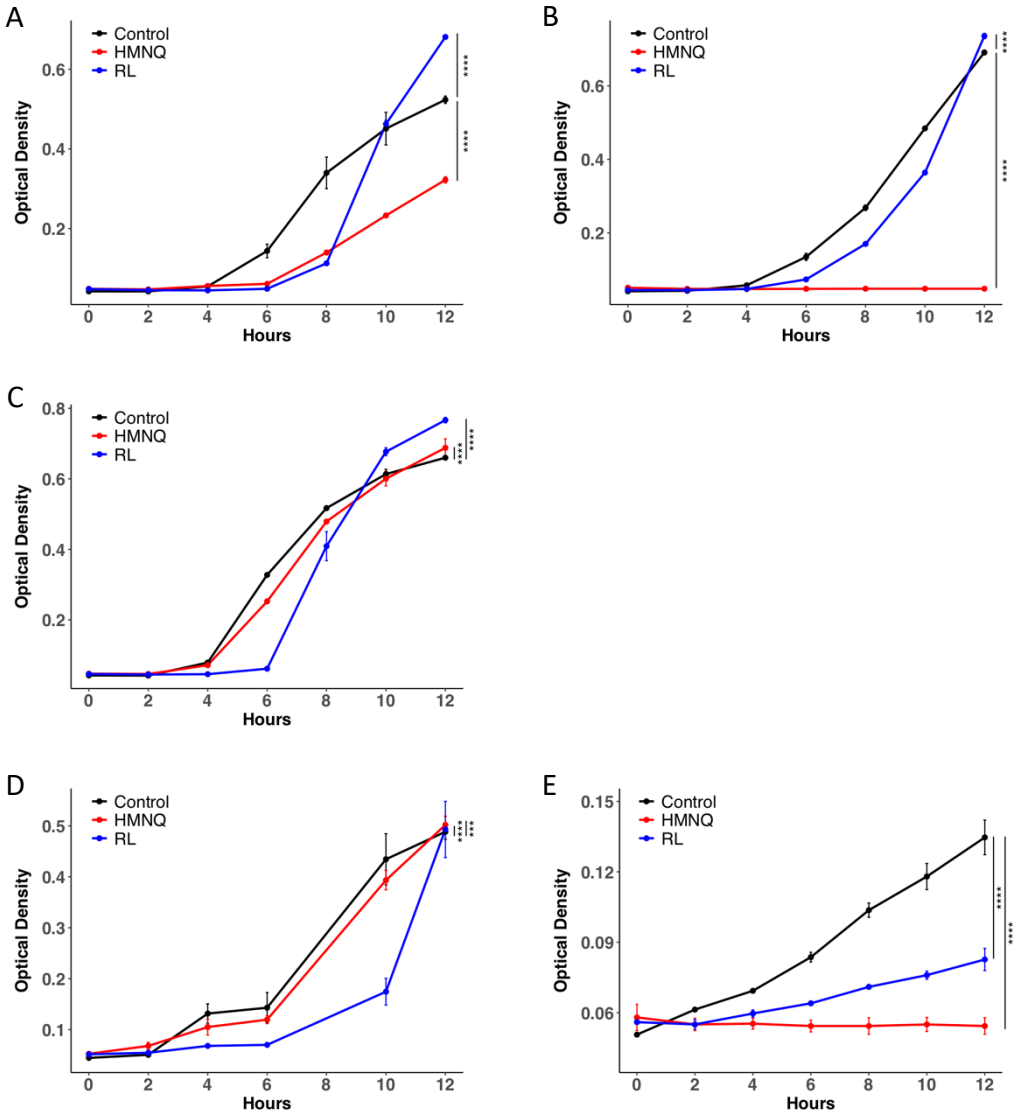

Figure 5-2. Evaluation of HMNQ and rhamnolipid inhibiting microbial growth in planktonic cultures with multidrug-resistant bacteria and fungi

Overnight cultures of with (**A**) MDR *A. baumannii*, (**B**) MRSA, (**C**) carbapenem-resistant *K. pneumoniae*, (**D**) *C. albicans*, and (**E**) *C. neoformans* were diluted 1:1000 in broth and treated with PBS, 100 μM HMNQ, or 64 μg/mL rhamnolipid in a total volume of 100 μL. OD_{600} was monitored for 12 hours. The results were analyzed using Chi squared test, *** $p < 0.001$, **** $p < 0.0001$.

Figure 5-3

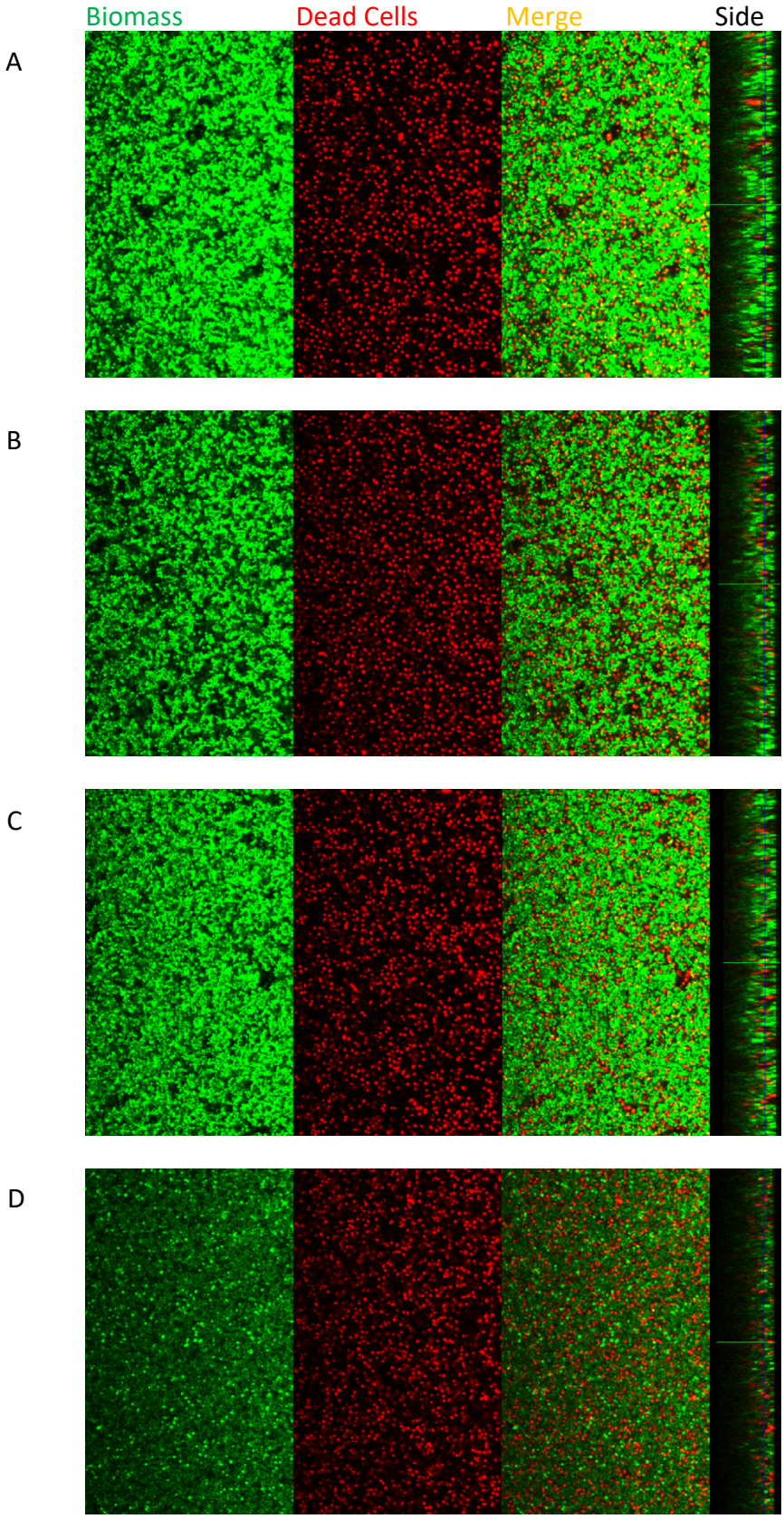

Figure 5-3. The bactericidal and antibiofilm effects of HMNQ and rhamnolipid against MRSA biofilm analyzed by fluorescent confocal microscopy

MRSA biofilms were grown on chambered-slides in TSB medium supplemented with 0.5% glucose for 48 hours. Biofilms were stained with LIVE/DEAD *Bac*Light fluorescent dye (SYTO 9/propidium iodide), then subjected to optical dissection using a Zeiss LSM 700 laser scanning confocal microscope. Images were acquired at 1.0 μm intervals down through the biofilm. At least seven image stacks were acquired at 400 x from each well. Post-acquisition analyses were performed using COMSTAT 2.0. Representative images of pre-formed biofilms treated with (**A**) water, (**B**) 200 μg/mL rhamnolipid, (**C**) 300 μM HMNQ, or (**D**) a combination of 200 μg/mL rhamnolipid with 300 μM HMNQ were acquired 1.5 hours after the treatment. Presented layers are 5 μm above the substratum in each image stacks. Green: total biomass; red: dead cell biomass; orange: merge; side: side view of biofilm thickness.

Figure 5-4

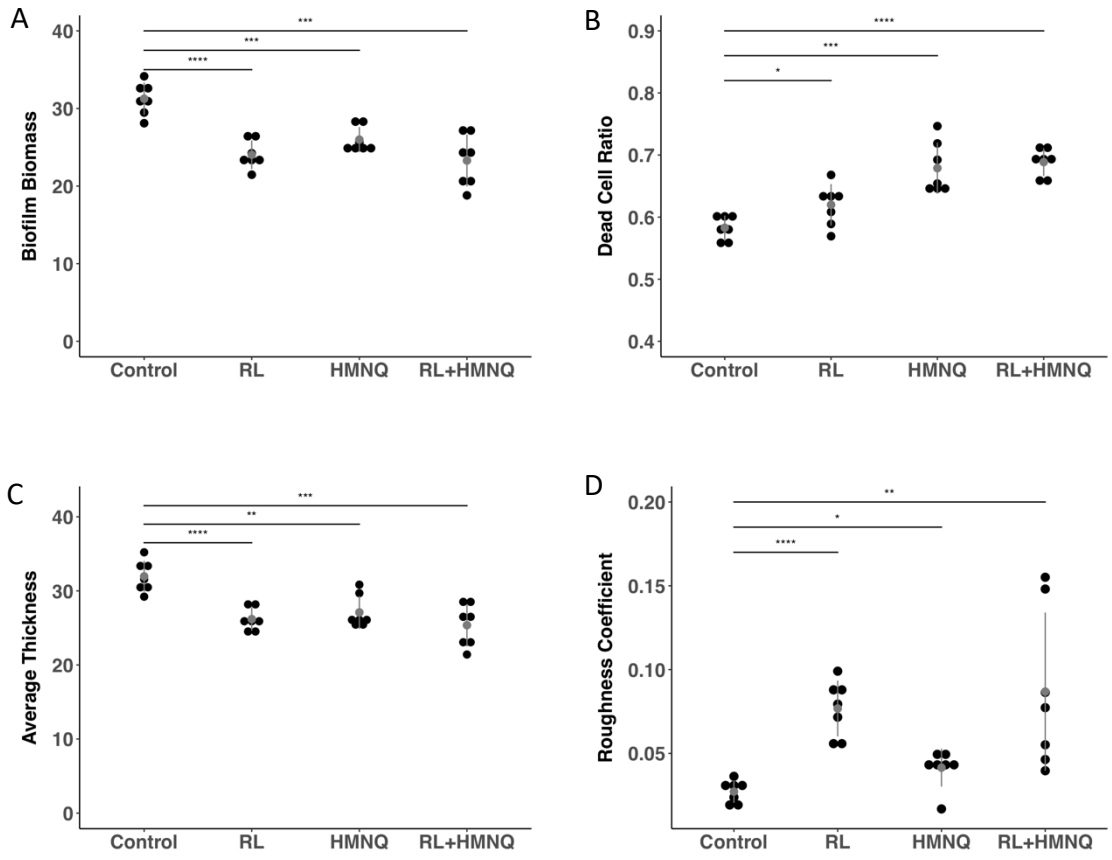
A
Biofilm Biomass
40
30
20
10
0
***
***
****
Control
RL
HMNQ
RL+HMNQ
B
Dead Cell Ratio
0.9
0.8
0.7
0.6
0.5
0.4
****
***
*
Control
RL
HMNQ
RL+HMNQ
C
Average Thickness
40
30
20
10
0
***
**
****
Control
RL
HMNQ
RL+HMNQ
D
Roughness Coefficient
0.20
0.15
0.10
0.05
**
*
****
Control
RL
HMNQ
RL+HMNQ

Figure 5-4. Post-acquisition analyses of fluorescent images of the MRSA biofilms treated with HMNQ and/or rhamnolipid

Post-acquisition analyses were performed using COMSTAT 2.0. MRSA biofilms treated with water, 200 μg/mL rhamnolipid, 300 μM HMNQ, or a combination of 200 μg/mL rhamnolipid with 300 μM HMNQ were compared in (**A**) biofilm biomass, (**B**) dead cell ratio, (**C**) average thickness, and (**D**) roughness coefficient. Roughness coefficients of the biofilms were calculated with COMSTAT 2.0 as an indication of biofilm healthiness and integrity. The results were analyzed using unpaired two-sample t-test. (* $p < 0.05$, ** $p < 0.01$, *** $p < 0.001$, **** $p < 0.0001$)

Figure 5-5

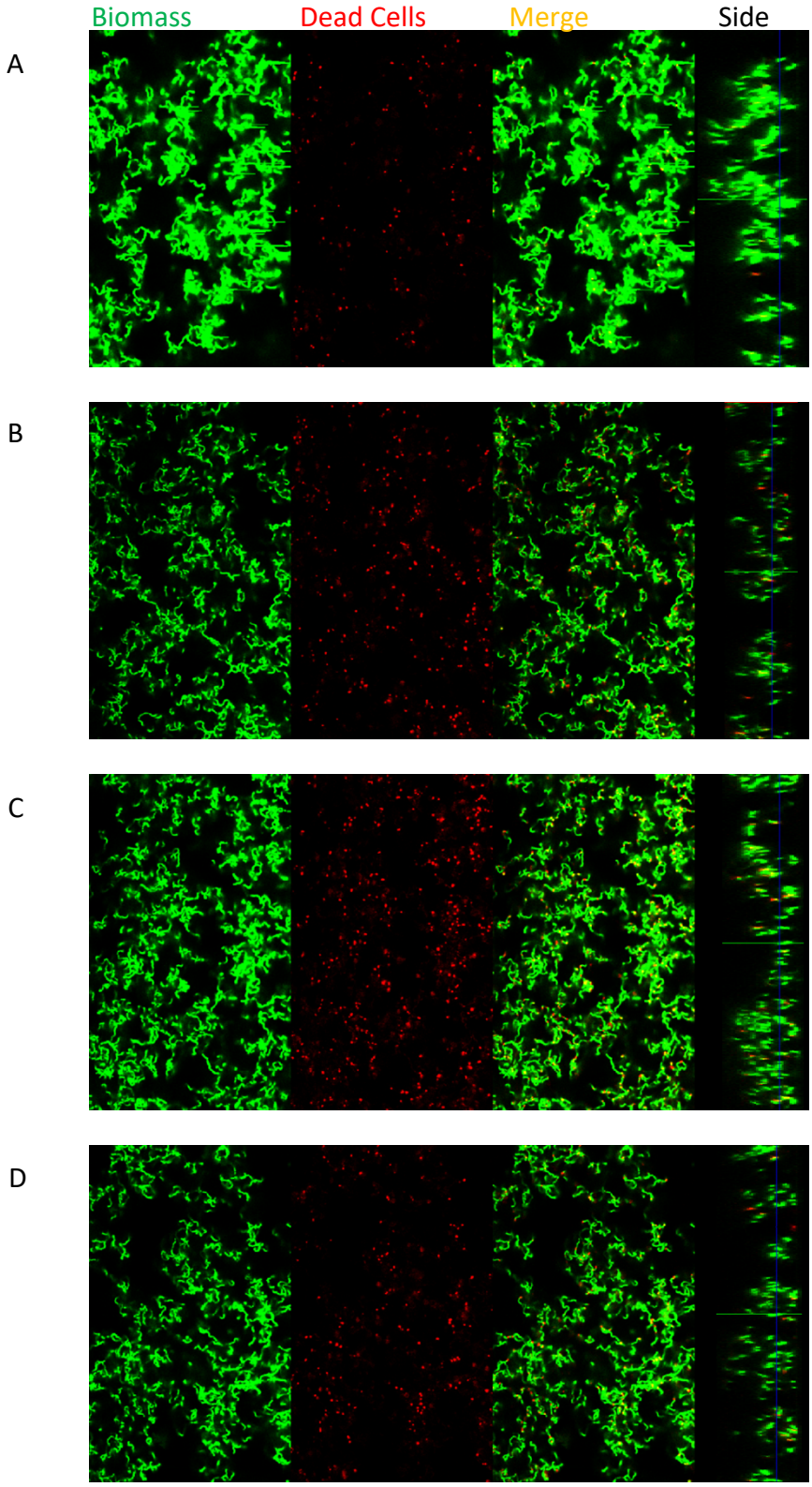

Figure 5-5. The bactericidal and antibiofilm effects of HMNQ and rhamnolipid against *S. mutans* biofilm analyzed by fluorescent confocal microscopy

S. mutans biofilms were grown on chambered-slides in BMGS medium. Biofilms were stained with LIVE/DEAD *Bac*Light fluorescent dye (SYTO 9/propidium iodide), then subjected to optical dissection using a Zeiss LSM 700 laser scanning confocal microscope. Images were acquired at 1.0 μm intervals down through the biofilm. At least seven image stacks were acquired at 400 x from each well. Post-acquisition analyses were performed using COMSTAT 2.0. Representative images of pre-formed biofilms treated with (**A**) water, (**B**) 200 μg/mL rhamnolipid, (**C**) 300 μM HMNQ, or (**D**) a combination of 200 μg/mL rhamnolipid with 300 μM HMNQ were acquired 1.5 hours after the treatment. Presented layers are 10 μm above the substratum in each image stacks. Green: total biomass; red: dead cell biomass; orange: merge; side: side view of biofilm thickness.

Figure 5-6

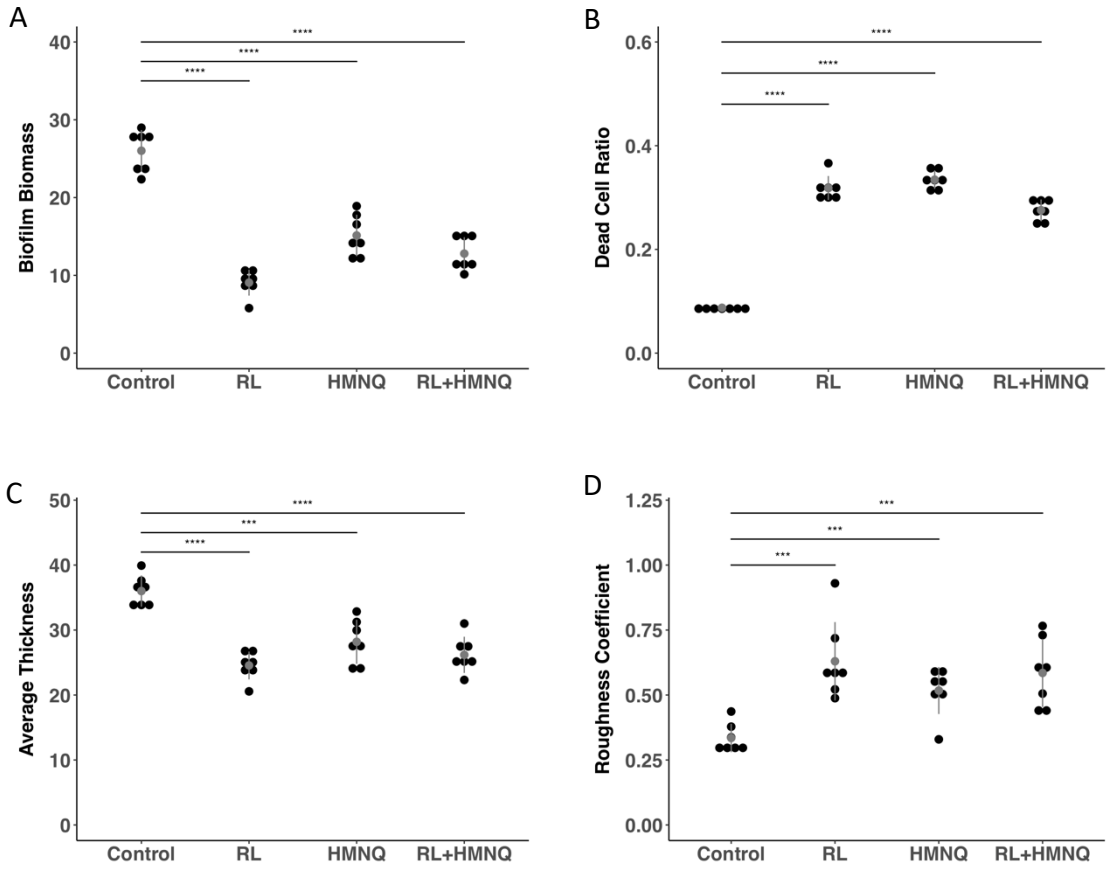
A
Biofilm Biomass
40
30
20
10
0
****
****
****
Control
RL
HMNQ
RL+HMNQ
B
Dead Cell Ratio
0.6
0.4
0.2
0.0
****
****
****
Control
RL
HMNQ
RL+HMNQ
C
Average Thickness
50
40
30
20
10
0
****
***
****
Control
RL
HMNQ
RL+HMNQ
D
Roughness Coefficient
1.25
1.00
0.75
0.50
0.25
0.00
***
***
***
Control
RL
HMNQ
RL+HMNQ

Figure 5-6. Post-acquisition analyses of fluorescent images of the *S. mutans* biofilms treated with HMNQ and/or rhamnolipid

Post-acquisition analyses were performed using COMSTAT 2.0. *S. mutans* biofilms treated with water, 200 μg/mL rhamnolipid, 300 μM HMNQ, or a combination of 200 μg/mL rhamnolipid with 300 μM HMNQ were compared in (**A**) biofilm biomass, (**B**) dead cell ratio, (**C**) average thickness, and (**D**) roughness coefficient. Roughness coefficients of the biofilms were calculated with COMSTAT 2.0 as an indication of biofilm healthiness and integrity. The results were analyzed using unpaired two-sample t-test. (* $p < 0.05$, ** $p < 0.01$, **** $p < 0.0001$)

Figure 5-7

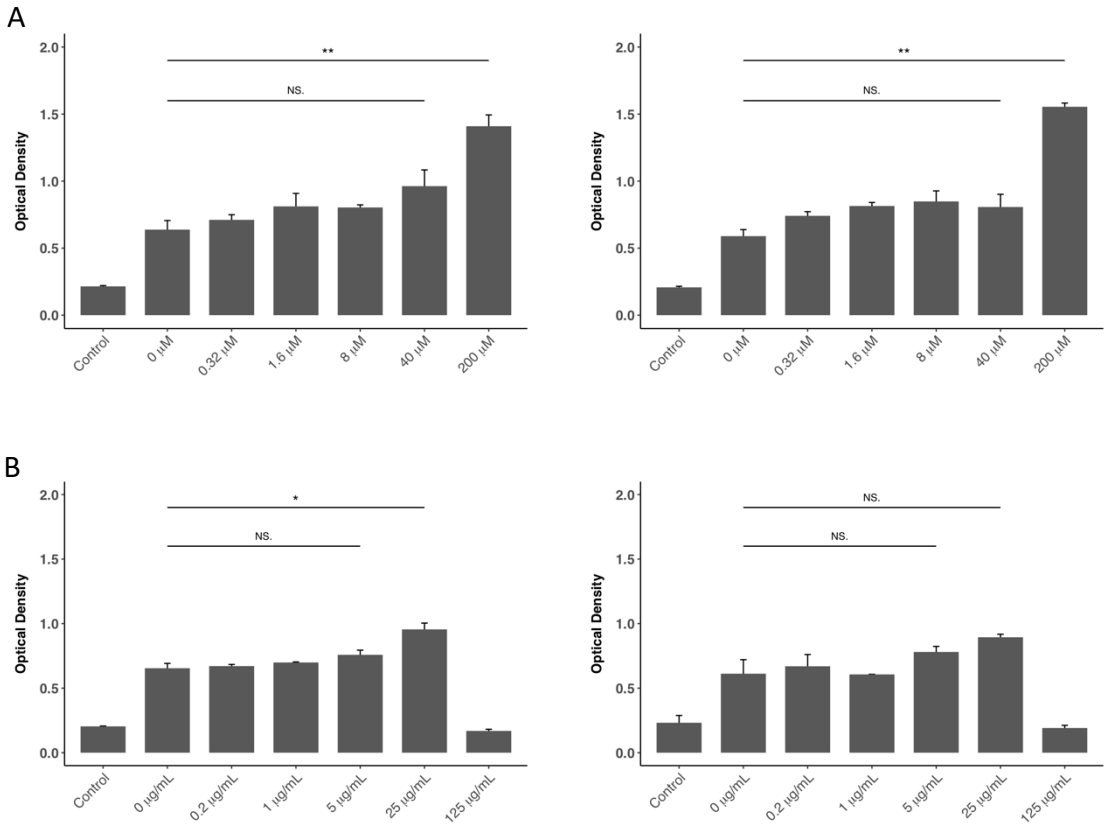
A
B
Optical Density
2.0
1.5
1.0
0.5
0.0
**
NS.
*
Control
0 μM
0.32 μM
1.6 μM
8 μM
40 μM
200 μM
0 μg/mL
0.2 μg/mL
1 μg/mL
5 μg/mL
25 μg/mL
125 μg/mL

Figure 5-7. Effects of HMNQ and rhamnolipid on NFκB activation in a macrophage cells line

NFκB reporter macrophage cells (1.25 x 10^5) were treated with increased concentrations of (**A**) HMNQ, or (**B**) rhamnolipid for 0 (left) or 2 (right) hours before stimulating with heat-killed MRSA (10^9 CFUs). After incubation for 18 hours, supernatant was collected from each treatment and diluted 1:10 with QUANTI-Blue reagent. After 6-hour incubation at 37°C, SEAP levels were detected as an indication of NFκB activation using a spectrophotometer at 620 nm. Control: culture medium alone.

Figure 5-8

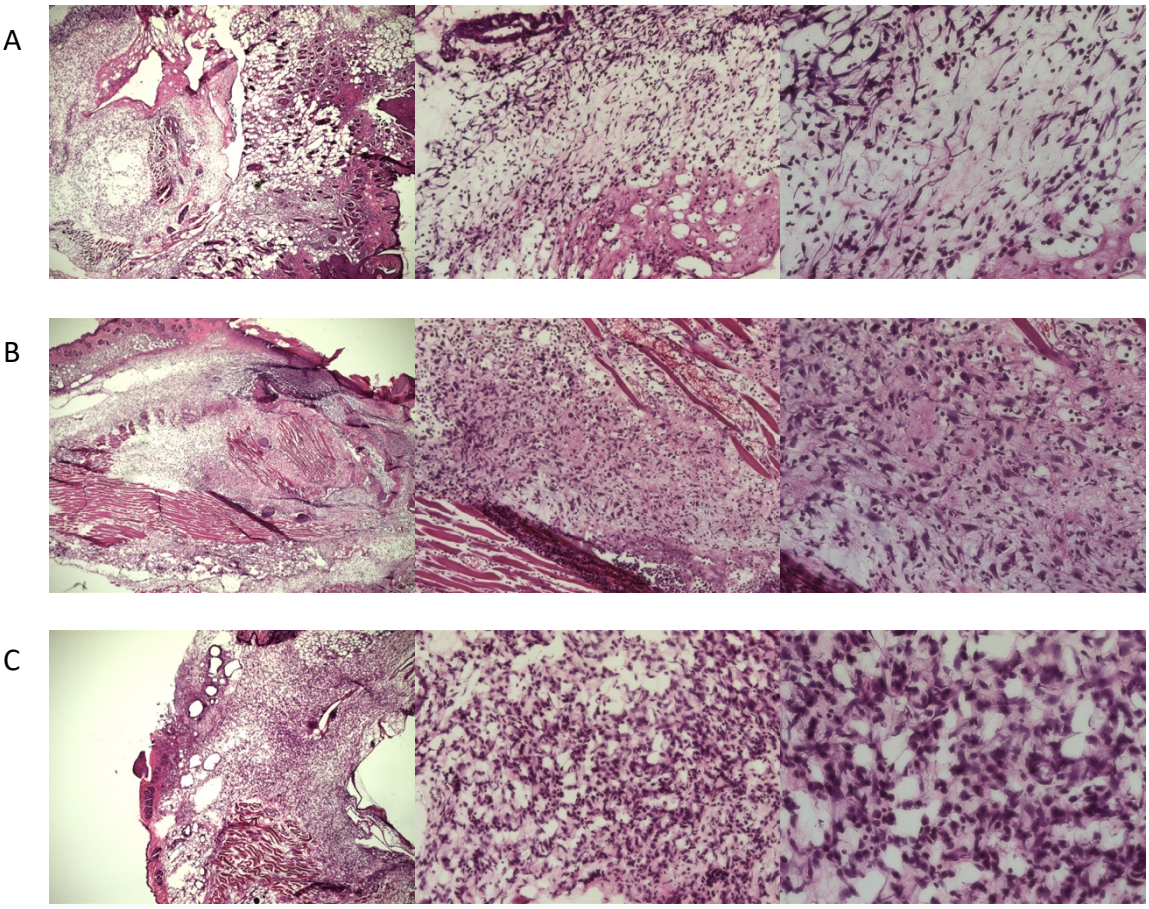

Figure 5-8. Histological analysis of uninfected wounds treated with HMNQ and rhamnolipid

Mice post wounding surgery were given increased doses of a combination of HMNQ and rhamnolipid daily for three days before sacrificed. Wound tissues treated with (**A**) PBS, or (**B, C**) a mixture of HMNQ and rhamnolipid were excised and cut into 10-μm-thick cryostat sections before H&E staining. Left: 4 x, middle: 20 x, right: 40 x magnification.

Figure 5-9

A

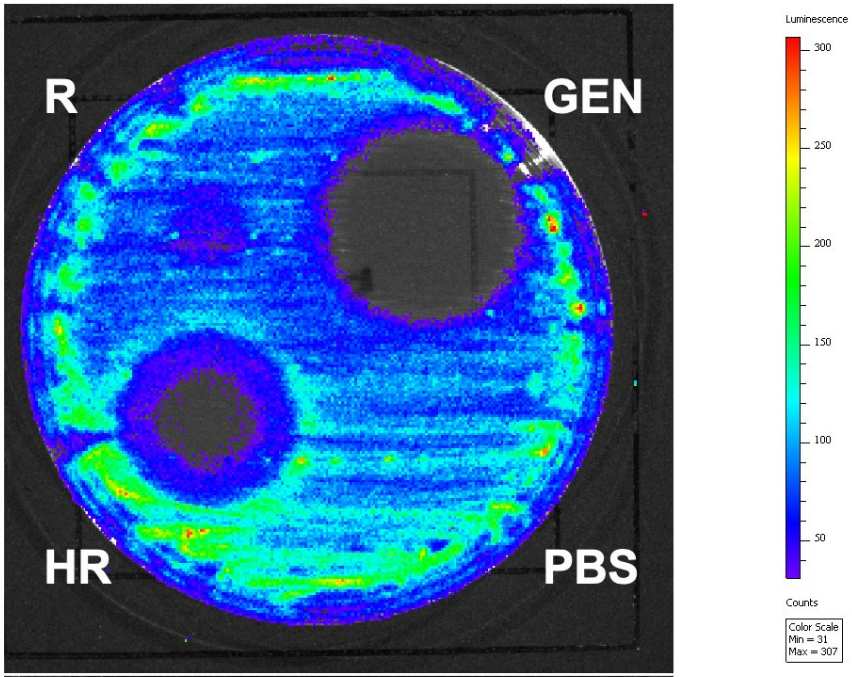
R
GEN
HR
PBS
Luminescence
300
250
200
150
100
50
Counts
Color Scale
Min = 31
Max = 307

B

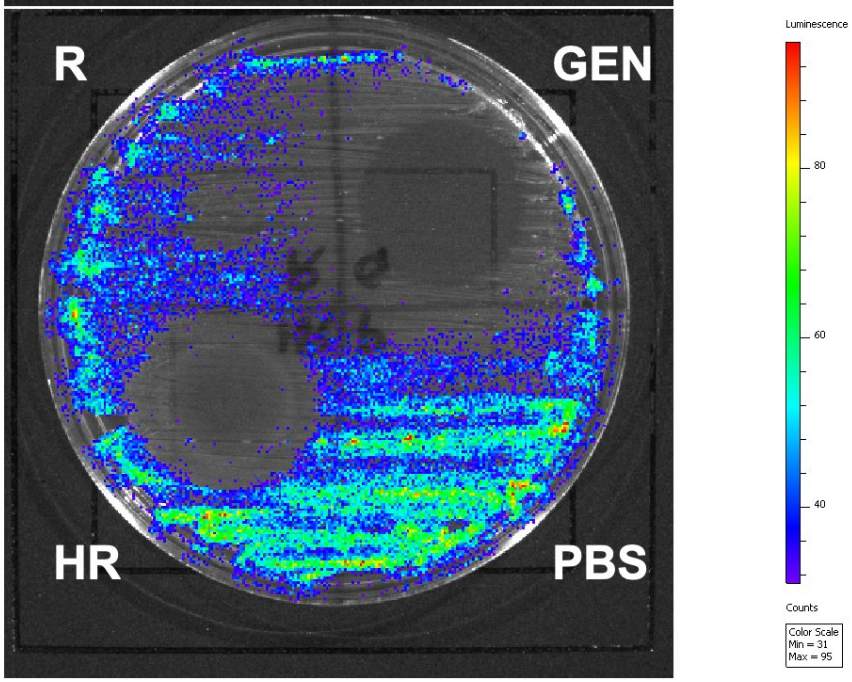
R
GEN
HR
PBS
Luminescence
80
60
40
Counts
Color Scale
Min = 31
Max = 95

Figure 5-9. The bactericidal activity of HMNQ and rhamnolipid against bioluminescent CA-MRSA imaged with IVIS

A fresh culture of bioluminescent CA-MRSA was streaked heavily onto an agar plate, and 10 μL of rhamnolipid (1.28 mg/mL), a mixture of HMNQ (2 mM) and rhamnolipid (1.28 mg/mL), gentamicin (1 mg/mL), or PBS were applied. The plate was incubated at room temperature for up to 72 hours and imaged with IVIS at 0 (**A**) and 72 (**B**) hours.

Figure 5-10

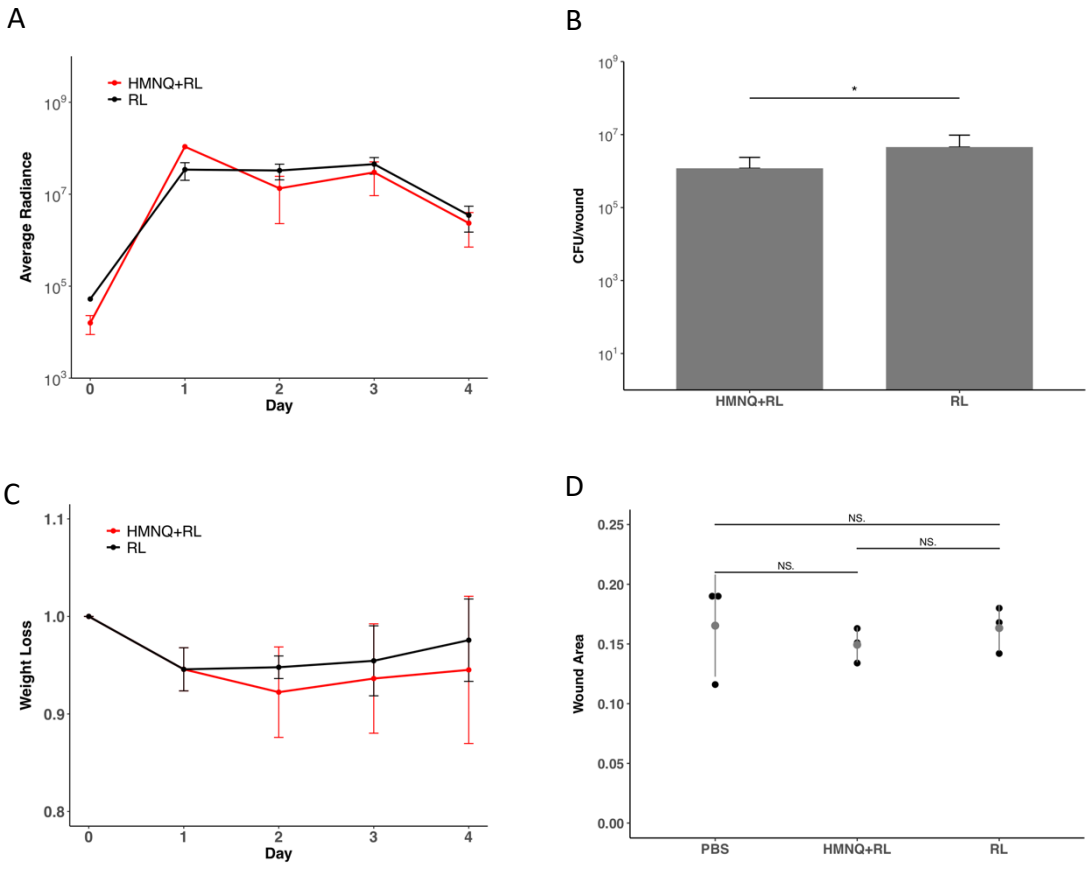
A
HMNQ+RL
RL
Average Radiance
Day
B
CFU/wound
*
HMNQ+RL
RL
C
HMNQ+RL
RL
Weight Loss
Day
D
Wound Area
NS.
NS.
NS.
PBS
HMNQ+RL
RL

Figure 5-10. Evaluation of the antimicrobial efficacy and wound healing capacity of HMNQ and rhamnolipid with a murine wound infection model

Mice post wounding surgery were infected with 10^5 CFUs of bioluminescent CA-MRSA and treated with a mixture of HMNQ (2 mM) and rhamnolipid (1.28 mg/mL) compared to rhamnolipid (1.28 mg/mL) alone. (**A**) Radiance plots of mouse wound bed as an indication of bacterial burdens. (**B**) CFU counting from wound tissues collected after euthanasia. (**C**) Daily mean group weights. (**D**) Wound area measurements at day 4 compared to PBS treated wounds in a previous experiment. (n = 3 for each treatment)

CHAPTER 6: Conclusion

In this work, we showed that *B. thailandensis* OMVs purified with either equilibrium density-gradient ultracentrifugation or size exclusion chromatography exhibited antimicrobial activity. Ultracentrifugation-purified OMVs inhibited the growth of *A. baumannii*, MDR *A. baumannii, S. aureus,* MRSA*, S. mutans, C. albicans,* and *C. neoformans* in planktonic cultures. In addition, our results indicated that *B. thailandensis* OMVs have the ability to disrupt pre-formed biofilms of *A. baumannii, E. faecalis, S. aureus,* and *S. mutans*. This antibiofilm activity was further examined against MRSA and *S. mutans* biofilms with more robust characterization. We showed that OMVs potently reduced the biomass, biofilm integrity, and cell viability of bacterial biofilms in a dose-dependent manner. Additionally, we observed a synergistic effect between *B. thailandensis* OMVs and gentamicin against *S. mutans* biofilms. In future studies, *B. thailandensis* OMVs should be evaluated against polymicrobial biofilms as well as fungal biofilms.

In deciphering the antimicrobial activity of *B. thailandensis* OMVs, we discovered that they contain not only peptidoglycan hydrolases but also HMNQ and long-chain rhamnolipid. HMNQ at a concentration of 100 μM inhibited the growth of *A. baumannii,* MDR *A. baumannii, E. coli, S. aureus,* MRSA, *S. mutans, C. albicans*, and *C. neoformans*, whereas rhamnolipid showed broader spectrum at 64 μg/mL working against these microorganisms as well as *K. pneumoniae* and carbapenem-resistant *K. pneumoniae*. Both HMNQ and rhamnolipid showed antibiofilm activity against MRSA and *S. mutans*. However, when applied together on pre-formed biofilms, we did not observe synergistic effects with the two molecules. Furthermore, there were no synergistic effects between

HMNQ and other antibiotics including ampicillin, gentamicin, rifampin, bacitracin, against any of the pathogens tested (data not shown).

Our preliminary *in vitro* experiment implied that HMNQ could modulate innate immune responses by inducing NFκB activation in macrophages, which influences neutrophil recruitment. Previous studies showed that innate immune defense especially neutrophil invasion is crucial for *S. aureus* control during infections[236,237]. The roles of HMNQ and rhamnolipid on innate immunity could be further characterized *in vivo* with immunohistochemical analysis and flow cytometry. When applied on infected wounds, HMNQ and rhamnolipid failed to reduce the bacterial burden compared to rhamnolipid alone according to luminescence data. However, wound tissue from the mixture-treated mice contained significantly less bacteria compared to wounds from rhamnolipid-treated mice. Thus, alternative models could be explored to better characterized the efficacy of HMNQ and rhamnolipid on topical infections. In addition, the rate of wound healing as well as collagen secretion, as an indication of scar tissue formation, should be monitored during the treatment.

To our knowledge, this is the first demonstration that HMNQ and rhamnolipid are secreted through OMVs by *B. thailandensis.* A recent study showed that the production of rhamnolipids in *B. thailandensis* is regulated by quorum sensing[116]. Interestingly, HMNQ has been shown to play a key role in the quorum sensing of *Burkholderia* species[103]. It will be interesting to investigate the correlation between the regulation and production of the two molecules and their secretion in OMVs. Considering its relationship to PQS, the roles of HMNQ in OMV production should be investigated in the future. In the current work, we also observed the presence of HAQ derivatives other than HMNQ within *B.*

thailandensis OMVs (data not shown). The roles of these derivatives during interspecies interactions and their relationship with OMVs remain unknown.

Here, we only characterized *B. thailandensis* OMVs derived from cultures grown in a nutrient-rich media. Future studies could evaluate the antimicrobial and antibiofilm activities of OMVs secreted by bacteria grown in non-conventional growth media, which influences cargo packaging and secretion[125]. In addition, the identification of HMNQ and rhamnolipid was determined by their activities against MRSA in a nutrient-rich environment, which doesn't necessarily mimic the environments in nature or during human infection. To tackle this problem, fractions from *B. thailandensis* OMVs could be screened against various pathogens grown in various conditions. Nevertheless, our findings indicate that *B. thailandensis* secretes antimicrobial OMVs that may impart a survival advantage by eliminating competition. In addition, with the mounting crisis of antimicrobial resistance, new therapeutic strategies with distinct mechanisms of action against MDR and biofilm-forming species are urgently needed to treat chronic and life-threatening infections. Bacterial OMVs may represent an untapped resource of novel therapeutics effective against biofilm-forming and multidrug-resistant organisms. OMV-derived compounds from *Burkholderia* or other soil bacteria could be further developed into new antibacterial agents. Modifications of the natural compounds using computational biology and structure-activity relationship studies could lead to novel antimicrobial products for clinical use or agricultural applications.

LIST OF REFERENCES

1 O'neill, J. Antimicrobial resistance: tackling a crisis for the health and wealth of nations. *Rev. Antimicrob. Resist* **20**, 1-16 (2014).

2 Blair, J. M., Webber, M. A., Baylay, A. J., Ogbolu, D. O. & Piddock, L. J. Molecular mechanisms of antibiotic resistance. *Nat Rev Microbiol* **13**, 42-51, doi:10.1038/nrmicro3380 (2015).

3 Andersson, D. I. & Hughes, D. Microbiological effects of sublethal levels of antibiotics. *Nat Rev Microbiol* **12**, 465-478, doi:10.1038/nrmicro3270 (2014).

4 Crofts, T. S., Gasparrini, A. J. & Dantas, G. Next-generation approaches to understand and combat the antibiotic resistome. *Nat Rev Microbiol* **15**, 422-434, doi:10.1038/nrmicro.2017.28 (2017).

5 Control, C. f. D. & Prevention. *Antibiotic resistance threats in the United States, 2013*. (Centres for Disease Control and Prevention, 2013).

6 Chang, Y. L., Yu, S. J., Heitman, J., Wellington, M. & Chen, Y. L. New facets of antifungal therapy. *Virulence* **8**, 222-236, doi:10.1080/21505594.2016.1257457 (2017).

7 Vandeputte, P., Ferrari, S. & Coste, A. T. Antifungal resistance and new strategies to control fungal infections. *Int J Microbiol* **2012**, 713687, doi:10.1155/2012/713687 (2012).

8 Fuentefria, A. M., Pippi, B., Dalla Lana, D. F., Donato, K. K. & de Andrade, S. F. Antifungals discovery: an insight into new strategies to combat antifungal resistance. *Lett Appl Microbiol* **66**, 2-13, doi:10.1111/lam.12820 (2018).

9 Magill, S. S. *et al.* Changes in Prevalence of Health Care-Associated Infections in U.S. Hospitals. *N Engl J Med* **379**, 1732-1744, doi:10.1056/NEJMoa1801550 (2018).

10 Perlin, D. S., Rautemaa-Richardson, R. & Alastruey-Izquierdo, A. The global problem of antifungal resistance: prevalence, mechanisms, and management. *Lancet Infect Dis* **17**, e383-e392, doi:10.1016/S1473-3099(17)30316-X (2017).

11 Brown, G. D. *et al.* Hidden killers: human fungal infections. *Sci Transl Med* **4**, 165rv113, doi:10.1126/scitranslmed.3004404 (2012).

12 Mpoza, E., Rhein, J. & Abassi, M. Emerging fluconazole resistance: Implications for the management of cryptococcal meningitis. *Med Mycol Case Rep* **19**, 30-32, doi:10.1016/j.mmcr.2017.11.004 (2018).

13 Chambers, H. F. & Deleo, F. R. Waves of resistance: Staphylococcus aureus in the antibiotic era. *Nat Rev Microbiol* **7**, 629-641, doi:10.1038/nrmicro2200 (2009).

14 Kreiswirth, B. *et al.* Evidence for a clonal origin of methicillin resistance in Staphylococcus aureus. *Science* **259**, 227-230, doi:10.1126/science.8093647 (1993).

15 Diekema, D. J. *et al.* Survey of infections due to Staphylococcus species: frequency of occurrence and antimicrobial susceptibility of isolates collected in the United States, Canada, Latin America, Europe, and the Western Pacific region for the SENTRY Antimicrobial Surveillance Program, 1997-1999. *Clin Infect Dis* **32 Suppl 2**, S114-132, doi:10.1086/320184 (2001).

16 Otto, M. Community-associated MRSA: what makes them special? *Int J Med Microbiol* **303**, 324-330, doi:10.1016/j.ijmm.2013.02.007 (2013).

17 Hiramatsu, K. *et al.* Methicillin-resistant Staphylococcus aureus clinical strain with reduced vancomycin susceptibility. *J Antimicrob Chemother* **40**, 135-136, doi:10.1093/jac/40.1.135 (1997).

18 Howden, B. P., Davies, J. K., Johnson, P. D., Stinear, T. P. & Grayson, M. L. Reduced vancomycin susceptibility in Staphylococcus aureus, including vancomycin-intermediate and heterogeneous vancomycin-intermediate strains: resistance mechanisms, laboratory detection, and clinical implications. *Clin Microbiol Rev* **23**, 99-139, doi:10.1128/CMR.00042-09 (2010).

19 Kluytmans, J., van Belkum, A. & Verbrugh, H. Nasal carriage of Staphylococcus aureus: epidemiology, underlying mechanisms, and associated risks. *Clin Microbiol Rev* **10**, 505-520 (1997).

20 Miller, L. G. & Diep, B. A. Clinical practice: colonization, fomites, and virulence: rethinking the pathogenesis of community-associated methicillin-resistant Staphylococcus aureus infection. *Clin Infect Dis* **46**, 752-760, doi:10.1086/526773 (2008).

21 Rhomberg, P. R. & Jones, R. N. Summary trends for the Meropenem Yearly Susceptibility Test Information Collection Program: a 10-year experience in the United States (1999-2008). *Diagn Microbiol Infect Dis* **65**, 414-426, doi:10.1016/j.diagmicrobio.2009.08.020 (2009).

22 Cisneros, J. M. *et al.* Bacteremia due to Acinetobacter baumannii: epidemiology, clinical findings, and prognostic features. *Clin Infect Dis* **22**, 1026-1032, doi:10.1093/clinids/22.6.1026 (1996).

23 Seifert, H., Strate, A. & Pulverer, G. Nosocomial bacteremia due to Acinetobacter baumannii. Clinical features, epidemiology, and predictors of mortality. *Medicine (Baltimore)* **74**, 340-349, doi:10.1097/00005792-199511000-00004 (1995).

24 Wisplinghoff, H., Perbix, W. & Seifert, H. Risk factors for nosocomial bloodstream infections due to Acinetobacter baumannii: a case-control study of adult burn patients. *Clin Infect Dis* **28**, 59-66, doi:10.1086/515067 (1999).

25 Davis, K. A., Moran, K. A., McAllister, C. K. & Gray, P. J. Multidrug-resistant Acinetobacter extremity infections in soldiers. *Emerg Infect Dis* **11**, 1218-1224, doi:10.3201/1108.050103 (2005).

26 Wise, K. A. & Tosolini, F. A. Epidemiological surveillance of Acinetobacter species. *J Hosp Infect* **16**, 319-329, doi:10.1016/0195-6701(90)90004-8 (1990).

27 Siegman-Igra, Y., Bar-Yosef, S., Gorea, A. & Avram, J. Nosocomial acinetobacter meningitis secondary to invasive procedures: report of 25 cases and review. *Clin Infect Dis* **17**, 843-849, doi:10.1093/clinids/17.5.843 (1993).

28 Dijkshoorn, L., Nemec, A. & Seifert, H. An increasing threat in hospitals: multidrug-resistant Acinetobacter baumannii. *Nat Rev Microbiol* **5**, 939-951, doi:10.1038/nrmicro1789 (2007).

29 Joly-Guillou, M. L. Clinical impact and pathogenicity of Acinetobacter. *Clin Microbiol Infect* **11**, 868-873, doi:10.1111/j.1469-0691.2005.01227.x (2005).

30 Seward, R. J., Lambert, T. & Towner, K. J. Molecular epidemiology of aminoglycoside resistance in Acinetobacter spp. *J Med Microbiol* **47**, 455-462, doi:10.1099/00222615-47-5-455 (1998).

31 Doi, Y. *et al.* Spread of novel aminoglycoside resistance gene aac(6')-Iad among Acinetobacter clinical isolates in Japan. *Antimicrob Agents Chemother* **48**, 2075-2080, doi:10.1128/aac.48.6.2075-2080.2004 (2004).

32 Vila, J., Ruiz, J., Goni, P. & Jimenez de Anta, T. Quinolone-resistance mutations in the topoisomerase IV parC gene of Acinetobacter baumannii. *J Antimicrob Chemother* **39**, 757-762, doi:10.1093/jac/39.6.757 (1997).

33 Huys, G. *et al.* Distribution of tetracycline resistance genes in genotypically related and unrelated multiresistant Acinetobacter baumannii strains from different European hospitals. *Res Microbiol* **156**, 348-355, doi:10.1016/j.resmic.2004.10.008 (2005).

34 Fournier, P. E. *et al.* Comparative genomics of multidrug resistance in Acinetobacter baumannii. *PLoS Genet* **2**, e7, doi:10.1371/journal.pgen.0020007 (2006).

35 WHO. Global priority list of antibiotic-resistant bacteria to guide research, discovery, and development of new antibiotics. Geneva: WHO; 2017. (World Health Organization, 2017).

36 Davies, D. Understanding biofilm resistance to antibacterial agents. *Nat Rev Drug Discov* **2**, 114-122, doi:10.1038/nrd1008 (2003).

37 P. Stoodley, K. Sauer, D. G. Davies & Costerton, J. W. Biofilms as Complex Differentiated Communities. *Annual Review of Microbiology* **56**, 187-209, doi:10.1146/annurev.micro.56.012302.160705 (2002).

38 Costerton, J. W., Stewart, P. S. & Greenberg, E. P. Bacterial biofilms: a common cause of persistent infections. *Science* **284**, 1318-1322, doi:10.1126/science.284.5418.1318 (1999).

39 Flemming, H. C. *et al.* Biofilms: an emergent form of bacterial life. *Nat Rev Microbiol* **14**, 563-575, doi:10.1038/nrmicro.2016.94 (2016).

40 Boles, B. R., Thoendel, M. & Singh, P. K. Self-generated diversity produces "insurance effects" in biofilm communities. *Proc Natl Acad Sci U S A* **101**, 16630-16635, doi:10.1073/pnas.0407460101 (2004).

41 Yang, L. *et al.* Combating biofilms. *FEMS Immunol Med Microbiol* **65**, 146-157, doi:10.1111/j.1574-695X.2011.00858.x (2012).

42 NIH. *Research on microbial biofilms.*, <https://grants.nih.gov/grants/guide/pa-files/pa-03-047.html> (2002).

43 Mihai, M. M. *et al.* Microbial biofilms: impact on the pathogenesis of periodontitis, cystic fibrosis, chronic wounds and medical device-related infections. *Curr Top Med Chem* **15**, 1552-1576, doi:10.2174/1568026615666150414123800 (2015).

44 Stacy, A., McNally, L., Darch, S. E., Brown, S. P. & Whiteley, M. The biogeography of polymicrobial infection. *Nat Rev Microbiol* **14**, 93-105, doi:10.1038/nrmicro.2015.8 (2016).

45 Xu, K. D., Stewart, P. S., Xia, F., Huang, C. T. & McFeters, G. A. Spatial physiological heterogeneity in Pseudomonas aeruginosa biofilm is determined by oxygen availability. *Appl Environ Microbiol* **64**, 4035-4039 (1998).

46 James, G. A. *et al.* Biofilms in chronic wounds. *Wound Repair Regen* **16**, 37-44, doi:10.1111/j.1524-475X.2007.00321.x (2008).

47 Stewart, P. S. & Franklin, M. J. Physiological heterogeneity in biofilms. *Nat Rev Microbiol* **6**, 199-210, doi:10.1038/nrmicro1838 (2008).

48 Flemming, H. C. & Wingender, J. The biofilm matrix. *Nat Rev Microbiol* **8**, 623-633, doi:10.1038/nrmicro2415 (2010).

49 Stewart, P. S. A review of experimental measurements of effective diffusive permeabilities and effective diffusion coefficients in biofilms. *Biotechnol Bioeng* **59**, 261-272 (1998).

50 Mulcahy, L. R., Burns, J. L., Lory, S. & Lewis, K. Emergence of Pseudomonas aeruginosa strains producing high levels of persister cells in patients with cystic fibrosis. *J Bacteriol* **192**, 6191-6199, doi:10.1128/JB.01651-09 (2010).

51 Fisher, R. A., Gollan, B. & Helaine, S. Persistent bacterial infections and persister cells. *Nat Rev Microbiol* **15**, 453-464, doi:10.1038/nrmicro.2017.42 (2017).

52 Stewart, P. S. & Costerton, J. W. Antibiotic resistance of bacteria in biofilms. *Lancet* **358**, 135-138, doi:10.1016/s0140-6736(01)05321-1 (2001).

53 Payne, D. J., Gwynn, M. N., Holmes, D. J. & Pompliano, D. L. Drugs for bad bugs: confronting the challenges of antibacterial discovery. *Nat Rev Drug Discov* **6**, 29-40, doi:10.1038/nrd2201 (2007).

54 Tommasi, R., Brown, D. G., Walkup, G. K., Manchester, J. I. & Miller, A. A. ESKAPEing the labyrinth of antibacterial discovery. *Nat Rev Drug Discov* **14**, 529-542, doi:10.1038/nrd4572 (2015).

55 Baker, S. J., Payne, D. J., Rappuoli, R. & De Gregorio, E. Technologies to address antimicrobial resistance. *Proc Natl Acad Sci U S A* **115**, 12887-12895, doi:10.1073/pnas.1717160115 (2018).

56 Brown, E. D. & Wright, G. D. Antibacterial drug discovery in the resistance era. *Nature* **529**, 336-343, doi:10.1038/nature17042 (2016).

57 Zlitni, S., Ferruccio, L. F. & Brown, E. D. Metabolic suppression identifies new antibacterial inhibitors under nutrient limitation. *Nat Chem Biol* **9**, 796-804, doi:10.1038/nchembio.1361 (2013).

58 Pethe, K. *et al.* Discovery of Q203, a potent clinical candidate for the treatment of tuberculosis. *Nat Med* **19**, 1157-1160, doi:10.1038/nm.3262 (2013).

59 Starkey, M. *et al.* Identification of anti-virulence compounds that disrupt quorum-sensing regulated acute and persistent pathogenicity. *PLoS Pathog* **10**, e1004321, doi:10.1371/journal.ppat.1004321 (2014).

60 Gonzalez-Bello, C. Antibiotic adjuvants - A strategy to unlock bacterial resistance to antibiotics. *Bioorg Med Chem Lett* **27**, 4221-4228, doi:10.1016/j.bmcl.2017.08.027 (2017).

61 Domalaon, R., Idowu, T., Zhanel, G. G. & Schweizer, F. Antibiotic Hybrids: the Next Generation of Agents and Adjuvants against Gram-Negative Pathogens? *Clin Microbiol Rev* **31**, doi:10.1128/CMR.00077-17 (2018).

62 Martens, E. & Demain, A. L. The antibiotic resistance crisis, with a focus on the United States. *J Antibiot (Tokyo)* **70**, 520-526, doi:10.1038/ja.2017.30 (2017).

63 Harms, A., Maisonneuve, E. & Gerdes, K. Mechanisms of bacterial persistence during stress and antibiotic exposure. *Science* **354**, doi:10.1126/science.aaf4268 (2016).

64 Hoiby, N., Bjarnsholt, T., Givskov, M., Molin, S. & Ciofu, O. Antibiotic resistance of bacterial biofilms. *Int J Antimicrob Agents* **35**, 322-332, doi:10.1016/j.ijantimicag.2009.12.011 (2010).

65 Lewis, K. Riddle of biofilm resistance. *Antimicrob Agents Chemother* **45**, 999-1007, doi:10.1128/AAC.45.4.999-1007.2001 (2001).

66 Kaplan, J. B. Antibiotic-induced biofilm formation. *Int J Artif Organs* **34**, 737-751, doi:10.5301/ijao.5000027 (2011).

67 Fernicola, S. *et al.* In Silico Discovery and In Vitro Validation of Catechol-Containing Sulfonohydrazide Compounds as Potent Inhibitors of the Diguanylate Cyclase PleD. *J Bacteriol* **198**, 147-156, doi:10.1128/JB.00742-15 (2016).

68 Sambanthamoorthy, K. *et al.* Identification of small molecules that antagonize diguanylate cyclase enzymes to inhibit biofilm formation. *Antimicrob Agents Chemother* **56**, 5202-5211, doi:10.1128/AAC.01396-12 (2012).

69 Fleming, D., Chahin, L. & Rumbaugh, K. Glycoside Hydrolases Degrade Polymicrobial Bacterial Biofilms in Wounds. *Antimicrob Agents Chemother* **61**, doi:10.1128/AAC.01998-16 (2017).

70 Ryan, R. P., An, S. Q., Allan, J. H., McCarthy, Y. & Dow, J. M. The DSF Family of Cell-Cell Signals: An Expanding Class of Bacterial Virulence Regulators. *PLoS Pathog* **11**, e1004986, doi:10.1371/journal.ppat.1004986 (2015).

71 Marques, C. N., Davies, D. G. & Sauer, K. Control of Biofilms with the Fatty Acid Signaling Molecule cis-2-Decenoic Acid. *Pharmaceuticals (Basel)* **8**, 816-835, doi:10.3390/ph8040816 (2015).

72 Anderson, J. K. *et al.* Chemorepulsion from the Quorum Signal Autoinducer-2 Promotes Helicobacter pylori Biofilm Dispersal. *MBio* **6**, e00379, doi:10.1128/mBio.00379-15 (2015).

73 DiGiandomenico, A. *et al.* Identification of broadly protective human antibodies to Pseudomonas aeruginosa exopolysaccharide Psl by phenotypic screening. *J Exp Med* **209**, 1273-1287, doi:10.1084/jem.20120033 (2012).

74 Flores-Mireles, A. L., Pinkner, J. S., Caparon, M. G. & Hultgren, S. J. EbpA vaccine antibodies block binding of Enterococcus faecalis to fibrinogen to prevent catheter-associated bladder infection in mice. *Sci Transl Med* **6**, 254ra127, doi:10.1126/scitranslmed.3009384 (2014).

75 Koo, H., Allan, R. N., Howlin, R. P., Stoodley, P. & Hall-Stoodley, L. Targeting microbial biofilms: current and prospective therapeutic strategies. *Nat Rev Microbiol* **15**, 740-755, doi:10.1038/nrmicro.2017.99 (2017).

76 Zazo, H., Colino, C. I. & Lanao, J. M. Current applications of nanoparticles in infectious diseases. *J Control Release* **224**, 86-102, doi:10.1016/j.jconrel.2016.01.008 (2016).

77 Cipolla, D., Blanchard, J. & Gonda, I. Development of Liposomal Ciprofloxacin to Treat Lung Infections. *Pharmaceutics* **8**, doi:10.3390/pharmaceutics8010006 (2016).

78 Clancy, J. P. *et al.* Phase II studies of nebulised Arikace in CF patients with Pseudomonas aeruginosa infection. *Thorax* **68**, 818-825, doi:10.1136/thoraxjnl-2012-202230 (2013).

79 Gao, L. *et al.* Nanocatalysts promote Streptococcus mutans biofilm matrix degradation and enhance bacterial killing to suppress dental caries in vivo. *Biomaterials* **101**, 272-284, doi:10.1016/j.biomaterials.2016.05.051 (2016).

80 Lewis, K. Antibiotics: Recover the lost art of drug discovery. *Nature* **485**, 439-440, doi:10.1038/485439a (2012).

81 Cox, G. *et al.* A Common Platform for Antibiotic Dereplication and Adjuvant Discovery. *Cell Chem Biol* **24**, 98-109, doi:10.1016/j.chembiol.2016.11.011 (2017).

82 Liu, X. & Cheng, Y. Q. Genome-guided discovery of diverse natural products from Burkholderia sp. *J Ind Microbiol Biotechnol* **41**, 275-284, doi:10.1007/s10295-013-1376-1 (2014).

83 Seyedsayamdost, M. R. High-throughput platform for the discovery of elicitors of silent bacterial gene clusters. *Proc Natl Acad Sci U S A* **111**, 7266-7271, doi:10.1073/pnas.1400019111 (2014).

84 Okada, B. K., Wu, Y., Mao, D., Bushin, L. B. & Seyedsayamdost, M. R. Mapping the Trimethoprim-Induced Secondary Metabolome of Burkholderia thailandensis. *ACS Chem Biol* **11**, 2124-2130, doi:10.1021/acschembio.6b00447 (2016).

85 Vial, L., Groleau, M. C., Dekimpe, V. & Deziel, E. Burkholderia diversity and versatility: an inventory of the extracellular products. *J Microbiol Biotechnol* **17**, 1407-1429 (2007).

86 Depoorter, E. *et al.* Burkholderia: an update on taxonomy and biotechnological potential as antibiotic producers. *Appl Microbiol Biotechnol* **100**, 5215-5229, doi:10.1007/s00253-016-7520-x (2016).

87 Coenye, T. & Vandamme, P. Diversity and significance of Burkholderia species occupying diverse ecological niches. *Environ Microbiol* **5**, 719-729 (2003).

88 Compant, S., Nowak, J., Coenye, T., Clement, C. & Ait Barka, E. Diversity and occurrence of Burkholderia spp. in the natural environment. *FEMS Microbiol Rev* **32**, 607-626, doi:10.1111/j.1574-6976.2008.00113.x (2008).

89 Yabuuchi, E. *et al.* Proposal of Burkholderia gen. nov. and transfer of seven species of the genus Pseudomonas homology group II to the new genus, with the type species Burkholderia cepacia (Palleroni and Holmes 1981) comb. nov. *Microbiol Immunol* **36**, 1251-1275, doi:10.1111/j.1348-0421.1992.tb02129.x (1992).

90 Blin, K. *et al.* antiSMASH 2.0--a versatile platform for genome mining of secondary metabolite producers. *Nucleic Acids Res* **41**, W204-212, doi:10.1093/nar/gkt449 (2013).

91 Medema, M. H. *et al.* antiSMASH: rapid identification, annotation and analysis of secondary metabolite biosynthesis gene clusters in bacterial and fungal genome sequences. *Nucleic Acids Res* **39**, W339-346, doi:10.1093/nar/gkr466 (2011).

92 Sawana, A., Adeolu, M. & Gupta, R. S. Molecular signatures and phylogenomic analysis of the genus Burkholderia: proposal for division of this genus into the emended genus Burkholderia containing pathogenic organisms and a new genus Paraburkholderia gen. nov. harboring environmental species. *Front Genet* **5**, 429, doi:10.3389/fgene.2014.00429 (2014).

93 Wiersinga, W. J., van der Poll, T., White, N. J., Day, N. P. & Peacock, S. J. Melioidosis: insights into the pathogenicity of Burkholderia pseudomallei. *Nat Rev Microbiol* **4**, 272-282, doi:10.1038/nrmicro1385 (2006).

94 Galyov, E. E., Brett, P. J. & DeShazer, D. Molecular insights into Burkholderia pseudomallei and Burkholderia mallei pathogenesis. *Annu Rev Microbiol* **64**, 495-517, doi:10.1146/annurev.micro.112408.134030 (2010).

95 Brett, P. J., DeShazer, D. & Woods, D. E. Burkholderia thailandensis sp. nov., a Burkholderia pseudomallei-like species. *Int J Syst Bacteriol* **48 Pt 1**, 317-320, doi:10.1099/00207713-48-1-317 (1998).

96 Knappe, T. A. *et al.* Isolation and structural characterization of capistruin, a lasso peptide predicted from the genome sequence of Burkholderia thailandensis E264. *J Am Chem Soc* **130**, 11446-11454, doi:10.1021/ja802966g (2008).

97 Biggins, J. B., Ternei, M. A. & Brady, S. F. Malleilactone, a polyketide synthase-derived virulence factor encoded by the cryptic secondary metabolome of Burkholderia pseudomallei group pathogens. *J Am Chem Soc* **134**, 13192-13195, doi:10.1021/ja3052156 (2012).

98 Nguyen, T. *et al.* Exploiting the mosaic structure of trans-acyltransferase polyketide synthases for natural product discovery and pathway dissection. *Nat Biotechnol* **26**, 225-233, doi:10.1038/nbt1379 (2008).

99 Biggins, J. B., Gleber, C. D. & Brady, S. F. Acyldepsipeptide HDAC inhibitor production induced in Burkholderia thailandensis. *Org Lett* **13**, 1536-1539, doi:10.1021/ol200225v (2011).

100 Liu, X. *et al.* Genomics-guided discovery of thailanstatins A, B, and C As pre-mRNA splicing inhibitors and antiproliferative agents from Burkholderia thailandensis MSMB43. *J Nat Prod* **76**, 685-693, doi:10.1021/np300913h (2013).

101 Seyedsayamdost, M. R. *et al.* Quorum-sensing-regulated bactobolin production by Burkholderia thailandensis E264. *Org Lett* **12**, 716-719, doi:10.1021/ol902751x (2010).

102 Dubeau, D., Deziel, E., Woods, D. E. & Lepine, F. Burkholderia thailandensis harbors two identical rhl gene clusters responsible for the biosynthesis of rhamnolipids. *BMC Microbiol* **9**, 263, doi:10.1186/1471-2180-9-263 (2009).

103 Vial, L. *et al.* Burkholderia pseudomallei, B. thailandensis, and B. ambifaria produce 4-hydroxy-2-alkylquinoline analogues with a methyl group at the 3 position that is required for quorum-sensing regulation. *J Bacteriol* **190**, 5339-5352, doi:10.1128/jb.00400-08 (2008).

104 Carr, G., Seyedsayamdost, M. R., Chandler, J. R., Greenberg, E. P. & Clardy, J. Sources of diversity in bactobolin biosynthesis by Burkholderia thailandensis E264. *Org Lett* **13**, 3048-3051, doi:10.1021/ol200922s (2011).

105 Kondo, S., Horiuchi, Y., Hamada, M., Takeuchi, T. & Umezawa, H. A new antitumor antibiotic, bactobolin produced by Pseudomonas. *J Antibiot (Tokyo)* **32**, 1069-1071, doi:10.7164/antibiotics.32.1069 (1979).

106 Elshikh, M. *et al.* Rhamnolipids from non-pathogenic Burkholderia thailandensis E264: Physicochemical characterization, antimicrobial and antibiofilm efficacy against oral hygiene related pathogens. *N Biotechnol* **36**, 26-36, doi:10.1016/j.nbt.2016.12.009 (2017).

107 Wu, Y. & Seyedsayamdost, M. R. Synergy and Target Promiscuity Drive Structural Divergence in Bacterial Alkylquinolone Biosynthesis. *Cell Chem Biol* **24**, 1437-1444.e1433, doi:10.1016/j.chembiol.2017.08.024 (2017).

108 Duerkop, B. A. *et al.* Quorum-sensing control of antibiotic synthesis in Burkholderia thailandensis. *J Bacteriol* **191**, 3909-3918, doi:10.1128/JB.00200-09 (2009).

109 Deziel, E. *et al.* Analysis of Pseudomonas aeruginosa 4-hydroxy-2-alkylquinolines (HAQs) reveals a role for 4-hydroxy-2-heptylquinoline in cell-to-cell communication. *Proc Natl Acad Sci U S A* **101**, 1339-1344, doi:10.1073/pnas.0307694100 (2004).

110 Jarvis, F. & Johnson, M. A glyco-lipide produced by Pseudomonas aeruginosa. *Journal of the American Chemical Society* **71**, 4124-4126 (1949).

111 Paulino, B. N. *et al.* Current status in biotechnological production and applications of glycolipid biosurfactants. *Appl Microbiol Biotechnol* **100**, 10265-10293, doi:10.1007/s00253-016-7980-z (2016).

112 Costa, S. G., Deziel, E. & Lepine, F. Characterization of rhamnolipid production by Burkholderia glumae. *Lett Appl Microbiol* **53**, 620-627, doi:10.1111/j.1472-765X.2011.03154.x (2011).

113 De Rienzo, M. A. & Martin, P. J. Effect of Mono and Di-rhamnolipids on Biofilms Pre-formed by Bacillus subtilis BBK006. *Curr Microbiol* **73**, 183-189, doi:10.1007/s00284-016-1046-4 (2016).

114 Vatsa, P., Sanchez, L., Clement, C., Baillieul, F. & Dorey, S. Rhamnolipid biosurfactants as new players in animal and plant defense against microbes. *Int J Mol Sci* **11**, 5095-5108, doi:10.3390/ijms11125095 (2010).

115 Wood, T. L. *et al.* Rhamnolipids from Pseudomonas aeruginosa disperse the biofilms of sulfate-reducing bacteria. *NPJ Biofilms Microbiomes* **4**, 22, doi:10.1038/s41522-018-0066-1 (2018).

116 Victor, I. U. *et al.* Quorum sensing as a potential target for increased production of rhamnolipid biosurfactant in Burkholderia thailandensis E264. *Appl Microbiol Biotechnol* **103**, 6505-6517, doi:10.1007/s00253-019-09942-5 (2019).

117 Deatherage, B. L. & Cookson, B. T. Membrane vesicle release in bacteria, eukaryotes, and archaea: a conserved yet underappreciated aspect of microbial life. *Infect Immun* **80**, 1948-1957, doi:10.1128/iai.06014-11 (2012).

118 Beveridge, T. J., Makin, S. A., Kadurugamuwa, J. L. & Li, Z. Interactions between biofilms and the environment. *FEMS Microbiology Reviews* **20**, 291-303 (1997).

119 Bonnington, K. E. & Kuehn, M. J. Protein selection and export via outer membrane vesicles. *Biochim Biophys Acta* **1843**, 1612-1619, doi:10.1016/j.bbamcr.2013.12.011 (2014).

120 Tashiro, Y. *et al.* Characterization of phospholipids in membrane vesicles derived from Pseudomonas aeruginosa. *Biosci Biotechnol Biochem* **75**, 605-607, doi:10.1271/bbb.100754 (2011).

121 Nieves, W. *et al.* A naturally derived outer-membrane vesicle vaccine protects against lethal pulmonary Burkholderia pseudomallei infection. *Vaccine* **29**, 8381-8389, doi:10.1016/j.vaccine.2011.08.058 (2011).

122 Sjostrom, A. E., Sandblad, L., Uhlin, B. E. & Wai, S. N. Membrane vesicle-mediated release of bacterial RNA. *Sci Rep* **5**, 15329, doi:10.1038/srep15329 (2015).

123 Dorward, D. W. & Garon, C. F. DNA Is Packaged within Membrane-Derived Vesicles of Gram-Negative but Not Gram-Positive Bacteria. *Appl Environ Microbiol* **56**, 1960-1962 (1990).

124 Mashburn-Warren, L. *et al.* Interaction of quorum signals with outer membrane lipids: insights into prokaryotic membrane vesicle formation. *Mol Microbiol* **69**, 491-502, doi:10.1111/j.1365-2958.2008.06302.x (2008).

125 Baumgarten, T. *et al.* Membrane vesicle formation as a multiple-stress response mechanism enhances Pseudomonas putida DOT-T1E cell surface hydrophobicity and biofilm formation. *Appl Environ Microbiol* **78**, 6217-6224, doi:10.1128/AEM.01525-12 (2012).

126 Mashburn-Warren, L. M. & Whiteley, M. Special delivery: vesicle trafficking in prokaryotes. *Mol Microbiol* **61**, 839-846, doi:10.1111/j.1365-2958.2006.05272.x (2006).

127 Kaparakis-Liaskos, M. & Ferrero, R. L. Immune modulation by bacterial outer membrane vesicles. *Nat Rev Immunol* **15**, 375-387, doi:10.1038/nri3837 (2015).

128 Alves, N. J., Turner, K. B., Medintz, I. L. & Walper, S. A. Protecting enzymatic function through directed packaging into bacterial outer membrane vesicles. *Sci Rep* **6**, 24866, doi:10.1038/srep24866 (2016).

129 Kadurugamuwa, J. L. & Beveridge, T. J. Bacteriolytic effect of membrane vesicles from Pseudomonas aeruginosa on other bacteria including pathogens: conceptually new antibiotics. *J Bacteriol* **178**, 2767-2774, doi:10.1128/jb.178.10.2767-2774.1996 (1996).

130 Wilkins, A. L. & Snape, M. D. Emerging clinical experience with vaccines against group B meningococcal disease. *Vaccine* **36**, 5470-5476, doi:10.1016/j.vaccine.2017.07.056 (2018).

131 Schooling, S. R. & Beveridge, T. J. Membrane vesicles: an overlooked component of the matrices of biofilms. *J Bacteriol* **188**, 5945-5957, doi:10.1128/jb.00257-06 (2006).

132 Li, Z., Clarke, A. J. & Beveridge, T. J. A major autolysin of Pseudomonas aeruginosa: subcellular distribution, potential role in cell growth and division and secretion in surface membrane vesicles. *J Bacteriol* **178**, 2479-2488, doi:10.1128/jb.178.9.2479-2488.1996 (1996).

133 Li, Z., Clarke, A. J. & Beveridge, T. J. Gram-negative bacteria produce membrane vesicles which are capable of killing other bacteria. *J Bacteriol* **180**, 5478-5483 (1998).

134 MacDonald, K. L. & Beveridge, T. J. Bactericidal effect of gentamicin-induced membrane vesicles derived from Pseudomonas aeruginosa PAO1 on gram-positive bacteria. *Can J Microbiol* **48**, 810-820, doi:10.1139/w02-077 (2002).

135 Vasilyeva, N. V., Tsfasman, I. M., Suzina, N. E., Stepnaya, O. A. & Kulaev, I. S. Secretion of bacteriolytic endopeptidase L5 of Lysobacter sp. XL1 into the medium by means of outer membrane vesicles. *FEBS J* **275**, 3827-3835, doi:10.1111/j.1742-4658.2008.06530.x (2008).

136 Berleman, J. E. *et al.* The lethal cargo of Myxococcus xanthus outer membrane vesicles. *Front Microbiol* **5**, 474, doi:10.3389/fmicb.2014.00474 (2014).

137 Evans, A. G. *et al.* Predatory activity of Myxococcus xanthus outer-membrane vesicles and properties of their hydrolase cargo. *Microbiology* **158**, 2742-2752, doi:10.1099/mic.0.060343-0 (2012).

138 Berleman, J. E. & Kirby, J. R. Deciphering the hunting strategy of a bacterial wolfpack. *FEMS Microbiol Rev* **33**, 942-957, doi:10.1111/j.1574-6976.2009.00185.x (2009).

139 Velicer, G. J. & Mendes-Soares, H. Bacterial predators. *Curr Biol* **19**, R55-56, doi:10.1016/j.cub.2008.10.043 (2009).

140 Vollmer, W., Joris, B., Charlier, P. & Foster, S. Bacterial peptidoglycan (murein) hydrolases. *FEMS Microbiol Rev* **32**, 259-286, doi:10.1111/j.1574-6976.2007.00099.x (2008).

141 Vollmer, W., Blanot, D. & de Pedro, M. A. Peptidoglycan structure and architecture. *FEMS Microbiol Rev* **32**, 149-167, doi:10.1111/j.1574-6976.2007.00094.x (2008).

142 Sharif, S., Singh, M., Kim, S. J. & Schaefer, J. Staphylococcus aureus peptidoglycan tertiary structure from carbon-13 spin diffusion. *J Am Chem Soc* **131**, 7023-7030, doi:10.1021/ja808971c (2009).

143 Chambless, J. D., Hunt, S. M. & Stewart, P. S. A three-dimensional computer model of four hypothetical mechanisms protecting biofilms from antimicrobials. *Appl Environ Microbiol* **72**, 2005-2013, doi:10.1128/AEM.72.3.2005-2013.2006 (2006).

144 Bjarnsholt, T., Ciofu, O., Molin, S., Givskov, M. & Hoiby, N. Applying insights from biofilm biology to drug development - can a new approach be developed? *Nat Rev Drug Discov* **12**, 791-808, doi:10.1038/nrd4000 (2013).

145 Kuehn, M. J. & Kesty, N. C. Bacterial outer membrane vesicles and the host-pathogen interaction. *Genes Dev* **19**, 2645-2655, doi:10.1101/gad.1299905 (2005).

146 Jan, A. T. Outer Membrane Vesicles (OMVs) of Gram-negative Bacteria: A Perspective Update. *Front Microbiol* **8**, 1053, doi:10.3389/fmicb.2017.01053 (2017).

147 Mashburn, L. M. & Whiteley, M. Membrane vesicles traffic signals and facilitate group activities in a prokaryote. *Nature* **437**, 422-425, doi:10.1038/nature03925 (2005).

148 Renelli, M., Matias, V., Lo, R. Y. & Beveridge, T. J. DNA-containing membrane vesicles of Pseudomonas aeruginosa PAO1 and their genetic transformation potential. *Microbiology* **150**, 2161-2169, doi:10.1099/mic.0.26841-0 (2004).

149 Klimentova, J. & Stulik, J. Methods of isolation and purification of outer membrane vesicles from gram-negative bacteria. *Microbiol Res* **170**, 1-9, doi:10.1016/j.micres.2014.09.006 (2015).

150 Keenan, J. I., Davis, K. A., Beaugie, C. R., McGovern, J. J. & Moran, A. P. Alterations in Helicobacter pylori outer membrane and outer membrane vesicle-associated lipopolysaccharides under iron-limiting growth conditions. *Innate Immun* **14**, 279-290, doi:10.1177/1753425908096857 (2008).

151 Macdonald, I. A. & Kuehn, M. J. Stress-induced outer membrane vesicle production by Pseudomonas aeruginosa. *J Bacteriol* **195**, 2971-2981, doi:10.1128/JB.02267-12 (2013).

152 Tashiro, Y. *et al.* Variation of physiochemical properties and cell association activity of membrane vesicles with growth phase in Pseudomonas aeruginosa. *Appl Environ Microbiol* **76**, 3732-3739, doi:10.1128/AEM.02794-09 (2010).

153 Oishi, S. *et al.* Cellular locations of proteinases and association with vesicles in Porphyromonas gingivalis. *Eur J Med Res* **15**, 397-402, doi:10.1186/2047-783x-15-9-397 (2010).

154 Kulp, A. & Kuehn, M. J. Biological functions and biogenesis of secreted bacterial outer membrane vesicles. *Annu Rev Microbiol* **64**, 163-184, doi:10.1146/annurev.micro.091208.073413 (2010).

155 Bauman, S. J. & Kuehn, M. J. Purification of outer membrane vesicles from Pseudomonas aeruginosa and their activation of an IL-8 response. *Microbes Infect* **8**, 2400-2408, doi:10.1016/j.micinf.2006.05.001 (2006).

156 Post, D. M. *et al.* Biochemical and functional characterization of membrane blebs purified from Neisseria meningitidis serogroup B. *J Biol Chem* **280**, 38383-38394, doi:10.1074/jbc.M508063200 (2005).

157 Monguio-Tortajada, M., Galvez-Monton, C., Bayes-Genis, A., Roura, S. & Borras, F. E. Extracellular vesicle isolation methods: rising impact of size-exclusion chromatography. *Cell Mol Life Sci* **76**, 2369-2382, doi:10.1007/s00018-019-03071-y (2019).

158 McNamara, R. P. & Dittmer, D. P. Modern Techniques for the Isolation of Extracellular Vesicles and Viruses. *J Neuroimmune Pharmacol*, doi:10.1007/s11481-019-09874-x (2019).

159 Nieves, W. *et al.* A Burkholderia pseudomallei outer membrane vesicle vaccine provides protection against lethal sepsis. *Clin Vaccine Immunol* **21**, 747-754, doi:10.1128/cvi.00119-14 (2014).

160 Petersen, H., Nieves, W., Russell-Lodrigue, K., Roy, C. J. & Morici, L. A. Evaluation of a Burkholderia pseudomallei Outer Membrane Vesicle Vaccine in Nonhuman Primates. *Procedia Vaccinol* **8**, 38-42, doi:10.1016/j.provac.2014.07.007 (2014).

161 Zaragoza, O. *et al.* The capsule of the fungal pathogen Cryptococcus neoformans. *Adv Appl Microbiol* **68**, 133-216, doi:10.1016/S0065-2164(09)01204-0 (2009).

162 Papenfort, K. & Bassler, B. L. Quorum sensing signal-response systems in Gram-negative bacteria. *Nat Rev Microbiol* **14**, 576-588, doi:10.1038/nrmicro.2016.89 (2016).

163 Rutherford, S. T. & Bassler, B. L. Bacterial quorum sensing: its role in virulence and possibilities for its control. *Cold Spring Harb Perspect Med* **2**, doi:10.1101/cshperspect.a012427 (2012).

164 Whiteley, M., Diggle, S. P. & Greenberg, E. P. Progress in and promise of bacterial quorum sensing research. *Nature* **551**, 313-320, doi:10.1038/nature24624 (2017).

165 Peleg, A. Y., Seifert, H. & Paterson, D. L. Acinetobacter baumannii: emergence of a successful pathogen. *Clin Microbiol Rev* **21**, 538-582, doi:10.1128/CMR.00058-07 (2008).

166 Thompson, M. G. *et al.* Validation of a novel murine wound model of Acinetobacter baumannii infection. *Antimicrob Agents Chemother* **58**, 1332-1342, doi:10.1128/AAC.01944-13 (2014).

167 Greene, C., Wu, J., Rickard, A. H. & Xi, C. Evaluation of the ability of Acinetobacter baumannii to form biofilms on six different biomedical relevant surfaces. *Lett Appl Microbiol* **63**, 233-239, doi:10.1111/lam.12627 (2016).

168 Mohamed, J. A. & Huang, D. B. Biofilm formation by enterococci. *J Med Microbiol* **56**, 1581-1588, doi:10.1099/jmm.0.47331-0 (2007).

169 Mohamed, J. A., Huang, W. X., Nallapareddy, S. R., Teng, F. & Murray, B. E. Influence of origin of isolates, especially endocarditis isolates, and various genes

on biofilm formation by Enterococcus faecalis (vol 72, pg 3658, 2004). *Infection and Immunity* **73**, 7075-7075, doi:10.1128/Iai.73.10.7075.2005 (2005).

170 McCarthy, H. *et al.* Methicillin resistance and the biofilm phenotype in Staphylococcus aureus. *Front Cell Infect Microbiol* **5**, 1, doi:10.3389/fcimb.2015.00001 (2015).

171 Percival, S. L., Emanuel, C., Cutting, K. F. & Williams, D. W. Microbiology of the skin and the role of biofilms in infection. *Int Wound J* **9**, 14-32, doi:10.1111/j.1742-481X.2011.00836.x (2012).

172 Petersen, P. E. & Ogawa, H. Prevention of dental caries through the use of fluoride - the WHO approach. *Community Dent Hlth* **33**, 66-68, doi:10.1922/CDH_Petersen03 (2016).

173 Loesche, W. J. Role of Streptococcus mutans in human dental decay. *Microbiol Rev* **50**, 353-380 (1986).

174 Koo, H., Xiao, J. & Klein, M. I. Extracellular polysaccharides matrix--an often forgotten virulence factor in oral biofilm research. *Int J Oral Sci* **1**, 229-234, doi:10.4248/IJOS.09086 (2009).

175 Lemos, J. A., Quivey, R. G., Jr., Koo, H. & Abranches, J. Streptococcus mutans: a new Gram-positive paradigm? *Microbiology* **159**, 436-445, doi:10.1099/mic.0.066134-0 (2013).

176 Loo, C. Y., Corliss, D. A. & Ganeshkumar, N. Streptococcus gordonii biofilm formation: identification of genes that code for biofilm phenotypes. *J Bacteriol* **182**, 1374-1382, doi:10.1128/jb.182.5.1374-1382.2000 (2000).

177 Bitoun, J. P. *et al.* BrpA is involved in regulation of cell envelope stress responses in Streptococcus mutans. *Appl Environ Microbiol* **78**, 2914-2922, doi:10.1128/AEM.07823-11 (2012).

178 Wen, Z. T. & Burne, R. A. Functional genomics approach to identifying genes required for biofilm development by Streptococcus mutans. *Appl Environ Microbiol* **68**, 1196-1203, doi:10.1128/aem.68.3.1196-1203.2002 (2002).

179 DeFrancesco, A. S. *et al.* Genome-wide screen for genes involved in eDNA release during biofilm formation by Staphylococcus aureus. *Proc Natl Acad Sci U S A* **114**, E5969-E5978, doi:10.1073/pnas.1704544114 (2017).

180 Heydorn, A. *et al.* Quantification of biofilm structures by the novel computer program COMSTAT. *Microbiology* **146 (Pt 10)**, 2395-2407, doi:10.1099/00221287-146-10-2395 (2000).

181 Korber, D., Lawrence, J., Hendry, M. & Caldwell, D. Analysis of spatial variability within Mot+ and Mot− Pseudomonas fluorescens biofilms using representative elements. *Biofouling* **7**, 339-358 (1993).

182 Vorregaard, M. *Comstat2-a modern 3D image analysis environment for biofilms*, Citeseer, (2008).

183 de Queiroz, V. S. *et al.* Influence of the Culture Medium in Dose-Response Effect of the Chlorhexidine on Streptococcus mutans Biofilms. *Scientifica (Cairo)* **2016**, 2816812, doi:10.1155/2016/2816812 (2016).

184 Koo, H. *et al.* Inhibition of Streptococcus mutans biofilm accumulation and polysaccharide production by apigenin and tt-farnesol. *J Antimicrob Chemother* **52**, 782-789, doi:10.1093/jac/dkg449 (2003).

185 Bitoun, J. P., Nguyen, A. H., Fan, Y., Burne, R. A. & Wen, Z. T. Transcriptional repressor Rex is involved in regulation of oxidative stress response and biofilm formation by Streptococcus mutans. *FEMS Microbiol Lett* **320**, 110-117, doi:10.1111/j.1574-6968.2011.02293.x (2011).

186 Wen, Z. T., Baker, H. V. & Burne, R. A. Influence of BrpA on critical virulence attributes of Streptococcus mutans. *J Bacteriol* **188**, 2983-2992, doi:10.1128/JB.188.8.2983-2992.2006 (2006).

187 Wen, Z. T., Suntharaligham, P., Cvitkovitch, D. G. & Burne, R. A. Trigger factor in Streptococcus mutans is involved in stress tolerance, competence development, and biofilm formation. *Infect Immun* **73**, 219-225, doi:10.1128/IAI.73.1.219-225.2005 (2005).

188 Mah, T. F. Establishing the minimal bactericidal concentration of an antimicrobial agent for planktonic cells (MBC-P) and biofilm cells (MBC-B). *J Vis Exp*, e50854, doi:10.3791/50854 (2014).

189 Reen, F. J. *et al.* The Pseudomonas quinolone signal (PQS), and its precursor HHQ, modulate interspecies and interkingdom behaviour. *FEMS Microbiol Ecol* **77**, 413-428, doi:10.1111/j.1574-6941.2011.01121.x (2011).

190 Inaba, T., Oura, H., Morinaga, K., Toyofuku, M. & Nomura, N. The Pseudomonas Quinolone Signal Inhibits Biofilm Development of Streptococcus mutans. *Microbes Environ* **30**, 189-191, doi:10.1264/jsme2.ME14140 (2015).

191 Bryan, L. E. & Van Den Elzen, H. M. Effects of membrane-energy mutations and cations on streptomycin and gentamicin accumulation by bacteria: a model for

entry of streptomycin and gentamicin in susceptible and resistant bacteria. *Antimicrob Agents Chemother* **12**, 163-177, doi:10.1128/aac.12.2.163 (1977).

192 Martin, N. L. & Beveridge, T. J. Gentamicin interaction with Pseudomonas aeruginosa cell envelope. *Antimicrob Agents Chemother* **29**, 1079-1087, doi:10.1128/aac.29.6.1079 (1986).

193 Deng, D. M. *et al.* Influence of Streptococcus mutans on Enterococcus faecalis biofilm formation. *J Endod* **35**, 1249-1252, doi:10.1016/j.joen.2009.05.038 (2009).

194 Nobile, C. J. & Johnson, A. D. Candida albicans Biofilms and Human Disease. *Annu Rev Microbiol* **69**, 71-92, doi:10.1146/annurev-micro-091014-104330 (2015).

195 Ramage, G. & Williams, C. The clinical importance of fungal biofilms. *Adv Appl Microbiol* **84**, 27-83, doi:10.1016/B978-0-12-407673-0.00002-3 (2013).

196 Walsh, T. J., Schlegel, R., Moody, M. M., Costerton, J. W. & Salcman, M. Ventriculoatrial Shunt Infection Due to Cryptococcus-Neoformans - an Ultrastructural and Quantitative Microbiological Study. *Neurosurgery* **18**, 373-375, doi:Doi 10.1227/00006123-198603000-00025 (1986).

197 Kunze, B., Bedorf, N., Kohl, W., Hofle, G. & Reichenbach, H. Myxochelin A, a new iron-chelating compound from Angiococcus disciformis (Myxobacterales). Production, isolation, physico-chemical and biological properties. *J Antibiot (Tokyo)* **42**, 14-17, doi:10.7164/antibiotics.42.14 (1989).

198 Gerth, K. *et al.* The myxalamids, new antibiotics from Myxococcus xanthus (Myxobacterales). I. Production, physico-chemical and biological properties, and

mechanism of action. *J Antibiot (Tokyo)* **36**, 1150-1156, doi:10.7164/antibiotics.36.1150 (1983).

199 Xiao, Y., Gerth, K., Muller, R. & Wall, D. Myxobacterium-produced antibiotic TA (myxovirescin) inhibits type II signal peptidase. *Antimicrob Agents Chemother* **56**, 2014-2021, doi:10.1128/AAC.06148-11 (2012).

200 Mashburn-Warren, L. *et al.* Interaction of quorum signals with outer membrane lipids: insights into prokaryotic membrane vesicle formation. *Molecular Microbiology* **69**, 491-502, doi:10.1111/j.1365-2958.2008.06302.x (2008).

201 Tashiro, Y., Yawata, Y., Toyofuku, M., Uchiyama, H. & Nomura, N. Interspecies Interaction between Pseudomonas aeruginosa and Other Microorganisms. *Microbes Environ* **28**, 13-24, doi:10.1264/jsme2.ME12167 (2013).

202 Mashburn-Warren, L., Howe, J., Brandenburg, K. & Whiteley, M. Structural requirements of the Pseudomonas quinolone signal for membrane vesicle stimulation. *J Bacteriol* **191**, 3411-3414, doi:10.1128/JB.00052-09 (2009).

203 Toyofuku, M., Nakajima-Kambe, T., Uchiyama, H. & Nomura, N. The effect of a cell-to-cell communication molecule, Pseudomonas quinolone signal (PQS), produced by P. aeruginosa on other bacterial species. *Microbes Environ* **25**, 1-7, doi:10.1264/jsme2.me09156 (2010).

204 Li, L. *et al.* Identification and functional characterization of a peptidoglycan recognition protein from the cotton bollworm, Helicoverpa armigera. *Arch Insect Biochem Physiol* **86**, 240-258, doi:10.1002/arch.21174 (2014).

205 Rosenthal, R. S. & Dziarski, R. Isolation of peptidoglycan and soluble peptidoglycan fragments. *Methods Enzymol* **235**, 253-285, doi:10.1016/0076-6879(94)35146-5 (1994).

206 Mellroth, P., Karlsson, J. & Steiner, H. A scavenger function for a Drosophila peptidoglycan recognition protein. *J Biol Chem* **278**, 7059-7064, doi:10.1074/jbc.M208900200 (2003).

207 Fukushima, T. & Sekiguchi, J. Zymographic Techniques for the Analysis of Bacterial Cell Wall in Bacillus. *Methods Mol Biol* **1440**, 87-98, doi:10.1007/978-1-4939-3676-2_7 (2016).

208 Buist, G., Steen, A., Kok, J. & Kuipers, O. P. LysM, a widely distributed protein motif for binding to (peptido)glycans. *Mol Microbiol* **68**, 838-847, doi:10.1111/j.1365-2958.2008.06211.x (2008).

209 van Asselt, E. J. *et al.* Crystal structure of Escherichia coli lytic transglycosylase Slt35 reveals a lysozyme-like catalytic domain with an EF-hand. *Structure* **7**, 1167-1180, doi:10.1016/s0969-2126(00)80051-9 (1999).

210 Powell, A. J., Liu, Z. J., Nicholas, R. A. & Davies, C. Crystal structures of the lytic transglycosylase MltA from N.gonorrhoeae and E.coli: insights into interdomain movements and substrate binding. *J Mol Biol* **359**, 122-136, doi:10.1016/j.jmb.2006.03.023 (2006).

211 van Asselt, E. J., Thunnissen, A. M. & Dijkstra, B. W. High resolution crystal structures of the Escherichia coli lytic transglycosylase Slt70 and its complex with a peptidoglycan fragment. *J Mol Biol* **291**, 877-898, doi:10.1006/jmbi.1999.3013 (1999).

212 Kerff, F. *et al.* Specific structural features of the N-acetylmuramoyl-L-alanine amidase AmiD from Escherichia coli and mechanistic implications for enzymes of this family. *J Mol Biol* **397**, 249-259, doi:10.1016/j.jmb.2009.12.038 (2010).

213 Rawlings, N. D. & Barrett, A. J. Evolutionary families of metallopeptidases. *Methods Enzymol* **248**, 183-228, doi:10.1016/0076-6879(95)48015-3 (1995).

214 Oshida, T. *et al.* A Staphylococcus aureus autolysin that has an N-acetylmuramoyl-L-alanine amidase domain and an endo-beta-N-acetylglucosaminidase domain: cloning, sequence analysis, and characterization. *Proc Natl Acad Sci U S A* **92**, 285-289, doi:10.1073/pnas.92.1.285 (1995).

215 Lin, J., Cheng, J., Wang, Y. & Shen, X. The Pseudomonas Quinolone Signal (PQS): Not Just for Quorum Sensing Anymore. *Front Cell Infect Microbiol* **8**, 230, doi:10.3389/fcimb.2018.00230 (2018).

216 Kim, K. *et al.* HHQ and PQS, two Pseudomonas aeruginosa quorum-sensing molecules, down-regulate the innate immune responses through the nuclear factor-kappaB pathway. *Immunology* **129**, 578-588, doi:10.1111/j.1365-2567.2009.03160.x (2010).

217 Hooi, D. S., Bycroft, B. W., Chhabra, S. R., Williams, P. & Pritchard, D. I. Differential immune modulatory activity of Pseudomonas aeruginosa quorum-sensing signal molecules. *Infect Immun* **72**, 6463-6470, doi:10.1128/IAI.72.11.6463-6470.2004 (2004).

218 Skindersoe, M. E. *et al.* Pseudomonas aeruginosa quorum-sensing signal molecules interfere with dendritic cell-induced T-cell proliferation. *FEMS*

Immunol Med Microbiol **55**, 335-345, doi:10.1111/j.1574-695X.2008.00533.x (2009).

219 Lepine, F., Milot, S., Deziel, E., He, J. X. & Rahme, L. G. electrospray/mass spectrometric identification and analysis of 4-hydroxy-2-alkylquinolines (HAQs) produced by Pseudomonas aeruginosa. *J Am Soc Mass Spectr* **15**, 862-869 (2004).

220 Calfee, M. W., Shelton, J. G., McCubrey, J. A. & Pesci, E. C. Solubility and bioactivity of the Pseudomonas quinolone signal are increased by a Pseudomonas aeruginosa-produced surfactant. *Infect Immun* **73**, 878-882, doi:10.1128/iai.73.2.878-882.2005 (2005).

221 Haba, E. *et al.* Physicochemical characterization and antimicrobial properties of rhamnolipids produced by Pseudomonas aeruginosa 47T2 NCBIM 40044. *Biotechnol Bioeng* **81**, 316-322, doi:10.1002/bit.10474 (2003).

222 Abdel-Mawgoud, A. M., Lepine, F. & Deziel, E. Rhamnolipids: diversity of structures, microbial origins and roles. *Appl Microbiol Biotechnol* **86**, 1323-1336, doi:10.1007/s00253-010-2498-2 (2010).

223 Boles, B. R., Thoendel, M. & Singh, P. K. Rhamnolipids mediate detachment of Pseudomonas aeruginosa from biofilms. *Mol Microbiol* **57**, 1210-1223, doi:10.1111/j.1365-2958.2005.04743.x (2005).

224 Mireles, J. R., 2nd, Toguchi, A. & Harshey, R. M. Salmonella enterica serovar typhimurium swarming mutants with altered biofilm-forming abilities: surfactin inhibits biofilm formation. *J Bacteriol* **183**, 5848-5854, doi:10.1128/JB.183.20.5848-5854.2001 (2001).

225 Irie, Y., O'Toole G, A. & Yuk, M. H. Pseudomonas aeruginosa rhamnolipids disperse Bordetella bronchiseptica biofilms. *FEMS Microbiol Lett* **250**, 237-243, doi:10.1016/j.femsle.2005.07.012 (2005).

226 Elshikh, M. *et al.* Rhamnolipids and lactonic sophorolipids: natural antimicrobial surfactants for oral hygiene. *J Appl Microbiol* **123**, 1111-1123, doi:10.1111/jam.13550 (2017).

227 Stipcevic, T., Pijac, A. & Pijac, G. Enhanced healing of full-thickness burn wounds using di-rhamnolipid. *Burns* **32**, 24-34, doi:10.1016/j.burns.2005.07.004 (2006).

228 Shen, C. *et al.* Targeted killing of myofibroblasts by biosurfactant di-rhamnolipid suggests a therapy against scar formation. *Sci Rep* **6**, 37553, doi:10.1038/srep37553 (2016).

229 Piljac, A., Stipcevic, T., Piljac-Zegarac, J. & Piljac, G. Successful treatment of chronic decubitus ulcer with 0.1% dirhamnolipid ointment. *J Cutan Med Surg* **12**, 142-146, doi:10.2310/7750.2008.07052 (2008).

230 Galiano, R. D., Michaels, J. t., Dobryansky, M., Levine, J. P. & Gurtner, G. C. Quantitative and reproducible murine model of excisional wound healing. *Wound Repair Regen* **12**, 485-492, doi:10.1111/j.1067-1927.2004.12404.x (2004).

231 Wang, X., Ge, J., Tredget, E. E. & Wu, Y. The mouse excisional wound splinting model, including applications for stem cell transplantation. *Nat Protoc* **8**, 302-309, doi:10.1038/nprot.2013.002 (2013).

232 Dunn, L. *et al.* Murine model of wound healing. *J Vis Exp*, e50265, doi:10.3791/50265 (2013).

233 Plaut, R. D., Mocca, C. P., Prabhakara, R., Merkel, T. J. & Stibitz, S. Stably Luminescent Staphylococcus aureus Clinical Strains for Use in Bioluminescent Imaging. *Plos One* **8**, doi:ARTN e5923210.1371/journal.pone.0059232 (2013).

234 Inoue, Y., Izawa, K., Kiryu, S., Tojo, A. & Ohtomo, K. Diet and abdominal autofluorescence detected by in vivo fluorescence imaging of living mice. *Mol Imaging* **7**, 21-27 (2008).

235 Ulitzur, S., Reinhertz, A. & Hastings, J. W. Factors affecting the cellular expression of bacterial luciferase. *Arch Microbiol* **129**, 67-71, doi:10.1007/bf00417183 (1981).

236 Verdrengh, M. & Tarkowski, A. Role of neutrophils in experimental septicemia and septic arthritis induced by Staphylococcus aureus. *Infect Immun* **65**, 2517-2521 (1997).

237 Rigby, K. M. & DeLeo, F. R. Neutrophils in innate host defense against Staphylococcus aureus infections. *Semin Immunopathol* **34**, 237-259, doi:10.1007/s00281-011-0295-3 (2012).

BIOGRAPHY

Yihui Wang was born on August 21, 1992 in Handan, China, to her parents, Ke Wang and Yanchun Li, as their only child. She grew up in this small city in northern China. After graduating high school in 2009, she moved to the south to attend Xiamen University, ultimately receiving a degree of Bachelor of Science in Pharmacy in 2013. During her junior year, she decided to explore her interest in research and go abroad for graduate studies. In 2015, she graduated from University of Southern California with a Master of Science in Molecular Pharmacology and Toxicology. In the same year, she was accepted into the Biomedical Sciences Graduate Program at Tulane University. She moved to New Orleans for her PhD study in the fall of 2015.